Design and Characterization of Twisted and Coiled Polymers and Their Applications as Soft Actuators

A thesis submitted

in partial fulfillment of the requirements for the degree of

MASTER OF APPLIED SCIENCE

in Biomedical Engineering

By

Jacob Martin

February 2023

Ottawa-Carleton Institute for Biomedical Engineering

Department of Mechanical Engineering

University of Ottawa

Ottawa, Ontario, Canada K1N 6N5

ABSTRACT

Current progress in mobility assistive devices revolves around traditional actuation methods including electric motors, hydraulics, and pneumatic cylinders to provide assistive joint torques to the user. While these mechanisms are effective at providing the torques needed, they are often bulky, heavy, and suffer from poor alignment with the joints of the user. These drawbacks have created a need for novel technologies that can provide a more compact and compliant form of actuation.

Twisted and coiled polymers, under the thermomechanical class of smart material actuators, have emerged as a strong candidate for use as soft actuators in assistive devices due to their low cost, commercial availability, high stroke capacity, and power density. Progress to their development is currently limited by lack of proper standardization in the fabrication process, along with incomplete characterization of its quasi-static mechanical and thermal behaviours and how the performance is influenced by various design considerations.

This thesis defined a fabrication process of twisted coiled polymer actuators and evaluated the trends between design considerations and their impacts on the final actuator performance. In this work, a fabrication rig was developed to manufacture consistent and repeatable actuators, while enabling the control of various identified design parameters. Subsequently, a comprehensive experimental evaluation was accomplished which resulted in a better understanding of the relationships between these parameters and the actuator performance including its tensile stroke, force generation, and variable stiffness properties. The results provided a foundation for designers to consider which variables should be controlled during both actuator fabrication and operation, in order to optimize its final performance to meet a set of prescribed requirements.

ACKNOWLEDGEMENTS

My Master's thesis is the culmination of all of the education I have received throughout the years and would not have been possible without the support and encouragement from countless individuals.

First and foremost, I would like to express my sincerest gratitude to my supervisor, Dr. Marc Doumit, for his continued support and guidance throughout this journey and for giving me the inspiration to study this field of research. I am extremely grateful for the invaluable mentorship and guidance which helped me in achieving this goal.

I would also like to express my appreciation to the University of Ottawa, the Department of Mechanical Engineering and all its faculty members and support staff for their assistance over the years in helping me achieve my academic goals. In particular, I would like to thank members of the machine shop, electronics shop, and more specifically Leo Denner, for his boundless assistance in helping me fix the numerous technical challenges faced in this work. His knowledge and experience contributed directly to this achievement.

I would like to thank my fellow graduate students, colleagues, and especially the peers in my research group for the roles they have played in helping me achieve my personal and professional goals.

I finally wish to express my love and sincere gratitude to my mom and dad, my brother and sister, and my dogs for their continuous and limitless support through all my years of education and specifically in this chapter of my life. Completing this challenging endeavour in the middle of a global pandemic would not have been possible without their support and encouragement.

TABLE OF CONTENTS

LIST OF FIGURES

LIST OF TABLES

LIST OF ABBREVIATIONS

Abbreviation	Meaning
C	Spring Index
CNT	Carbon Nanotube
CP	Conductive Polymer
CTE	Coefficient of Thermal Expansion
DEA	Dielectric Elastomer Actuator
DMA	Dynamic Mechanical Analysis
DSC	Differential Scanning Calorimetry
EAP	Electroactive Polymer
IR	Infrared
LCE	Liquid Crystal Elastomer
LCF	Length Contraction Factor
LVDT	Linear Variable Differential Transformer
MWNT	Multiwalled Nanotubes
NiTi	Nickel Titanium
PAM	Pneumatic Artificial Muscle
PVDF	Poly (Vinyl Difluoride)
SMA	Shape Memory Alloy
SME	Shape Memory Effect
SMP	Shape Memory Polymer
SWNT	Single Wall Nanotubes
TCP	Twisted and Coiled Polymer
TMA	Thermomechanical Analysis
UHMWPE	Ultra High Molecular Weight Polyethylene

Chapter 1

Introduction

According to the 2017 Canadian Survey on Disability, nearly 2.7 million Canadians aged 15 or older live with a mobility disability, which represents close to 10% of the population [1]. Those with mobility disabilities must modify their gait by relying on compensation mechanisms in the body to accommodate the insufficiencies or require full powered assistance making it harder to perform daily activities. As Canada's population ages and grows, the number of people with mobility disabilities are expected to increase, creating a need for improved personal assistive devices that can be tailored for individual users and specific deficiencies. These devices include walkers and canes, orthoses and prostheses, and passive and powered exoskeletons.

Current assistive devices are typically fabricated from rigid components such as metal or plastic links, hydraulic or pneumatic cylinders, and electric motors that work in synchrony to provide assistive joint torques to the user. While these mechanisms can bear significant loads and transmit large torques at high bandwidths, they are usually heavy, bulky, expensive, noisy, and suffer from poor alignment with the user joints. This introduces additional weight and inertia to the system that usually has a negative influence on the gait of the user, while increasing their metabolic energy expenditures. Though these devices are now common, patients who require their use have reported experiencing discomfort and lack of proper assistance that ultimately leads to rejection of such devices and limited mobility [2].

Recent trends have shifted towards soft assistive devices as a method to address these concerns. To start, the use of stretchable textiles has been employed with pneumatic artificial muscles (PAM) or Bowden cables as an alternative to rigid links and transmission systems. While the compliance of the textile straps has led to improved comfort and mobility for some users, the need for an on-board or off-board actuation mechanism consisting of heavy tanks or electric motors limits the practical daily use of such devices. As an alternative solution, the use of smart materials as soft actuators has gained significant attention in recent years, specifically in the fields of robotics and assistive devices. Smart materials are materials that can alter their mechanical properties or configurations in response to external stimuli, enabled by the coupling of variables

in different physical domains. These stimuli have included electric and magnetic fields, light, heat, and chemical absorption, among others.

In particular, the recent discovery of inexpensive, commercially available, high stroke, and power dense twisted and coiled polymers as soft actuators has become a promising contender for integration into large scale devices. These materials can provide high stress linear contraction in compact volumes, making them attractive alternatives to the conventional rotary actuators of powered assistive devices. Additionally, when prepared as an actuator, these materials have an inherent ability to vary in stiffness by several orders of magnitude making them appealing candidates for mimicking biological muscles. Progress is currently limited by lack of proper characterisation and inconsistencies in the fabrication process, inefficient actuators requiring large amounts of input energy, and the low force generation of individual actuators. These limitations must be addressed to further develop novel and successful assistive devices.

1.1 – Objectives

Consequently, the objectives of this thesis are organized in three steps. The first objective was to gain a foundational knowledge of the working mechanisms behind the actuation of twisted and coiled polymers, and to identify any fabrication and operation parameters that may influence the final actuator performance. These specific performance metrics include the tensile stroke, force generation capacity, and range of achievable stiffness of the individual actuators. The next objective was to develop a reliable fabrication procedure enabling control of specific parameters during fabrication, such that consistent and repeatable actuators can be manufactured. Lastly, this thesis aimed to characterize the mechanical and thermal quasi-static behaviours of several twisted and coiled polymer actuator prototypes with individually controlled design or operating parameters to illustrate the relationships between the identified fabrication and operation parameters with the final actuator performance.

1.2 – Methodology

To satisfy the main thesis objectives, a three-part methodology was applied to guide the research. First, a comprehensive literature survey was conducted, and eight unique fabrication and operation parameters were identified that may have effects on the tensile stroke, force generation, or variable stiffness actuator properties. After identifying the parameters to be isolated during

fabrication of the prototypes, a fabrication rig was built enabling control of individual parameters. This allowed sets of prototypes to be fabricated for each isolated parameter, where samples were prepared with wide ranges of properties for testing. Finally, the effects of varying each isolated fabrication or operation parameter on the final actuator performance was determined through a thorough experimental evaluation. Three unique experimental setups were designed to test the three biological muscle contraction types, namely isotonic contraction, isometric contraction, and eccentric contraction. Qualitative and quantitative trends between the actuator performance and the fabrication and operation parameters used were presented based on the analysis of each experiment.

1.3 – Contributions

This thesis provides a thorough literature review outlining the current state of twisted and coiled polymer (TCP) actuators, their mechanisms of actuation, basic fabrication procedure, common properties, advantages, and limitations to their use. From this review, a lack of consistency and standardization in the fabrication process was noticed in the reported results, and 8 design parameters were identified that may influence the final performance of the actuator. These parameters included the operating conditions, precursor fibre diameter, spring index, twist density and coil bias angle, twist insertion speed, training load, amount of pre-stretch in the precursor fibre, and amount of pre-stretch in the fully coiled sample during annealing. A fabrication rig was constructed and validated, capable of manufacturing consistent and repeatable actuators while enabling the control of each individual parameter.

The thesis provides a comprehensive experimental evaluation of nylon-6 TCP actuators and the relationships between identified fabrication and operation parameters, and the final actuator performance. This included relationships between design parameters and their effects on the variable stiffness properties of the actuator, which to date is missing from the literature.

Based on this experimental evaluation, many trade-offs in performance were identified along with certain optimal fabrication or operating conditions that yielded the best performance, including highest tensile stroke, largest generated actuator forces, and largest magnitude of variation in stiffness.

Finally, a novel method of training was explored by training the prototypes dynamically against extension springs of varying stiffness. Based on this training method, repeatable actuation strokes can be achieved without the noticeable changes in initial sample length that typically accompanies training under static masses.

1.4 – Thesis Outline

This thesis is organized into 5 chapters. Chapter 1 presents an introduction of the TCP actuator and the motivations behind its further study, the thesis objectives, the adopted methodology, and main contributions of this work. Chapter 2 presents the results of the literature review and is divided into three main sections. First, existing classes of electromechanical and thermomechanical soft actuators are presented. Next, an overview of twisted and coiled polymer actuators is presented including its mechanism of actuation, the fabrication procedure and identification of design parameters that may influence actuator performance, and the main properties, advantages, and disadvantages of these materials. Lastly, different methods of upscaling the performance of individual actuators into larger devices are presented including various textile processing techniques and biomimetic inspirations.

Chapter 3 presents the experimental setup and is organized into three main subsections. First, three experimental setups designed to enable isotonic, isometric, and eccentric muscle contraction of the fabricated prototypes will be presented. Next, an overview of the custom fabrication rig used to manufacture the prototypes is presented. This fabrication rig was then validated by manufacturing samples with consistent initial properties and testing the samples following the experimental setups outlined to ensure consistent and repeatable actuators can be produced. Lastly, the chapter concludes with the precursor fibre material selection to be used in the development of the actuator prototypes. The precursor fibres and associated mechanical and thermal properties were then determined experimentally or through open literature sources.

Chapter 4 presents the experimental evaluation and is divided into 8 sections, each presenting the experimental results of the independent fabrication or operation parameter that were investigated. These subsections are further organized into four main subsections, each presenting the changes to the fabrication procedure, experimental results, analysis, and discussion of the isotonic, isometric, and eccentric contraction tests. Numerous trends between the individual

fabrication or operation parameters and the final actuator performance were identified and discussed in the context of optimizing actuator stroke, force generation, or variable stiffness properties.

Chapter 5 presents the thesis conclusions, and provides recommendations for future work in this subject, including modifications to the fabrication rig and experimental setups, and suggestions for further research based on limitations in the current experimental evaluation

Chapter 2

Literature Review

In this chapter, a comprehensive literature review was conducted and the relevant topics within the scope of this thesis were reported. The review first provides context on existing soft actuating technologies such as electromechanical and thermomechanical actuators, along with the unique advantages and limitations of each. Next, an overview on twisted and coiled polymer actuators including the mechanisms of actuation, their fabrication procedures and design considerations, and typical properties, advantages, and drawbacks to their use was presented. Finally, a summary of different upscaling techniques is presented including existing textile processing methods and biomimetic inspirations.

2.1 – Existing Soft Actuators

2.1.1 – Electromechanical Actuators

The first class of soft actuators presented are those which are actuated through electrical stimulation and are referred to as electromechanical actuators. Specifically, a class of polymer materials have emerged that can change their properties or configurations in response to electrical and ionic stimuli and are known as electroactive polymers (EAP). Conductive polymers (CP) are within the ionic subclass of EAPs, and its actuation behaviour depends on the diffusion of ions between an electrolyte and the polymer structure. Upon a given electric potential, the CP electrodes become charged and ions from the electrolyte diffuse into the polymers leading to swelling, which can be exploited for actuation [3], [4]. Actuator strains are typically within 2-10%, which correlate with operating stresses between 1 to 34 MPa and work densities as high as 100 MJ/m^3 [3]–[5]. CPs suffer from low electromechanical coupling efficiency of typically less than 1%, which requires large amounts of electrical energy to be shunted. This inefficiency, and the need for an encapsulated electrolyte may limit the practical use of CP actuators [3], [5].

Dielectric elastomer actuators (DEA) are within the electronic subclass of EAPs and consist of a thin elastomer film coated with a conductive powder or grease on opposite surfaces. When a voltage is applied across the thickness of the DEA, a Maxwell stress is induced forcing

the electrodes closer to each other. Compression over the elastomer thickness causes expansion normal to this direction, and these dimensional changes can be exploited for use as an actuator against a load [4]–[6]. Areal strains are usually in the range of 10-100% under normal operating conditions, while strains up to 380% have been reported under high applied fields. This yields exceptional work densities of up to 3.4 MJ/m^3, which is approximately 400 times larger than biological muscle [5]. Energy efficiencies have been reported as high as 90% for silicone-based DEAs, while bandwidths in the range of hundreds of hertz have been demonstrated. Drawbacks to DEAs include large electric field strengths up to 100-150 MV/m, or up to 10 kV of voltage for a common thin film configuration, which can be unsafe and impractical for wearable assistive applications [3], [5], [6].

Electrostrictive polymers are also within the electronic subclass of EAPs and consist of two main types: electrostrictive relaxor ferroelectrics, and electrostrictive graft elastomers. Upon application of an electric field, polarized domains within the polymer structure have their dipoles reoriented to align with the direction of the applied field. The resulting electric displacement of charges is the driving force behind actuation [5], [7], [8]. For electrostrictive relaxor ferroelectrics, strains have been reported between 4-7% with corresponding stresses up to 45 MPa, and energy densities as high as 1.1 MJ/m^3. Electrostrictive graft elastomers have demonstrated strains ranging from 2.5-4%, with corresponding energy densities up to 0.5 MJ/m^3 [3], [5], [7]–[9]. As with DEAs, high electric fields are required to induce these strains, which typically limits the configurations to thin films and fibres.

Carbon nanotubes (CNT) are unique materials with a combination of desirable electrical and mechanical properties and are generally classified as within the ionic subclass of EAPs. Single wall nanotubes (SWNT) consist of a single layer of graphene wrapped in a cylindrical tube of nanometer diameter, while multiwalled nanotubes (MWNT) are multiple SWNTs concentrically nested [5], [10]. CNTs can be actuated electrochemically through formation of a double layer of ions within an electrolyte, or electrothermally by infiltrating the CNT with a thermally expanding guest material. Interestingly, it was determined that torsional or tensile stroke of these actuators can be amplified by inserting high degrees of twist into the CNTs [11], [12]. This phenomenon has led to actuators capable of producing 5.6-33% strokes, with corresponding stresses as high as 88 MPa and work densities up to 2.2 kJ/kg [12]–[14]. The poor energy efficiency, difficulty

manufacturing and high cost have limited the use of CNT actuators in many applications [3], [12], [15].

2.1.2 – Thermomechanical Actuators

Thermomechanical actuators are those which respond to thermal stimuli. Liquid crystal elastomers (LCE) are polymer materials with solid and liquid states, along with an intermediary viscoelastic state enabled by liquid crystal molecules known as mesogens. When the material is cooled, it behaves as an anisotropic solid with the mesogens highly aligned. When heated, the mesogens become free to reorient into a more thermodynamically stable state, and the crosslinks perform mechanical work on the polymer backbone leading to macroscopic deformations that can be exploited for actuation [16]–[19]. LCEs have a lesser degree of crosslinking than some other liquid crystal polymer materials, allowing for larger deformations as the mesogens reorient themselves. Achievable strains have been reported as high as 45%, with corresponding stresses up to 280 kPa for fibre-form LCEs, which is comparable to the ranges of skeletal muscle [3], [17], [20], [21]. Limitations of LCEs include low thermomechanical coupling leading to poor energy efficiency, with low work densities ranging from 3-56 kJ/m^3 [5], [16], [20].

Shape memory alloys (SMA) are metallic materials that exhibit the shape memory effect (SME), a phenomenon which describes the ability for a material to recover a memorized shape upon activation with a stimulus after the material was deformed to a temporary shape [6]. At low temperatures, loading the SMA transforms the crystal lattice to a detwinned martensite structure. Once the material is heated beyond a critical temperature, the reverse martensite to austenite phase transformation occurs and the SMA recovers its permanent shape in its body centred cubic austenite phase [3], [6], [16], [17]. After cooling the material, the crystal lattice transforms back to a twinned martensite structure which restarts the cycle. A commercially available nickel titanium (NiTi) SMA wire can experience up to 5% contraction against a 200 MPa load, which yields power densities as high as 50 W/g [3], [4], [6], [16]. Furthermore, by coiling the wire around a mandrel, a similar SMA can experience up to 50% contraction while providing up to 46.8 MPa of stress. This impressive behaviour is enabled by the drastic variation in elastic moduli between the martensite and austenite phases, which can be increased by a factor of 2 to 3 when actuated [17], [22], [23]. As is common with many thermomechanical actuators, bandwidths are limited by

the cooling rates to the surrounding environment. Other limitations include significant hysteresis in the heating and cooling cycle, poor energy efficiency, as well as fatigue and creep behaviour [6], [16], [17].

Shape memory polymers (SMP) are another class of materials that exhibit the SME and are comprised of a stiffer permanent phase of chemical or physical crosslinks, and a reversible switching phase triggered by a transition temperature. The permanent phase retains high elasticity, while the switching phase can vary in stiffness by several orders of magnitude when activated [24]–[26]. A typical cycle is explained as follows, where a SMP is heated past its transition temperature and is subsequently loaded to deform to a temporary shape. The load is held as the material is cooled below the transition temperature, activating the switching segments to fix the temporary shape. Once the SMP is reheated above its transformation temperature, the switching segments are activated again and the stored strain energy from the temporary shape is released which leads to macroscopic permanent shape recovery [17], [24]–[27]. One of the main advantages to SMP actuators is the large recoverable strains up to 800%. This, however, comes at the expense of low stress generation typically in the range of 1-3 MPa [6], [17], [26]. SMPs are capable of varying in stiffness ranging from 0.01-3 GPa during actuation, which can be useful in robotic and assistive device applications. Long cooling times, and the need for an external force or antagonistic configuration to reset the temporary shape are some of the main drawbacks to SMP actuators [17], [24], [25].

2.2 – Overview of Twisted and Coiled Polymer Actuators

With many developed and novel smart materials suitable for use as soft actuators, there remains significant trade-offs in performance making it challenging to find actuation mechanisms that meet all prescribed requirements. Figure 1 shows a comparison of the stresses, strains, and energy densities of various actuator technologies [28]. SMA actuators have excellent power density but they generally suffer from hysteretic performance, lower achievable strains, high cost, and difficulty manufacturing. Conversely, DEAs have some of the largest achievable strokes compared to other soft actuators, and the rapid response times enable bandwidths on the order of hundreds of hertz. However, these actuators are limited by its low stress production, or demanding operating conditions on the power supply. The challenge in finding a suitable soft actuation

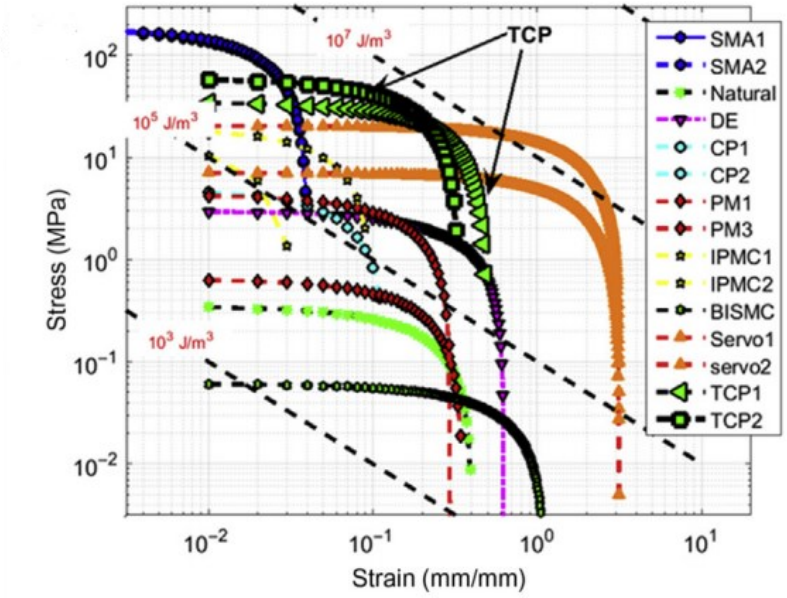

Figure 1: Blocked stress, free strain, and average energy density of various actuators and natural skeletal muscle. Reprinted from [28] with permission from © 2019 Elsevier.

mechanism arises from finding the optimal combination of desirable traits, while reducing the effects of actuator trade-offs.

This challenge has been met with considerable progress since 2014 upon the discovery by Haines et al. [29], where soft thermomechanical actuators with large stroke, high power density, and low hysteresis could be fabricated out of low-cost, commercially available high strength polymer fibres. More specifically, highly oriented semicrystalline polymer fibres like fishing lines or sewing threads can be configured into soft thermomechanical actuators by exploiting the anisotropic thermal expansion behaviour and directing the deformation along a particular direction. These precursor fibres, often made from nylon or polyethylene, have a semicrystalline structure composed of amorphous chains and surrounding crystalline domains that are highly aligned in the fibre draw direction. Furthermore, Haines et al. demonstrated that the anisotropic thermal expansion behavior can be further utilized after inserting such a high degree of twist into the fibre such that the twists spontaneously convert to form coils [29]. This configuration is referred to as twisted and coiled polymer (TCP) actuators and will be the focus of this review.

2.2.1 – Mechanism of Actuation

To better understand the origins of the TCP actuation mechanism, first the mechanism of actuating a straight cylindrical fibre will be discussed. As a straight precursor fibre, the amorphous chains and surrounding crystalline regions are highly aligned in the draw direction. During the drawing process, the amorphous tie molecules are extended in the fibre direction and retain rubber-like elasticity. As the fibre is heated, the modulus of the amorphous tie molecules increases and the stored elastic energy is released, allowing for the chains to reconfigure into a more stable state. The result is axial thermal contraction along the fibre axis, while the surrounding crystalline regions expand in volume perpendicular to the fibre axis as seen in Figure 2(a) [30]. A straight nylon 6-6 fibre can experience axial contraction as high as 4% when heated, which is comparable to that of commercial NiTi SMA wires [3], [17], [29].

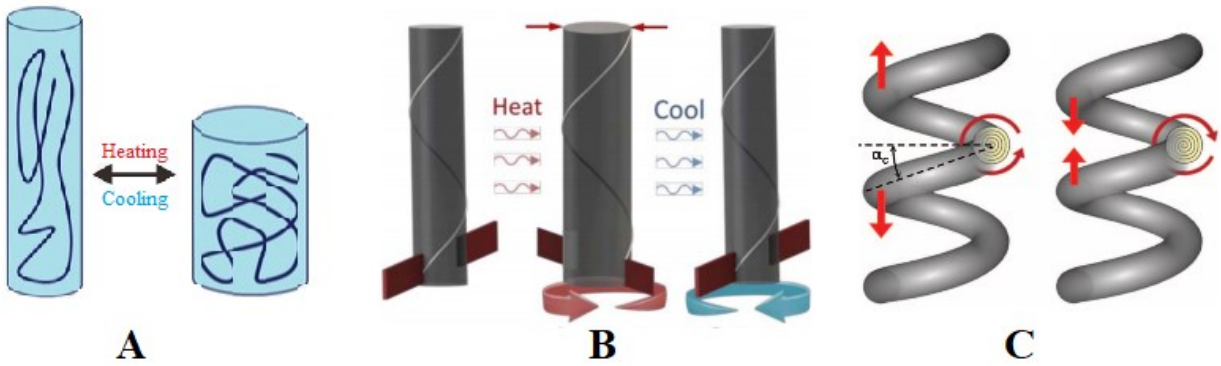

Figure 2: Schematic of thermal actuation of: A) precursor fibre; B) twisted fibre; C) heterochiral (left) and homochiral (right) TCP actuators. A) Reprinted from [30] with permission from © 2020 John Wiley and Sons. B) Reprinted from [32] with permission from © 2016 John Wilen and Sons. C) Reprinted from [29] with permission from © 2014 AAAS.

Similar to CNT actuators, torsional and tensile stroke can be amplified by inserting a high degree of twist into the precursor fibre. In highly twisted, non-coiled fibre bundles, the aligned amorphous chains and surrounding crystalline regions are now reoriented in a helical arrangement matching the chirality of the inserted twist. When the twisted bundle is heated, the amorphous chains contract in length along the helical path, while the crystalline regions expand in the radial direction. Now, both an increase in fibre diameter and a decrease in fibre length contribute to untwisting of the fibres, which can be exploited for torsional actuation or torque generation as shown in Figure 2(b) [11], [12], [29], [31], [32].

Once a critical amount of twist is inserted into the precursor fibre, coils spontaneously nucleate to minimize strain energy in the fibres [31]. Coiling of the twisted fibres reconfigures the

constituent elements into a macroscopic writhe arrangement, where the same thermal mechanisms apply. In this configuration, as the writhe is heated, radial expansion and axial contraction of the precursor fibre both additively contribute to fibre untwisting which generates internal torsion at the coil level. This forces adjacent coils to contract closer to each other, as shown in Figure 2(c). A similar nylon 6-6 fibre was shown to amplify its tensile stroke from 4% to 34% when actuated as a straight fibre or a writhe, respectively [29], [31]. An alternative method for coiling takes the twisted fibres before onset of coil nucleation and wraps the bundle around a mandrel of adjustable diameter. In this method, coils with opposite chirality can be produced by wrapping the twisted bundle in the opposite direction to the initial inserted twist. Once heated, the internal torsion from the thermal expansion forces coils apart from one another, which can also be exploited for actuation. Extensional and contractional actuators can be fabricated, and are known as heterochiral and homochiral actuators, respectively [29], [31].

To actuate semicrystalline polymer fibres and TCP actuators, the material must be heated beyond critical temperatures that enable macroscopic thermal expansion and contraction. In this case, this temperature range is at or near the glass transition temperature of the polymer, T_g. When performing a thermomechanical analysis during experiments, Haines et al. noticed two distinct regions of the stroke-temperature plot [29]. A region of lower temperature where stroke remained minimal was observed, followed by a region of higher temperature where greater tensile stroke was recorded. The authors attributed this behaviour to the transition from a stiffer, glassy state, to a softer elastic state beyond the glass transition temperature. During this transition, the negative axial coefficient of thermal expansion increased by an order of magnitude, which explains the drastic increase in tensile stroke. Furthermore, when evaluating the glass transition temperature of both the precursor fibre and the fully twisted and coiled fibres, Haines et al. measured an increase in the glass transition temperature of nylon 6-6 from 70°C to 89°C as a straight fibre and a fully twisted and coiled fibre, respectively [29], [31]. This indicates that a larger magnitude of thermal stimulus is required to enhance chain mobility and tensile actuation in coiled actuators as more twists are inserted.

Throughout the literature, many methods have been investigated for supplying heat to the TCP actuators, including photothermal actuation, convective and radiative heating, and electrothermal actuation [3], [29], [33]. In photothermal actuation, the heat is supplied to the

actuators from absorption of light at its surface. Haines et al. demonstrated a 7% contraction against a 25 MPa load when a single nylon 6-6 TCP actuator was activated by a 250 W incandescent lamp [29], while Mirvakili and Hunter showed that coating the actuators with graphene paint can improve optical and thermal properties of nylon bending actuators under two 6 W laser diodes [3], [34]. Convective heating requires the transfer of heat from the TCP actuators to a fluid, while radiative heating involves the absorption of electromagnetic waves at high frequencies. Haines et al. fabricated a nylon 6 TCP actuator which could hydrothermally actuate against a 500-gram load with 12% contraction at 0.2 Hz, when 25°C and 95°C water were alternated against the actuator. In addition, the authors demonstrated improved bandwidths up to 7.5 Hz when coating a nylon 6-6 fibre with a CNT sheet, and supplying helium gas of high thermal diffusivity to improve the cooling rates [29]. Moreover, a conventional microwave oven provided the radiation to actuate a 2-ply TCP muscle at 5.5% contraction against a 14 MPa load in 2 seconds, although this may be impractical for certain applications [29], [31]. A more practical alternative which is common in the literature is electrothermal actuation, where the TCP actuators are integrated with electrically conductive wires or coatings to supply heat through resistive (Joule) heating. Some of the materials investigated include copper and nichrome wires, graphene and silver coatings and paints, and CNT sheets and composites [3], [17], [29], [33]. Commercially available conductive silver-coated nylon fibres have also been used to demonstrate direct Joule heating for actuation [28], [35].

2.2.2 – Fabrication Procedures and Design Considerations

2.2.2.1 – Basic Fabrication Procedure

The fabrication process of TCP actuators involves four steps: twisting, coiling, annealing, and training, as illustrated in Figure 3. In this section, each fabrication step will be outlined for a generic aligned, semicrystalline polymer precursor fibre. After that, different design considerations reported in the literature which can influence the TCP actuator performance will be discussed.

The first step of the fabrication process is twist insertion. From Figure 3(a), the process begins with a straight precursor fibre that is attached to a motor at one end, and a dead weight is attached at the other end. The precursor fibre is typically about three times the desired length of the final actuator, and the dead weight should be large enough to keep the fibre taut and prevent

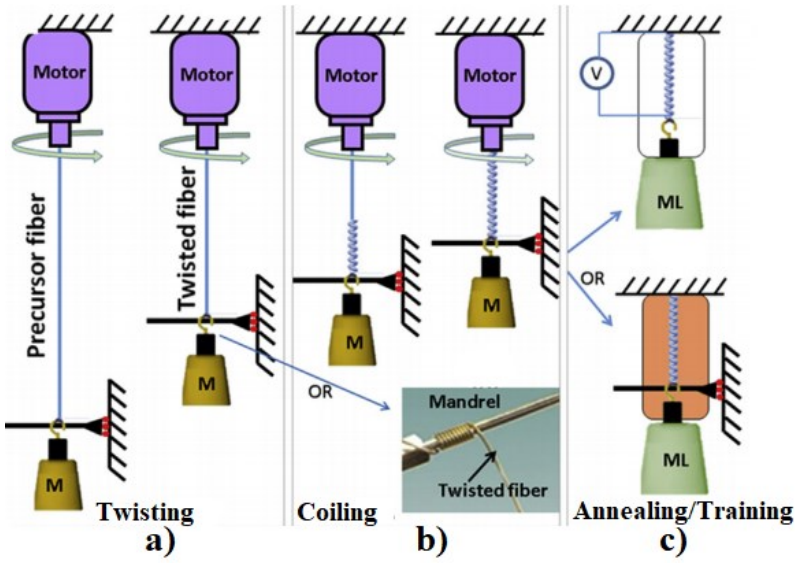

Figure 3: Schematic of fabrication steps of TCP actuators. a) Twisting of precursor fibre; b) Coiling of twisted fibre; c) Annealing and training of TCP actuator. Reprinted from [28] with permission from © 2019 Elsevier.

snarling, while ensuring that the fibre does not snap [28], [29], [36]. The dead weight is mechanically constrained to prevent fibre end rotations, such that rotations from the motor will fully convert to inserted twists in the fibre. As twists are inserted, the dead weight will translate vertically as the twisted fibre shortens in length. At this time, the twisted fibres are formed at an angle with the fibre axis known as the fibre bias angle, α_f, which can be approximated using equation 1:

$$\alpha_f = tan^{-1}(\pi DT) \tag{1}$$

Where D is the precursor fibre diameter, and T is the number of inserted twist per fibre length [31]. The choice of precursor fibre, dead weight, amount of twist inserted, and motor speed are all factors to consider before fabrication.

The next stage of fabrication involves coiling of the twisted fibres, which can be performed automatically or manually over a mandrel as shown in Figure 3(b). Nearing the end of the twist insertion stage, the fibre eventually reaches a critical limit beyond which it is unable to accommodate any more twists. This limit, known as the critical twist density, T_c, depends on the geometry and precursor fibre material properties, as well as the stress used during coiling as described by equation 2:

$$T_C = \frac{\sqrt{2\sigma E}}{\pi DG} \tag{2}$$

Where σ is the tensile coiling stress, D is the fibre diameter, and E and G are the material's elastic and shear moduli, respectively [31]. Once the critical twist density has been reached, coils begin to spontaneously nucleate at one or more points along the fibre as fibre twists are further converted into writhes [28], [29], [31], [36]. An alternative method for coiling involves taking the twisted fibre near or shortly after the point of critical twist density and wrapping the twisted fibres around a mandrel of customizable size and shape. Besides the ability to fabricate extensional actuators with opposite chirality as previously discussed, mandrel coiling offers the ability to tune the outer coil diameter along with the macroscopic coil shape. The relationship between the change in coil length, ΔL, and the change in fibre twist, ΔT, can be described using equation 3:

$$\frac{\Delta L}{L} = \frac{l^2 \Delta T}{LN} \tag{3}$$

Where L is the coil length, l is the length of the fibre in the coil, and N is the number of coil turns [31]. Using mandrels, Haines et al. produced TCP actuators around mandrels including steel wires of less than a millimeter diameter, and rods up to several millimeters in diameter [28], [29]. The authors later demonstrated that when using a conical mandrel, the geometry enabled coils to pass through each other during actuation, eventually leading to stroke up to 200% as actuator contraction converts into extension in the opposite direction beyond 100% stroke [31]. Once the fibre has fully coiled, Haines et al. observed that the coil shape was set by plastic deformation and the number of coils remained unchanged as additional twists were added or removed. However, the coil diameter and fibre length varied as twists were added or removed. Further addition of twists into a fully coiled TCP actuator caused the coil length to decrease and the diameter to increase due to the coils tightening. Conversely, removing twists reduced the coil diameter while increasing the coil length [29].

As both twisting and coiling are cold working processes, they leave behind residual stresses within the material structure that cause a tendency to untwist the fibres. Proper heat treatment through annealing has proven to be a solution, where the TCP actuators are heated above the glass transition temperature but below the polymer melting point while under a tensile load [29], [36]. Depending on the fibre and the heat source, annealing can be performed electrothermally through Joule heating or from a convective or radiative heat source, as shown in Figure 3(c). For any TCPs actuated electrothermally, it is important to consider oxidation of the conductive elements that can reduce the conductivity over time, ultimately limiting the actuator performance and cycle life.

Mediums other than air have been investigated for use during annealing to prevent oxidation of the conductive elements, including vacuums, argon, and nitrogen [28], [29], [37]. Electrothermal annealing is usually performed in cycles, where different currents are supplied for shorter periods of time. Many factors relate to the current needed to heat the actuator, and too much current can overheat the material leading to actuator degradation. To overcome this, mathematical relationships between the supplied current and actuator temperature have been derived [35], while manual control of the current and monitoring actuator temperature has commonly been used as a simpler method [28], [36], [38]. Furnaces, ovens, and microwaves have been used effectively for TCPs actuated by convective or radiative heat. Most of the literature describes shape setting of the actuator after one to two hours of annealing, although this can vary depending on the size of the precursor fibre, the amount of space introduced between neighbouring coils, and the twist density within the coils [28], [29], [37], [39].

The final step involves training the actuator. Training is a similar process to annealing; however, the requirement is to obtain consistent and repeatable actuation cycles against a load. The size of the load used during training depends on the actuator's intended use, and the load can be adjusted to ensure there is adequate space between coils to contract. For electrothermal actuators, training is typically performed in cycles similar to the annealing process, however some authors have reported using 50% duty cycle as being sufficient to achieve consistent reversible actuation [28], [36]. For TCPs actuated without conductive elements, alternating hot and cold fluids such as water and air have demonstrated effective actuator training [28], [29], [40]. This static training method is well documented and has been the primary method found in the literature; however, dynamic training effects under a bias load could be of practical importance to some researchers and has not been fully evaluated [28]. In many practical applications, the actuators will not be loaded with constant forces. Loading effects could be investigated by training the actuator against a mechanical spring, where the load against the actuator increases as the actuator contracts. Once consistent and reversible actuation cycles have been obtained, the actuators can be prepared to be integrated into designs.

2.2.2.2 – Design Considerations and Their Effect on Actuator Performance

Many factors and design considerations influence the performance of TCP actuators, and researchers have attempted to analyze these factors to fully characterize the actuators, such that they can be implemented in designs for various applications. The first factor to consider is the precursor fibre selection. Starting with low cost, commercially available polymer fibres such as nylon, ultra high molecular weight polyethylene (UHMWPE), Kevlar, poly (vinyl difluoride) (PVDF), polyester, and polypropylene, after twisting, the fibres retain their thermal anisotropic properties that drives torsional and tensile actuation [3], [29], [31]. Materials with higher tensile moduli and lower coefficients of thermal expansion, such as Kevlar or UHMWPE, are useful in high-strength applications; however, the low coefficients of thermal expansion limit the actuator stroke. Conversely, materials with larger coefficients of thermal expansion including nylon, spandex, and PVDF generate larger actuator strokes at the expense of stress generation. Furthermore, Haines et al. [29], [31] demonstrated that it is not simply the negative axial coefficient of thermal expansion that drives contraction of twisted and coiled nylon fibres, but rather the degree of mismatch between axial and radial expansion coefficients. For example, a precursor polyester fibre has both positive axial and radial thermal expansion coefficients; however, once fully twisted and coiled the actuator still contracts along its length. Since the radial thermal expansion coefficient is sufficiently larger than the axial coefficient, the degree of anisotropy still causes a tendency for the fibre to untwist, which is the driving force behind torsional and tensile actuation. As such, precursor fibres with the largest degree of thermal anisotropy produce the greatest amount of torsional actuation, which is expected to yield the largest tensile strokes.

Karami et al. [41] built on the work of Choy et al. [42] and investigated the effects of temperature and draw ratio on the coefficients of thermal expansion for a nylon 6-6 fibre. Draw ratio is defined as the ratio of the fibre's initial length to the length of the fibre after drawing and twisting. Both the axial and radial coefficients of thermal expansion increased with increasing temperature, which is consistent with the observations from Haines et al. [29]. The coefficients of thermal expansion also depended on the draw ratio, where larger draw ratios yielded larger coefficients of thermal expansion, and greater anisotropy between the properties. Increasing the

draw ratio by pre-stretching or further drawing could be an effective solution to improving anisotropy in thermal expansion, which could lead to higher torsional and tensile strokes [43]. As such, more research is required to characterize the effects of anisotropy in thermal expansion on the coiled sample performance.

The next factor to be considered is heating element integration within the TCP actuator. Although many attempts have successfully actuated TCPs using convective, radiative, or light sources, the most common and convenient method in the literature has been electrothermal actuation through Joule heating. The challenge consists of maximizing the contact surface area between the heating element and the TCP actuator, while remaining compliant such that twisting, coiling, or TCP actuation is not hindered by the conductive component. If the heating element is not evenly distributed throughout the TCP, regions of localized heating may accumulate leading to possible actuator degradation, while also limiting the actuator performance. Haines et al. demonstrated successful electrothermal actuation by twisting a 25 μm diameter steel wire with a nylon 6 monofilament [29]. Similarly, Wu et al. maximized the contact surface area by wrapping a very thin nichrome wire around the precursor polymer fibre at a small pitch and constant speed, which enabled even heat distribution with little mechanical constraints during actuation [44]. Besides twisting or plying resistance wires with the precursor polymer fibres, other methods included conductive coatings, pastes, and paints to enable Joule heating. These included silver plated coatings, silver paints, silver-niobium nanowire paint, drawn MWNT sheets, and commercially available silver-coated nylon yarns [3], [29], [36]. Careful consideration should be taken when selecting the heating element, such that actuation performance can be optimized without risk of actuator degradation over many heating and cooling cycles.

With the actuation mechanisms better understood, it is important to evaluate which fabrication parameters yield the optimal torsional stroke and torque, which ultimately leads to improved tensile actuation. To start, Haines et al. set out to investigate the effects of twist density and load during twisting on the fibre bias angle and tensile actuation performance. The authors determined the applied load during twisting had little effect on the fibre bias angle. When the applied load was kept constant and the amounts of inserted twists varied, the authors noticed tensile stroke of twisted and non-coiled actuators remained relatively constant for lower twist densities. However, for higher twist densities, tensile stroke decreased rapidly with increasing inserted twist

[29], [31]. While tensile stroke of the twisted fibres was limited, torsional stroke was greatly enhanced, and this is the driving mechanism in coiled actuators. To build on this, Aziz et al. [32] investigated the effects of inserted twist and precursor fibre diameter on the torsional performance of twisted, non-coiled actuators. The authors first performed torsional stroke experiments against temperature for fibres of different diameter with the same amount of inserted twist. Results showed that torsional stroke was independent of the fibre diameter if the inserted twist was kept constant. However, when the fibre diameter was kept constant and the amount of inserted twist varied, torsional stroke increased with increasing amount of inserted twists. Next, the authors measured the generated actuator torque against temperature for fibres of different diameter with the same amount of inserted twist. The generated torque increased with increasing fibre diameter, which is consistent with the fact that fibres become increasingly stiffer with larger diameters. Similarly, when fibre diameter was controlled and the amount of inserted twists varied, the generated torque increased monotonically with increasing amounts of inserted twist [32]. While it is understood that the torsional performance of twisted and non-coiled bundles drives the tensile performance of fully coiled samples, more evidence is required to properly characterize this relationship.

One of the simpler approaches to tuning actuator performance involves changing the TCP actuator spring index, C, which is the ratio of the coil diameter, D, to the precursor fibre diameter, d. The spring index can be tuned either by varying the load used during coiling, or by coiling over a mandrel. The load used during coiling is important to consider because too much weight can cause the fibre to fail, while too little weight can cause the fibres to snarl rather than coil [29]. Once coils begin to nucleate, increasing the load during coiling or using a mandrel allows coils with larger spring indices to be fabricated. These actuators have more space between adjacent coils, which allows the coils to access a broader range of coil bias angles during actuation, yielding larger tensile strokes at the expense of reduced stiffness and load capacity. Conversely for TCPs with lower spring indices, these actuators behave similar to tight mechanical springs. While very stiff and able to withstand large stresses, the dense fibre packing within the coils restricts the possible range of coil bias angles before adjacent coils come into contact, which ultimately limits the actuator stroke [29], [31]. To demonstrate the effects of varying the TCP spring index on actuator performance, Haines et al. fabricated numerous TCP actuators with consistent properties prior to coiling, and varied the load used during coiling to produce three groups of actuators with distinct spring indices (C of 1.1, 1.4, and 1.7). Coils made with larger spring indices achieved

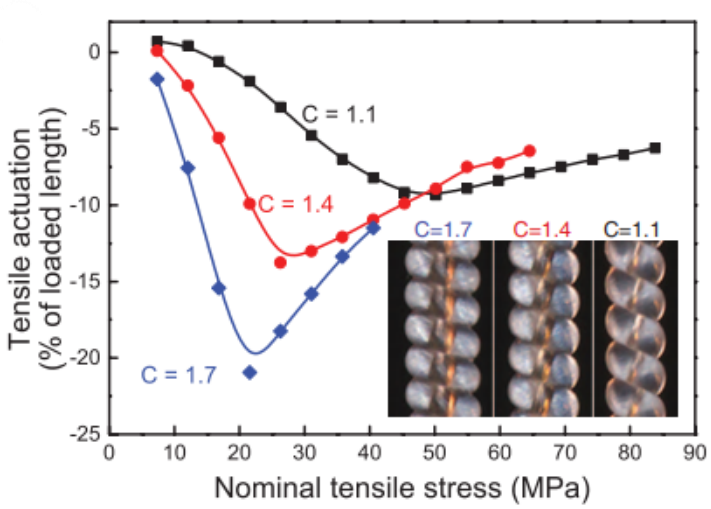

Figure 4: Variation in tensile stroke as a function of nominal tensile stress for TCP actuators with varying spring indices. Reprinted from [29] with permission from © 2014 AAAS.

larger tensile strokes against smaller nominal stresses, whereas coils made with smaller spring indices achieved smaller tensile strokes but could actuate against larger loads. For all coils, tensile stroke reached a maximum at a peak nominal stress, as seen in Figure 4, beyond which tensile actuation would decrease as the load increased [29], [31]. Tuning of the spring index either through varying the coiling load or using a mandrel is an effective method to adjust the trade-off in actuator performance between achievable stroke and output stress.

Work by Saharan and Tadesse attempted to characterize the effects of twist insertion speed on actuator performance for single, 2-ply, and 3-ply TCP actuators. Specifically, the output force, strain, stiffness, power generated and consumed were evaluated for each actuator made with different twist insertion speeds. While the authors did notice significant changes to actuator performance when varying the twist insertion speed, the observed trends were inconsistent and did not scale as expected as the number of plies increased [36]. These conclusions indicated that twist insertion speed may have a significant impact on actuator performance; however, further investigation is needed to fully characterize these effects.

Throughout the literature, many design parameters have been identified that can influence the final TCP actuator performance. While some of these parameters have been investigated individually, a comprehensive review designed to accurately compare all design parameters together was not found in the literature. This makes it increasingly difficult to compare results between authors using different methodologies. For these reasons, more research should be conducted to characterize the fabrication-performance relationships of various design parameters

collectively, since this would provide a useful tool for future designers of TCP actuators to tailor the performance to meet specific requirements.

2.2.3 – Properties, Advantages, and Limitations of TCP Actuators

The mechanical properties and actuator performance of TCPs is highly sensitive to the selection of precursor fibre, along with the fabrication procedures. Generally, TCP actuators are best known for its large achievable strokes, high power density, low cost, and ease of manufacturing. For nylon-based TCP actuators, Haines et al. [29] demonstrated the trade-off in performance when varying the actuator spring index. For tight coils with a spring index of 1.1, the maximum stroke was 9.3% while actuating against a 50 MPa stress. In contrast, when coiling the same precursor fibre around a mandrel for a spring index of 5.5, the maximum stroke increased to 49% while actuating against a 1 MPa stress. For precursor fibres of higher tensile strength and moduli, such as polyethylene, tensile strokes have been reported as high as 16%, while 140 MPa actuation stresses have been demonstrated for 4.5% stroke [3], [29]. More recently, highly stretchable spandex fibres achieved 45% contraction at lower temperatures compared with nylon or polyethylene, with achievable pulling stresses up to 0.758 MPa [17], [45]. These stress and strain ranges are comparable or greater to those achieved by natural skeletal muscle, indicating its potential application as soft actuators in mobility assistive devices.

With the ability to tune the actuator stress and stroke, TCP actuators have proven to exhibit high specific work capacity and power density. The specific work depends on the TCP spring index but can be as high as 2.48 kJ/kg for a nylon 6-6 actuator. Similarly, the average output power density during contraction was reported as high as 27.1 kW/kg, which is approximately 84 times greater than the peak output power produced by skeletal muscle [29]. Furthermore, work done by Haines et al. [29] and Aziz et al. [32] helped demonstrate the scalability of actuator performance with increasing or decreasing fibre diameter, since neither the fibre bias angle nor the torsional stroke depended on the fibre diameter. This is of particular interest for researchers in many fields, ranging from microfluidics and MEMS to assistive devices and deployable space structures, where high powered linear actuators in compact volumes are desired.

Another unique property of TCP actuators is its ability to vary in stiffness by several orders of magnitude. As the TCP actuator is heated, untwisting of the fibres forces adjacent coils to contract closer to each other, up until a point where adjacent coils are in contact and contraction is saturated. At the point of coil contact, negative axial thermal expansion transitions to positive thermal expansion in all directions at a rate similar to the radial thermal expansion. At this point, the coil geometry constrains it from further contraction as heat is added; however, the twisted fibres continue to expand and have a tendency to untwist, which builds up increasing internal torsion. As seen in Figure 5, this resulted in a 24-fold increase in the nominal modulus of a nylon 6-6 monofilament actuator, where initially the actuator stiffness decreased with increasing temperature up to the point of coil contact [29]. Such broad ranges of possible stiffness values are of great importance in the fields of soft robotics and assistive devices, where materials are desired that can transmit forces and withstand external loads in the active state, while remaining compliant and conforming in the resting state.

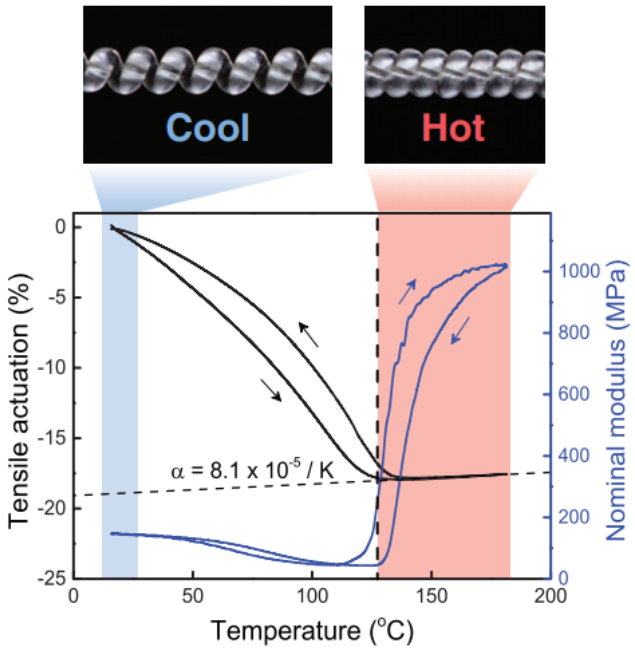

Figure 5: Variation of nominal modulus of a nylon 6-6 TCP actuator during saturated contraction. Reprinted from [29] with permission from © 2014 AAAS.

Another advantage of TCP actuators is the low hysteresis in the heating and cooling cycle in comparison to other smart materials. As shown in Figure 6, the tensile stroke of a nylon 6-6 TCP actuator follows a similar path during heating and cooling and the observed hysteresis was less than 1.2°C. In comparison, widely used and commercially available SMA actuators known for its power density and stress capacity, experience large hysteresis of up to 27°C in the heating

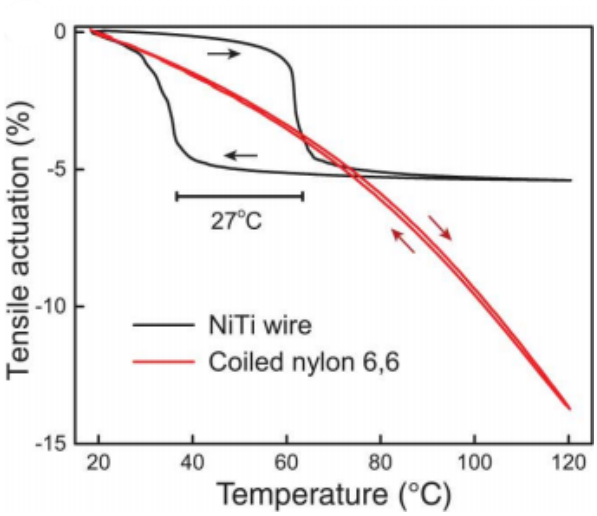

Figure 6: Measured hysteresis of a NiTi SMA wire and a nylon 6-6 monofilament TCP during heating and cooling cycle. Reprinted from [29] with permission from © 2014 AAAS.

and cooling cycle [29]. This hysteresis greatly complicates the actuator control strategy when attempting to control the actuator's position using an input stimulus. Although much less significant than SMAs and other smart materials, TCPs still experience some hysteresis due to the friction between fibres as they untwist during actuation. This hysteresis becomes more apparent for electrothermal actuators, and specifically at higher temperatures and strokes. Work done by Zhang et al. attempted to capture the hysteretic behaviour of TCP actuators using augmented linear and nonlinear models, and showed good agreement between the voltage input, temperature, and contraction length [46].

So far, TCPs have presented many promising mechanical properties and actuator performance that can enable its potential use over other smart materials as soft actuators. This performance, however, does have limitations that are common to many thermomechanical soft actuators. Low energy efficiencies are a limiting factor to TCPs that must be overcome if they are to be utilized as actuators over their traditional counterparts. The maximum energy conversion efficiencies during contraction of twisted and coiled nylon and polyethylene fibres were reported between 1.08% and 1.32%, respectively [29]. These values are comparable to the 1-2% efficiencies seen with SMA actuators, however they are far more inefficient than electromechanical actuators including DEAs and electric motors, with over 90% conversion efficiencies [3]. The actuator inefficiency creates a high demand on the power supply to provide the appropriate thermal stimulus to achieve actuation and this becomes increasingly important when actuating TCPs with larger diameters or multiple filaments. To address this problem, Saharan and Tadesse proposed a

mechanical locking mechanism for TCPs actuating a robotic hand where the position was locked in place and the input power could be removed [47]. While this method does bypass the need for continuous power supply once the actuator is locked in its final position, it may be impractical in applications where continuous, reversible contractions are required. Additional research is required to better improve the energy conversion efficiencies in TCP actuators.

Another limitation of TCPs common to many thermomechanical actuators are the long actuation and relaxation times due to the reliance of heat transfer between the TCP and its surrounding environment. Joule heating and doping the TCP with conductive particles helps speed up the actuation time; however, relaxation times are limited by the heat transfer rate to the surrounding environment. To address this concern, Haines et al. [29] implemented active cooling to improve the cooling rate during relaxation. In one experiment, the authors actuated a nylon 6 TCP actuator hydrothermally by alternating hot and cold water around the TCP to achieve bandwidths up to 1 Hz. In another experiment, a nylon 6-6 monofilament wrapped in a CNT sheet was actuated electrothermally at bandwidths up to 7.5 Hz when employing the high thermal diffusivity of helium gas [3], [29]. These achievable bandwidths are far lower than many other soft actuators, and as a result may restrict use of TCP actuators to low frequency, static, or quasi-static applications. Furthermore, the high temperatures required to reach full actuation stroke in certain polymers may be unsuitable for wearable applications close to the skin. This can be partially overcome by careful selection of the precursor fibre material or using thermally insulating sheaths and coatings.

While the specific work and power densities are exceptionally high in TCP actuators, the coil diameters are typically of millimeter scale that results in low pulling forces for individual actuators. Pulling forces can range from approximately 1 to 4 N for individual and multi-plied actuators, respectively [6], [29], [47]. Recruitment of additional actuators would be necessary for large-scale devices, and the low cost, ease of manufacturing, and scalability of TCP actuators should make upscaling realizable. Research into TCP actuators has not fully matured, and further work is necessary to fully characterize the behaviour and performance of individual actuators before they can be bundled to improve active force generation.

2.3 – Upscaling Actuator Properties

The fundamental characteristics of TCP actuators outlined in the previous section make them promising candidates for use in large scale devices such as robotic systems, space structures, and mobility assistive devices. However, one of the main limitations for use in such devices is the low performance of individual TCP actuators, where trade-offs exist between the output stress and stroke of the actuator. Higher strokes are generally attainable at the expense of reduced force generation; however, in many applications it is desired to have both characteristics maximized. To meet these demands, many approaches have been investigated to improve the force generation, stroke, and stiffness of TCP actuators using well-established textile processing techniques, biomimetic inspirations, and bundling and plying configurations [4], [29], [38], [48]–[50]. These techniques will be elaborated on in the following section.

Textile processing techniques such as knitting, weaving, and braiding are well established and can enable the mass production of textile fabrics from individual fibres or filaments. Since TCP actuators are already of fibre form, they can be upscaled using existing textile processing methods. When comparing different fabric morphologies, knitted fabrics are highly extensible from its loop geometry but generally suffer from lower stress capacity. Conversely woven materials are stiffer and can withstand higher stresses due to the interlocking of fibres in the warp and weft directions, but this constrains the possible fabric deformation. Braided materials generally have properties in between where they are highly extensible at lower loads, and subsequently stiffen as the constituent fibres align in the direction of the force [17]. Since these techniques have been automated for centuries, many researchers have attempted to exploit the morphology of the fabrics to amplify actuator stroke or pulling force.

An actuating textile consisting of TCP actuators was first reported by Haines et al. [29], where a tubular braid with 7 mm diameter was fabricated out of 32 2-ply nylon 6-6 TCP actuators (Figure 7(a)). When the actuator was heated over a 93°C-temperature range, the braid contracted by 16.4% against a 630 g load. The authors also used conventional weaving methods to manufacture a 15 mm by 70 mm rectangular fabric out of nylon actuators in the warp direction,

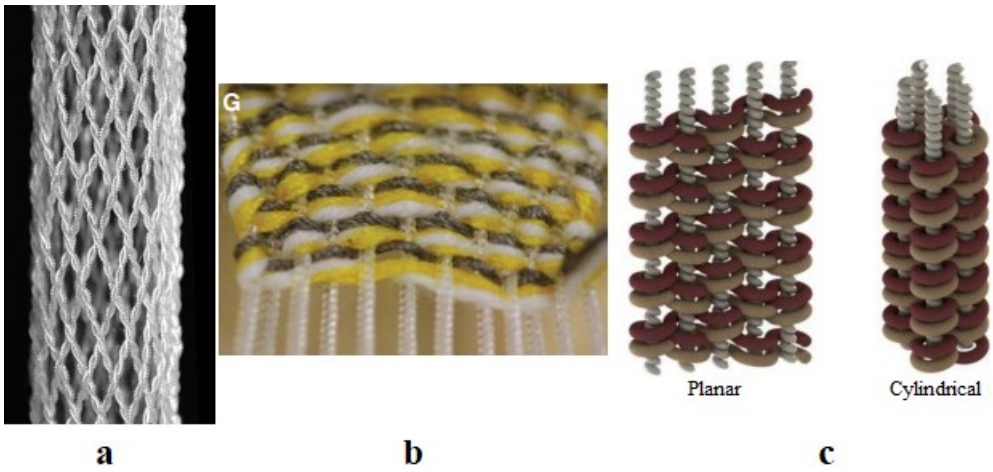

Figure 7: Bundled TCP configurations including a) Cylindrical braid; b) 2D Woven fabric; c) Planar and cylindrical weaves. Figures a), b) reprinted from [29] with permission from © 2014 AAAS. Figure c) reprinted from [51] with permission from © 2018 IEEE.

and a combination of polyester, cotton, and silver coated nylon fibres in the weft direction for structure and electrothermal actuation, as seen in Figure 7(b). Weighing less than a gram, the piece of actuating fabric could reversibly lift a 2 kg load at 12% stroke [29], [31]. Yang et al. built on this work and developed planar and cylindrical woven textiles out of spandex TCP actuators driven electrothermally (Figure 7(c)). In this work, the planar weave provided 34.3% contraction against a 4.91 N load, while the cylindrical weave provided 32.7% contraction against a 10.3 N load [51]. Recent analysis by Kongahage et al. further demonstrated that actuator force generation is almost linearly proportional to the number of active actuators for woven textiles, implying great scalability for larger devices [52]. While research demonstrated the potential of amplifying actuator properties using existing textile processing techniques, more work is required to fully model the behaviour of these fabrics, and how various design parameters and textile architectures may effect the bundled actuator performance.

Other researchers have used biology and nature for inspiration and have produced biomimetic configurations in an attempt to amplify individual actuator performance. In one study, Kianzad et al. investigated the effects of recruiting additional nylon TCP actuators on the force production and variable stiffness of a central tendon [49]. The researchers arranged 16 silver coated nylon actuators to either side of a central tendon at an angle of 20°, to mimic the pennate structure of human skeletal muscle as seen in Figure 8(a). Consistent with the reported literature, the authors noticed a proportional relationship between the force generated and the number of active actuators, ranging from 18 N to 45 N of pulling force on the central tendon when 0 and 16 actuators were

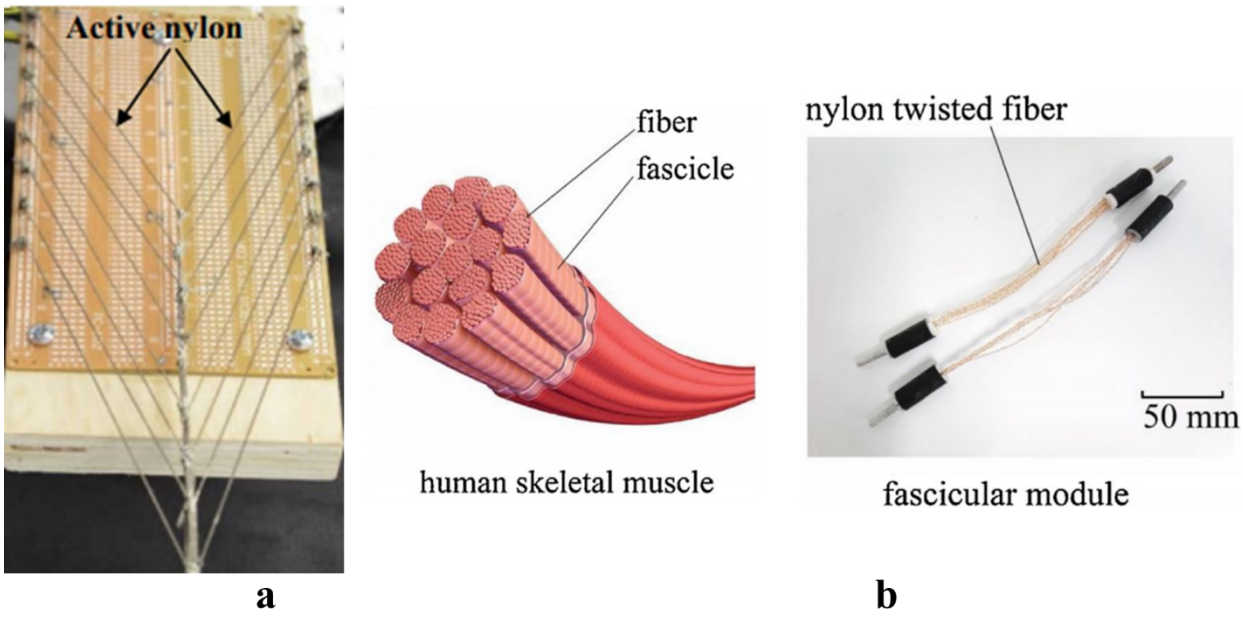

Figure 8: Biomimetic TCP configurations including a) Pennate structure; b) Fascicular module (right) based on human fascicle (left). Figure a) reprinted from [49] with permission from © 2015 SPIE. Figure b) reprinted from [48] with permission from © 2020 Elsevier.

activated, respectively [49]. Consequently, this resulted in the pennate structure varying in stiffness by a factor of 9 over this range.

To create a more compact arrangement, Liu et al. took inspiration from the anatomy of fascicles in human muscles and arranged 4 sets of nylon TCP actuators in parallel to amplify the force generation, as seen in Figure 8(b) [48]. These artificial fascicles were then arranged in series and parallel configurations for further enhanced force generation. The authors reported enhanced stroke capacity when actuating against a 500-gram load, where the stroke increased from 2.60% to 9.36% for a single TCP and an artificial fascicle, respectively. The main limitation to their work was the individual fibre performance, and specifically the lack of characterization and standardization of fabrication procedures. Currently, research is needed to optimize the precursor fibre material properties, to characterize the effects of design choices on actuator performance, and to standardize the fabrication procedures such that consistent and repeatable actuators can be formed. The amplified load capacity of fascicular TCP bundles can only be optimized once the underlying individual actuators are fully defined and optimized.

Some research groups set out to investigate the effects of using multiple filaments, plies, and bundling techniques on actuator performance. Research by Karami et al. [41] attempted to model the behaviour of single and two-ply TCP actuators and determine how increasing the

number of plies effects actuator performance. The researchers found that additional plies introduced increased stiffness to the TCP structure as the individual actuators worked in parallel, and as a result the load capacity can be increased when using multiple plies. Furthermore, the authors noticed that plying two TCPs together increased the length of the constituent fibres, which allows the TCP to untwist further when heated. The result was a greater actuator stroke when using multiple plies [41]. In a separate study, Saharan and Tadesse [36] investigated the effects of twist insertion speed on actuator performance for single, double, and triple plied TCP actuators. While the effects of twist insertion speed on actuator performance requires further investigation, the maximum stroke, force, and output power produced by the actuators were greater for double and triple plied actuators compared to individual TCPs. Lastly, recent work by Kongahage et al. investigated the effects of using multiple filaments prior to twisting when fabricating TCP actuators. Increasing the number of filaments did not increase actuator strain or active force, where additional filaments complicated the internal structure of the twisted fibres [38]. Additional research is required to develop fabrication-performance relationships for monofilament and non-plied TCP actuators before they can be upscaled using bundling or plying techniques.

2.4 – Conclusions

The emergence of TCP actuators as novel smart materials has produced a promising alternative to the limitations of current devices, including the low cost and ease of manufacturing, the inherent lightweight of the actuator, and the ability to generate tensile forces. While these materials present little hysteresis, with strokes and power densities far exceeding the benchmarks of human skeletal muscle, many limitations exist which restrict the integration of these actuators into small- and large-scale devices. Low thermomechanical coupling leads to poor energy conversion efficiency, which increases the demand on the power supply or creates a need for redundant locking mechanisms. Efforts should be focused on finding ways to improve the electrothermal or thermomechanical coupling efficiencies of these actuators. Additionally, more research must be conducted to fully characterize the behaviour of individual TCP actuators, along with the effects of different design and fabrication considerations on the overall performance. There remains a need to standardize the TCP fabrication procedure in order to produce consistent and repeatable actuators. This will allow designers to tailor the optimal performance of the actuator to meet the specific requirements of its intended application, which to date is missing from the

literature. Once individual actuators have been fully characterized and modeled, researchers can look into methods to properly upscale the force and stroke of individual actuators using existing textile processing methods, biomimetic configurations, and plying or bundling techniques. Additional research is necessary in order to model and characterize the effects of textile architecture, including the effects of varying the number of active actuators and their orientations on the overall performance of the textile. Once these concerns have been addressed, it is expected that TCP actuators will offer a convenient and practical solution to the limitations seen in current assistive device technologies.

Chapter 3

Experimental Setup

In this chapter, the experimental setup used to fabricate and test the TCP prototypes will be presented and is divided into three sections. The first section outlines the three experimental testing setups designed to mimic the selected contraction types and measure the actuator stroke, force, and stiffness. Next, an overview of the custom fabrication rig is presented and validated by creating initial prototypes with consistent properties and performance testing. The chapter concludes with the identification of precursor fibre materials and the determination of its key mechanical and thermal properties.

3.1 – Experimental Test Setups

To properly characterize the relationships between the performance of the actuator and the chosen fabrication and operating parameters, three primary experimental setups were assembled. These setups were designed to mimic isotonic, isometric, and eccentric contraction, while measuring the TCP actuator performance. For each testing configuration, an Instron 4202 universal tensile testing machine was used to acquire force and displacement data using a 500 N load cell, which is accurate to within 0.1 N [53]. In addition, a modified Instron environmental chamber was used to supply the thermal stimulus to the TCP samples, while a Watlow T-series thermocouple measured the temperature data at an accuracy of ± 1°C [54].

The concentric or isotonic contraction setup measures the muscle stroke as a function of temperature while operating against a constant external load. These tests are carried out using the experimental configuration shown in Figure 9. In this configuration, the TCP sample is attached to an aluminum rod and suspended vertically inside the environmental chamber. To record the displacement data, a linear variable differential transformer (LVDT) is used with a 0 to 150 mm working range, infinite resolution, and ± 0.5% linearity [55]. The LVDT is mounted in parallel with the aluminum rod, while the end of the core is coupled with the end of the TCP sample. A known mass is hung from the coupled ends, and the actuator stroke is measured as a function of temperature. When no external load is applied and the sample is heated, the displacement being measured is known as the free stroke and is an important metric in soft actuators. In all

a) b)

Figure 9: a) Experimental setup for isotonic contractions; b) Inside view of environmental chamber during actuation

experiments, tensile stroke is defined as the difference between the actuator initial loaded length and the final length, normalized by the initial loaded length.

The isometric contraction setup measures the generated muscle force as a function of temperature while maintaining a constant muscle length. These tests are conducted using the experimental setup shown in Figure 10. In this configuration, both ends of the TCP sample are fixed to aluminum rods extending above and below the environmental chamber, with the top end attached to the load cell and the bottom end secured to the Instron machine base fixture. The Instron machine introduces an initial extension and subsequent preload to the TCP sample. The sample is then heated in the environmental chamber, and the generated actuator force is measured as a function of temperature. When no initial extension is introduced and the sample is heated, the force being measured is known as the blocked force and is another important metric in soft actuators.

The eccentric contraction setup measures the TCP force and displacement at constant temperatures while an external opposing load exceeding the generated actuator force produces an extension of the muscle. These tests also used the setup in Figure 10 under isothermal conditions. The TCP samples are attached to both ends of the aluminum rods and the sample is heated inside

a) b)

Figure 10a) Experimental setup for isometric and eccentric contractions; b) Inside view of environmental chamber with TCP sample ends fixed

the environmental chamber to a constant temperature. Once steady-state temperature has been reached, a tensile test is performed at predetermined strain rates and the force and displacement data are recorded by the Instron load cell and displacement sensor, respectively. This setup is also used to characterize the TCP sample stiffness and its relationship with temperature by converting the force and elongation data to its corresponding stress and strain. For all experiments, measured stress is the load generated by or exerted on the actuator, normalized to the original precursor fibre cross-sectional area. The control of each experimental setup and data acquisition system is performed using the LabVIEW desktop software and MATLAB code was written to process and plot the experimental data.

3.2 – Automated Fabrication Rig

3.2.1 – Overview of Fabrication Setup

As was outlined in Chapter 2, progress in TCP actuator development is currently limited by incomplete characterization of the muscle mechanical and thermal properties and its

relationships with actuator performance, along with a lack of consistency in the fabrication procedure leading to a wide range of reported results with inconsistent performance. As a result, it proves challenging to determine if reported performance metrics are based on the parameters selected in the actuator design, or if variability arises due to the differences in fabrication procedures.

Consequently, before beginning to analyze the effects of design parameters and their relationships on the overall actuator performance, an automated fabrication setup must be built and validated to ensure that consistent TCP samples can be produced while enabling control of design variables. The fabrication rig is constructed to follow the primary steps: twisting, coiling, annealing, and training.

The twisting and coiling processes are performed on a custom fabrication rig shown in Figure 11. To provide the twists to the precursor fibre, a DC motor is mounted to the fabrication platform with a maximum speed of 8,500 rpm and maximum torque of 230mN·m [56]. The motor speed is controlled manually with a rotary potentiometer and a dual H-bridge motor driver. At the opposite end of the fabrication platform, a slider is mounted along two parallel rails that extend the length of the platform. A precursor fibre is connected to two paper clips, with each end hooked onto the ends of the DC motor and the slider as shown in Figure 11. The hook on the slider is fixed,

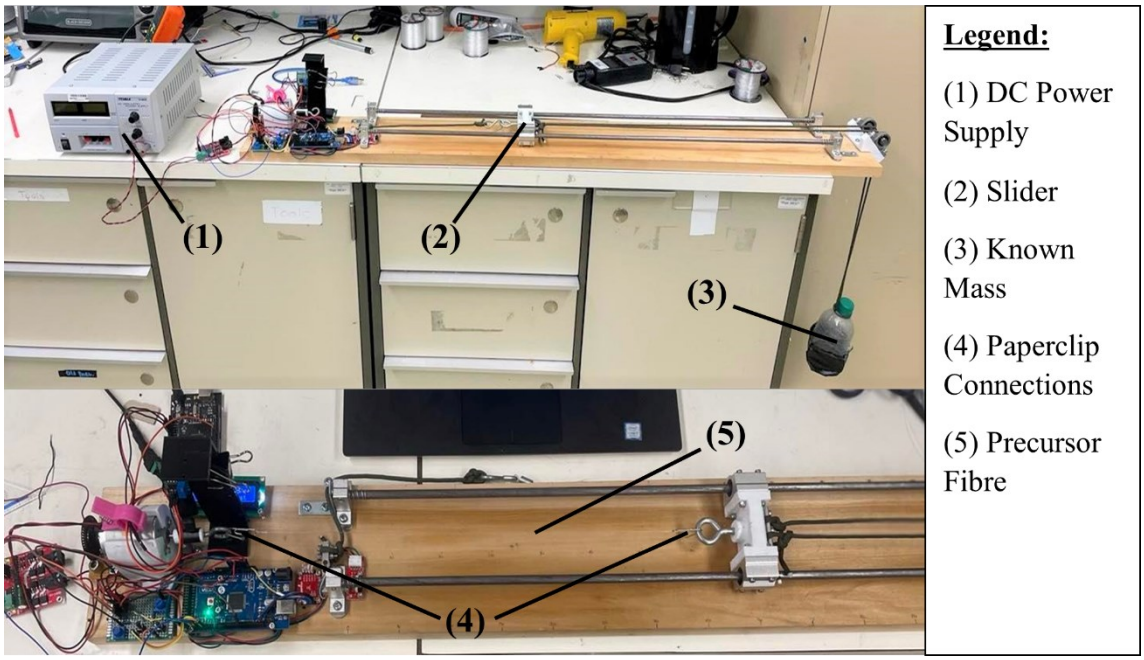

Figure 11: Automated fabrication setup for twisting and coiling (top); Close up view of precursor fibre prior to twist insertion (bottom)

such that all turns from the motor are converted into fibre twists. To ensure the fibre is under tension throughout the twisting and coiling processes, a known mass is attached to the back end of the slider and is suspended vertically off the end of the lab table. As the motor spins and twists are inserted into the fibre, the fibre begins to shorten in length, translating the slider along the rails and raising the mass vertically. The motor can be paused at any time if coiling is performed over a mandrel, otherwise coils spontaneously nucleate at one end of the fibre and continue along its length after a critical amount of twist has been reached.

To measure the number of inserted twists in the fibre along with the twist insertion speed, an infrared (IR) sensor was mounted above the output shaft of the DC motor as shown in Figure 12. The IR sensor reads the frequency of pulses from the output shaft into an Arduino Mega microcontroller, which converts the frequency reading into the corresponding motor speed and number of turns. These measurements are displayed in real time on the Arduino serial monitor. Once the fibre has fully coiled, a limit switch is pressed to stop the motor and the final number of twists are recorded. The TCP sample is then removed from the fabrication rig and placed on an oven rack in preparation for annealing, ensuring that no twists or tension is lost in the sample.

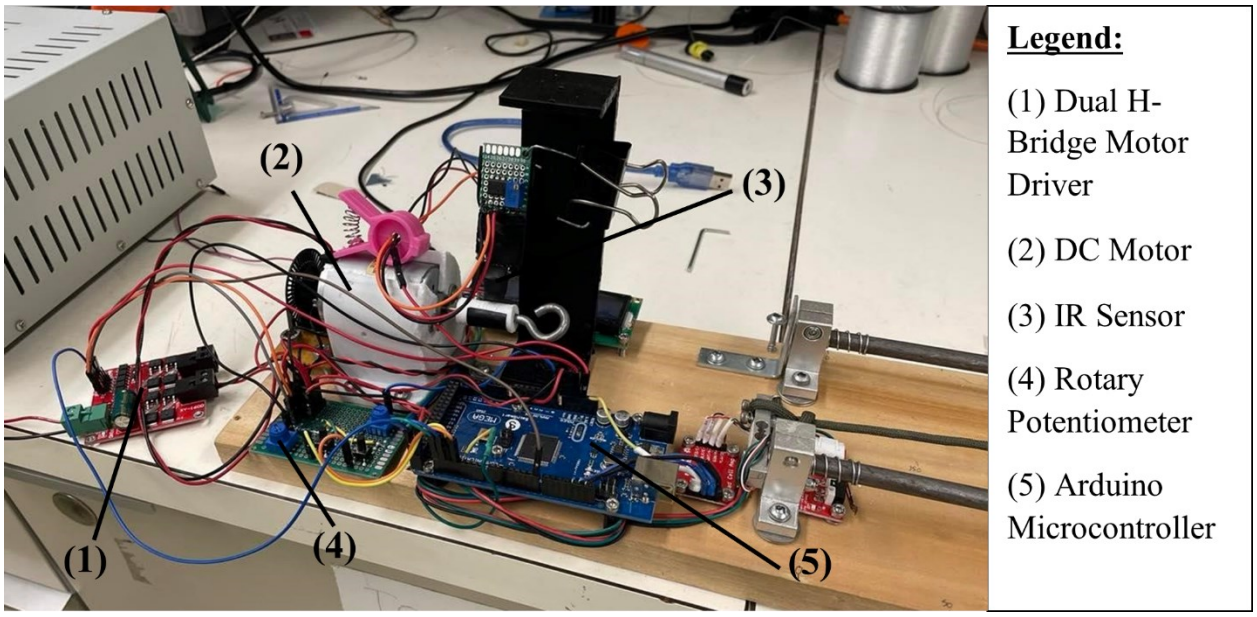

Figure 12: Overview of hardware and electronic components in fabrication rig

As twisting and coiling of polymers are cold-working processes, they leave behind residual stresses that must be removed before the actuators can successfully be operated. Throughout the literature, many methods have been investigated for annealing the TCP samples using various conditions depending on the precursor material and the selected fabrication parameters. In this

work, annealing is performed using the Instron environmental chamber to supply the required heat. Temperatures, length of time, number of cycles, and amount of pre-stretch are relevant variables in the annealing process that require further research and will be investigated in the coming chapters.

Training is a similar process to annealing, with the goal of this process to achieve consistent, reversible, and repeatable actuation strokes for each sample. In this setup, training is also performed using the Instron environmental chamber to supply the heat, while the actuator stroke is measured using an LVDT. The temperatures, number of cycles, and load used during training are additional important factors that require further research and will be investigated in the coming chapters.

3.2.2 – Validating Fabrication Setup

To better illustrate the fabrication rig and to validate the ability to create consistent actuators, 3 samples were fabricated using consistent properties as shown in Table 1. The samples were then tested using the experimental setups outlined in Chapter 3.1, with the goal to observe repeatable performance between the samples made with consistent properties.

Table 1: Measured properties of TCP samples made with consistent parameters

Sample Number	**1**	**2**	**3**
Precursor Fibre Length (mm)	337	343	345
Final Coiled Length, L_0 (mm)	88.74	90.34	93.37
Length Contraction Factor (LCF)	3.80	3.80	3.70
Coil Diameter D (mm)	1.02	1.03	1.02
Spring Index (C = D/d)	2.13	2.15	2.13
Average Motor Speed (rpm)	254	257	257
Number of Twists to Induce Coiling	193	187	200
Number of Twists to Fully Coil	309	323	325
Load Used During Coiling (g)	265.72	265.72	265.72
Final Length After Annealing, L_i (mm)	104.68	105.90	109.29

Individual strands of nylon-6 monofilament were cut to approximately 340 mm in length and attached to paper clips at either end. The precursor fibres were then attached to the ends of the motor and slider of the fabrication rig. Through a process of trial and error, it was determined that a load of 265.72 g was successful in providing enough tension during the twisting and coiling process, while remaining below the stress that would cause the fibre to fail during twisting. A motor speed was selected as 255 rpm, and this speed was manually controlled throughout the first stage of experiments.

Once the fibres had fully coiled, they were placed on an oven rack and annealed in the Instron environmental chamber. Through an iterative process, one annealing method was chosen that set the sample coiled structure, while ensuring enough space was present between the coils for the actuator to contract. First, the samples were annealed for one hour at 160°C. After one hour, the samples were removed from the oven and extended by moving one end of the sample to the adjacent wire on the rack as shown in Figure 13. The samples were placed back in the oven and annealed for another hour at 160°C. These annealing conditions were successful in retaining the coiled structure of the samples, although temperatures and lengths of time used are dependent on the properties selected during the first two stages of fabrication.

Figure 13: Pre-stretch introduced in TCP samples: (left) Before annealing; (right) After one hour of annealing

After the samples finished annealing, they were trained individually in the environmental chamber using the desired loads for its future application. In this case, masses were selected that consisted of six-0.1 lb masses attached to a mass holder for a total mass of 323.06 g. The samples were heated from room temperature to 200°C and back, while the displacement data was recorded by the LVDT. Training was complete once the actuation strokes reached consistent values, which

was found to be approximately 4 to 5 cycles. The load, temperatures and number of cycles used during training are dependent on the chosen fabrication properties, along with the intended final use of the muscles.

Results for TCP Samples Made with Consistent Properties

Once each of the samples achieved consistent and repeatable actuation cycles, they were tested using each of the experimental setups outlined in the previous sections. The first tests evaluated the TCP sample performance during concentric or isotonic contraction. Similar to the training process, a 323.06 g mass was suspended from the bottom end of the TCP samples, imposing an initial extension to the muscles. The samples were then heated from room temperature to 200°C, and the temperature and displacement data were acquired through the LabVIEW software. As seen in Figure 14, each sample achieved between 14-17% stroke when actuating

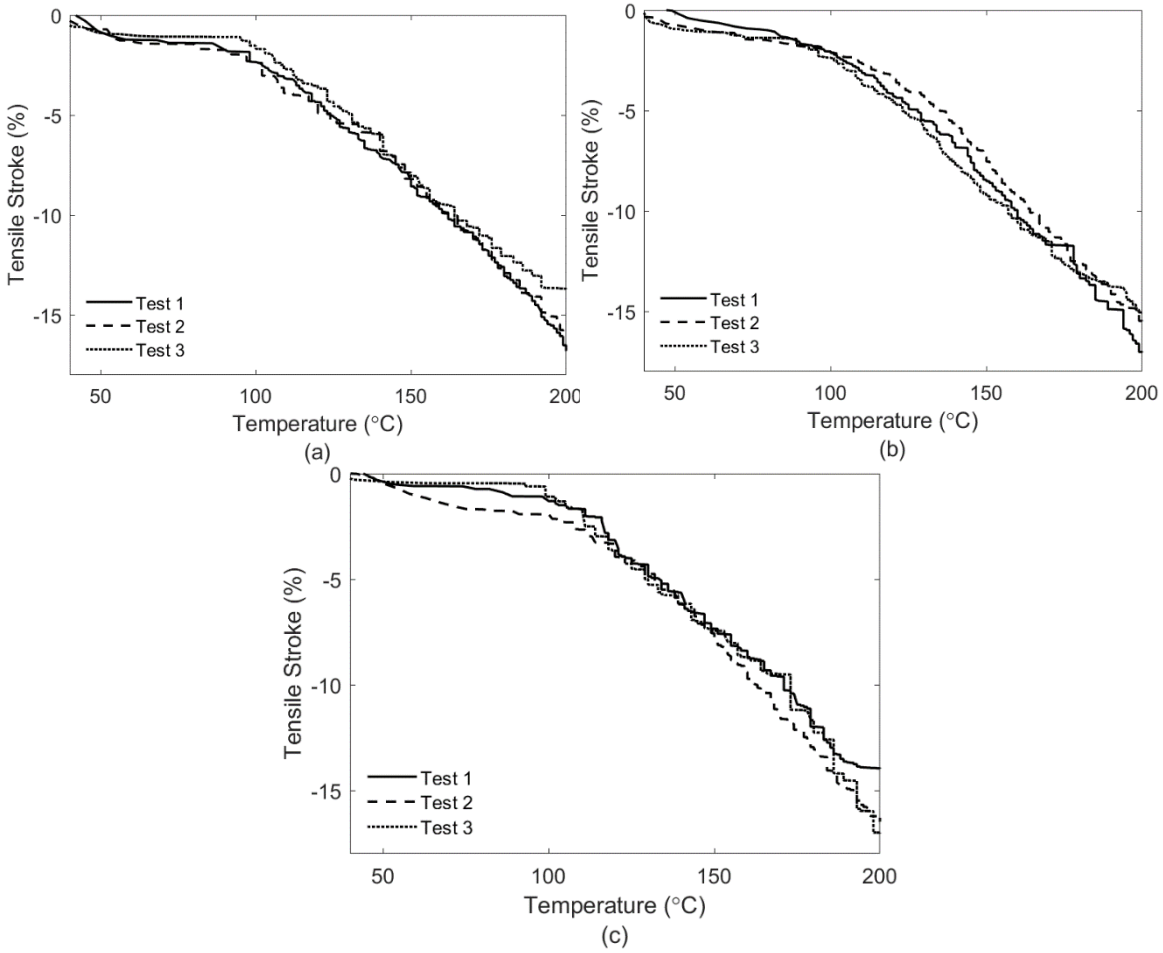

Figure 14: Results for isotonic tests for TCP samples made with consistent properties a) Sample 1; b) Sample 2; c) Sample 3

against a 17.51 MPa external load, and the temperature-stroke curves between samples follow similar paths.

The next set of experiments evaluated the TCP samples during isometric contraction. In this setup, both ends of the TCP samples were attached to the ends of the aluminum rods as shown in Figure 10b). The Instron machine was used to align the sample such that all slack was removed, while ensuring that no preload or initial extension was applied to the sample. The first sets of isometric experiments did not involve an initial preload, so the forces being measured are referred to as the blocked force of the actuators. After the samples were aligned vertically, the environmental chamber was heated from room temperature to 200°C, and the temperature and force data were acquired through the LabVIEW software. As can be seen from Figure 15, each sample was able to generate between 2-2.5 N of force when heated from room temperature to 200°C, and followed similar temperature-force paths between samples.

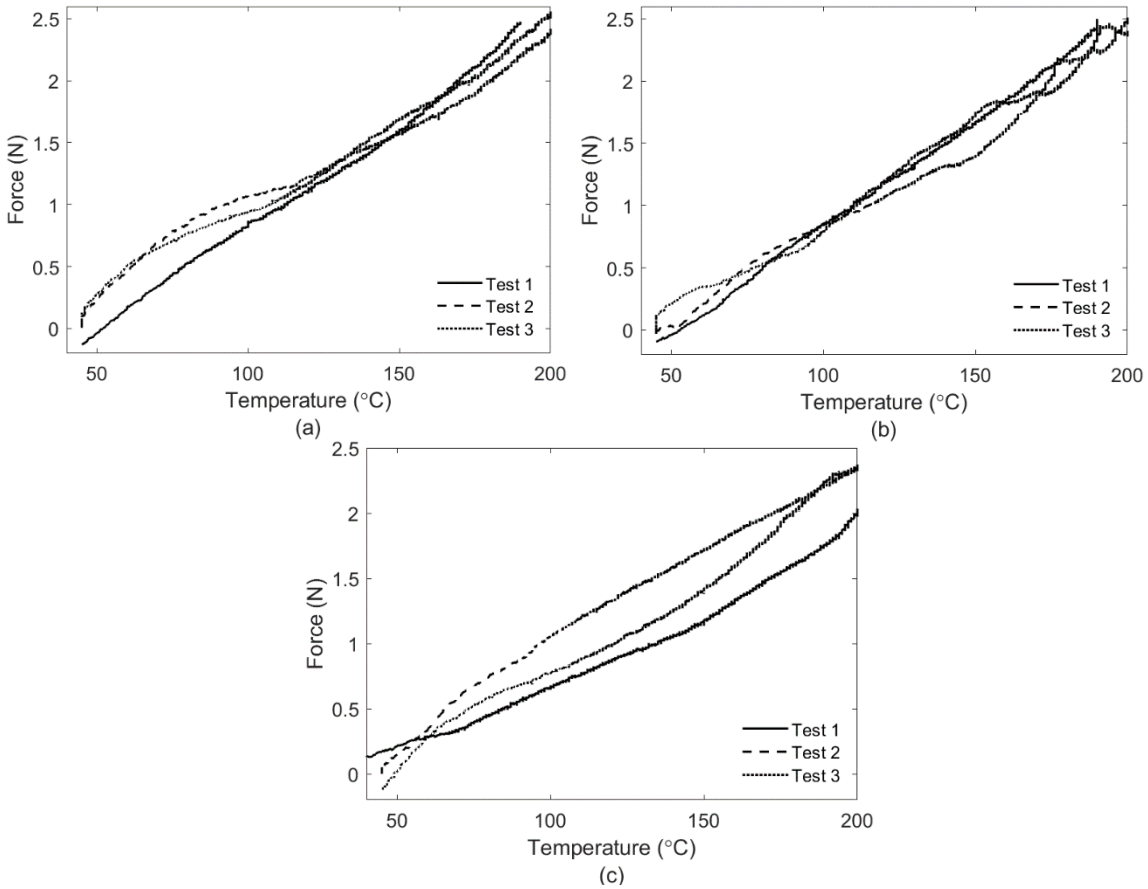

Figure 15: Results for isometric tests for TCP samples made with consistent properties. a) Sample 1; b) Sample 2; c) Sample 3

The final set of experiments evaluated the TCP samples during eccentric contraction. This setup follows a similar procedure to the isometric tests performed, with the distinction that the

Instron machine provided an external force that exceeded the generated TCP force. Each TCP sample was connected to the ends of the aluminum rods and aligned vertically to remove all slack or tension. The environmental chamber was then heated to different steady-state temperatures, while the muscle produced an initial tensile force on the load cell. Once steady-state temperatures had been reached, the load cell reading was noted, and a tensile test was performed on the samples. Starting at room temperature and testing at 10-degree increments until 200°C, the samples were loaded at a strain rate of 10 mm per minute to 40% strain, then unloaded and returned back to their original length. Force and displacement data were recorded by the load cell and displacement sensor of the Instron machine, respectively, and acquired by the LabVIEW software. As can be seen in Figure 16b), samples made with consistent properties had very similar loading and unloading curves when tested during eccentric contraction.

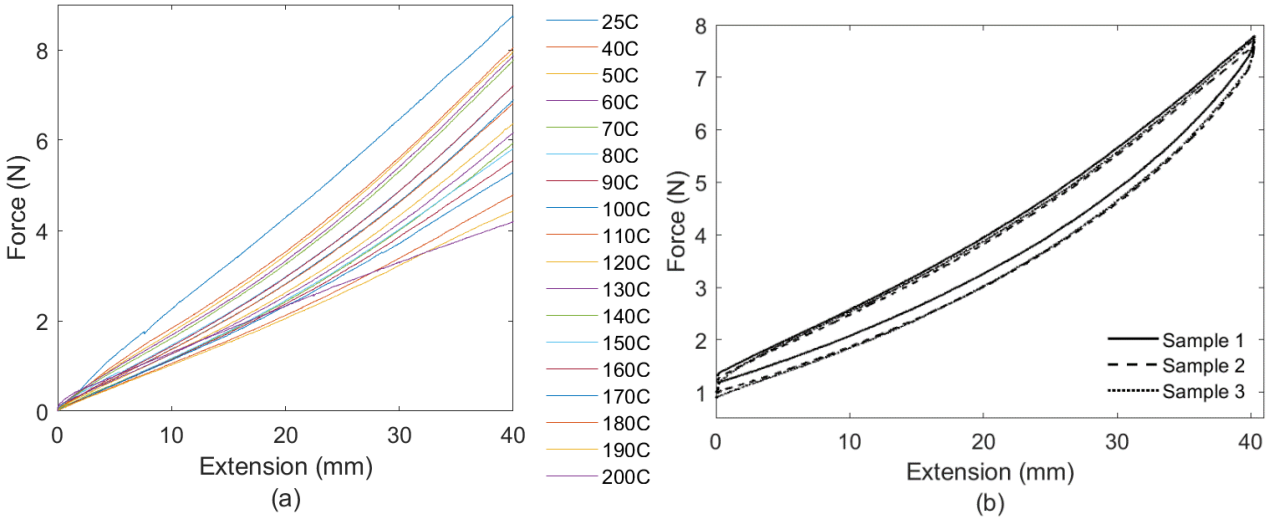

Figure 16: a) Results from eccentric tests from Sample 1 at various constant temperatures; b) Results from eccentric tests at 120°C for TCP samples made with consistent properties

From the results above, it is clear that the fabrication rig is capable of producing actuators with consistent performance when care is taken to control the properties used during manufacturing. This is an important step in the experimental procedure to ensure that results obtained in future stages of experiments can be attributed to the actual effect being investigated, and not to sources of error arising from the manufacturing process.

3.3 – Muscle Materials

Before investigating the effects of the design parameters on the actuator performance and characterizing the mechanical and thermal behaviours, the mechanical and thermal properties of the underlying precursor fibre material must be better understood.

The material investigated in this thesis is Trilene Big Game fishing line, a nylon-6 monofilament from Berkley Fishing [57]. Nylon-6 was selected for its low cost, commercial availability, high strength, and large anisotropy in thermal expansion. Four monofilaments were selected based on their advertised break strengths and average diameters that include 10 lb, 15 lb, 25lb, and 50 lb tests, for corresponding diameters of 0.21 mm, 0.38 mm, 0.48 mm, and 0.71 mm, respectively.

3.3.1 – Mechanical Properties of Precursor Fibres

To properly characterize the mechanical properties of the precursor fibre, a series of uniaxial tensile tests were performed. First, three samples of the 25 lb test break strength precursor fibre were cut to approximately 12 cm in length and were clamped to the Instron end fixture grips. While keeping the fibres at room temperature, the sample was stretched at rates of 2, 8, and 16 mm/min up until the point of failure, while load and displacement data were recorded. As seen in Figure 17, the slope of the loading curves increases with increasing strain rate. All samples failed between 16% and 20% strain at corresponding ultimate tensile strengths ranging from 270 MPa to 337 MPa.

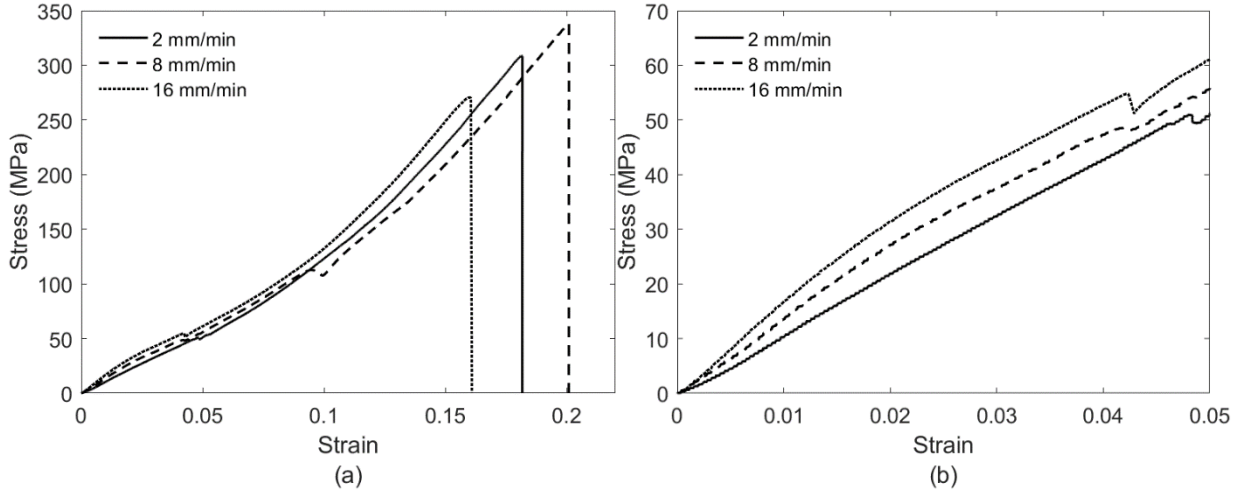

Figure 17: a) Stress vs strain diagram of nylon-6 precursor fibre; b) Results from a) with focus on first 5% strain

Also from Figure 17, each sample demonstrated an elastic region within the first 5% strain, corresponding to yield strengths in the range of 53 MPa to 65 MPa, which is within the expected ranges reported in the literature [58]. The modulus of elasticity, E, for the precursor fibre is calculated from the slope of the stress-strain curve in the elastic region of Figure 17b). From these curves, the measured elastic moduli ranges from 1.07 GPa to 1.22 GPa when loaded at 2 mm per minute to 16 mm per minute, respectively. These values are also within the expected ranges reported in the literature [58]. As is common with most semicrystalline polymers, the modulus of elasticity depends not only on the strain rate, but is also expected to degrade with increasing temperature beyond the glass transition temperature.

Similar to natural skeletal muscles, TCP actuators must be investigated for their time-dependent mechanical properties to capture the viscoelastic effects of the material. This behaviour arises when a material's mechanical response to an applied load or extension depends not only on the input but also on the history of previous loading and thermal stimuli [59]. Consequently, three time-dependent phenomena are important to consider when testing TCP actuators: creep, stress relaxation, and hysteresis. When testing the actuators under isotonic conditions, a material exhibits creep if the muscle length changes over time at constant applied stress, possibly leading to permanent changes in the muscle resting length. Additionally, when testing actuators under isometric conditions, a material exhibits stress relaxation if the stored stress is reduced over time at constant muscle length. This can lead to degradation in strength of the TCP actuator and can limit its force production. When testing under eccentric conditions, a material exhibits hysteresis if the loading and unloading curves from a cyclic test follow separate paths, indicating the stress at a given instant depends on the loading history [59]. Hysteresis can complicate the soft actuator control if the desired muscle length can be obtained at two independent temperatures.

To investigate these phenomena, three samples of the 25 lb test break strength precursor fibre were cut to 120 mm in length and tested under the three experimental setups. First, one sample was placed in the environmental chamber under the isotonic experimental setup and was heated to 150°C. The sample was then loaded with a static mass of 1.7 kg, inducing an initial strain on the sample of approximately 9%. The sample was held at 150°C under a constant load, and the change in sample length was measured over time. Figure 18 shows creep within the first 45 minutes, where the strain increased from approximately 9% to 10.2%. The secondary creep region exhibited a

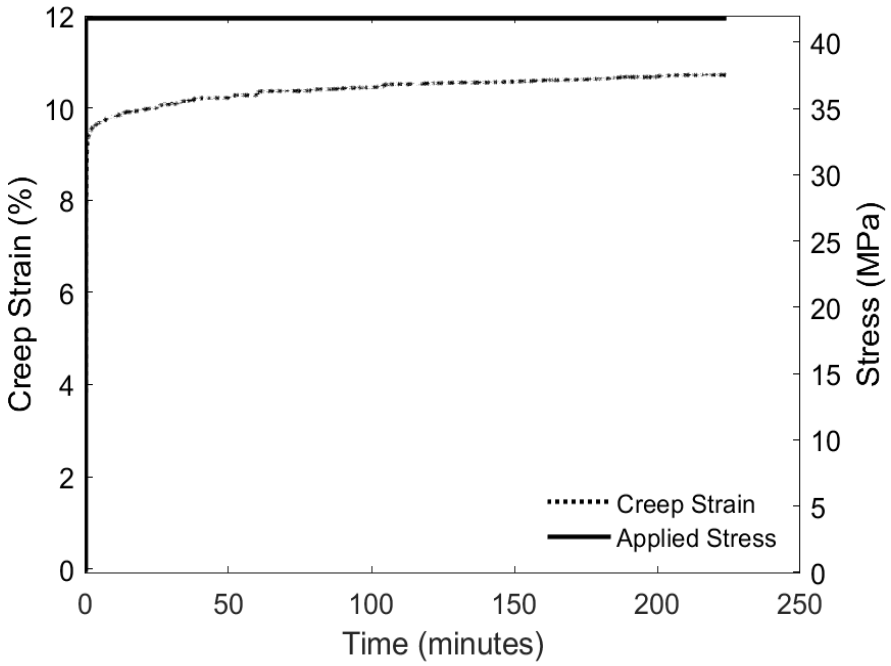

Figure 18: Tensile creep test of 120 mm nylon-6 sample at 150°C under 42 MPa static load

minor increase in creep strain; however, changes in sample length were minimal beyond 4 hours of testing. Under static and quasi-static applications, TCP actuators should be designed to account for changes in sample length that occur at elevated temperatures when the sample is loaded for extended periods of time.

Next, a precursor fibre sample was placed in the environmental chamber following the isometric experimental setup, and was subsequently heated to 150°C. At 150°C, the sample was rapidly stretched to 13.81% strain, inducing a tensile stress of approximately 126 MPa on the sample. The sample was held at constant length, and the change in stored stress within the material was measured over time. Figure 19 shows a steep reduction in the stress within the first 5 minutes, followed by a gradual reduction in stress for the remainder of the test period. Results show that the generated stress in the sample remained relatively constant beyond 3 hours, settling at just above 33 MPa. This relaxation in stored stress is another important factor to consider in TCP actuator design when used in static or quasi-static applications at elevated temperatures.

Lastly, to capture the hysteretic effects of the material, three 120 mm samples of 25 lb test break strength precursor fibre were secured to the Instron machine following the eccentric experimental setup. At room temperature, the samples were loaded to just over 4% strain at various strain rates and subsequently unloaded back to their initial lengths. Figure 20 shows the loading

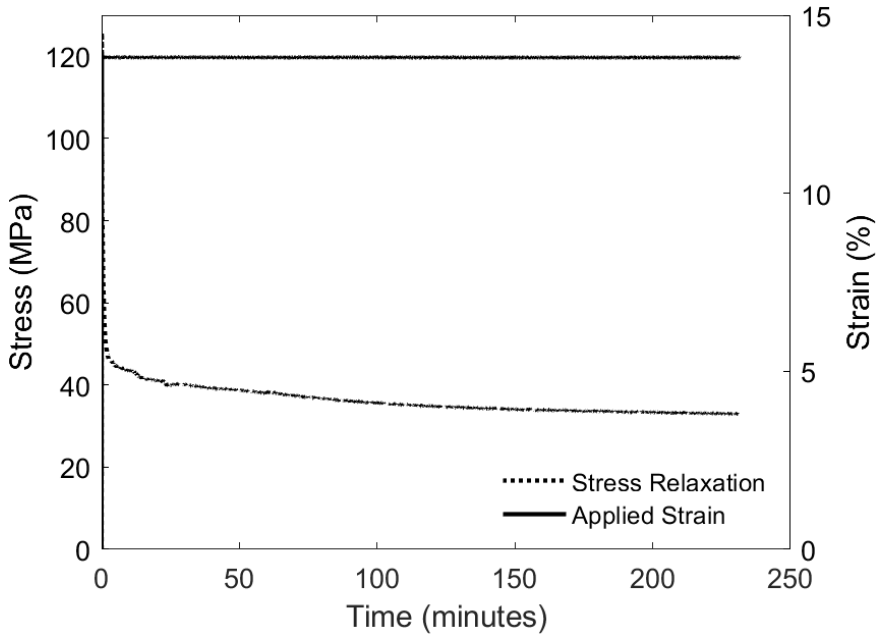

Figure 19: Stress relaxation test of nylon-6 fibre at 150°C at constant strain of 13.81%

and unloading curves for the samples tested at strain rates of 2, 8, and 16 mm per minute. Hysteresis was present in each of the samples when loaded at room temperature; however, the magnitude of the hysteresis does not appear to be influenced by the strain rate. The slope of the loading and unloading curves increases with increasing strain rate, which is consistent with the results observed from Figure 17. The hysteretic behaviour of these materials must also be accounted for in the design and control of TCP actuators, and many attempts have already been made to model these effects [46].

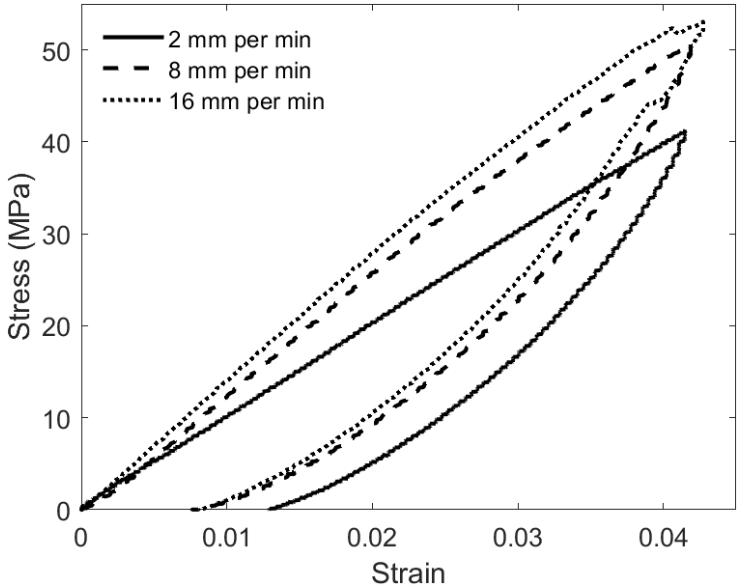

Figure 20: Load-Unload tests of nylon-6 fibres at various strain rates

3.3.2 – Thermal Properties of Precursor Fibres

With the TCP actuator mechanisms depending on heat transfer, it is also paramount to understand the thermal properties of the underlying precursor fibre material. The relevant thermal properties include material operating temperature ranges, linear coefficients of thermal expansion and corresponding anisotropy in thermal expansion, material specific heat capacity, and thermal conductivity. The operating temperature range is primarily dependent on the polymer glass transition temperature, T_g, while temperatures should not exceed the polymer melting temperature, T_m.

Absent proper traditional thermomechanical testing methods for deriving these properties such as differential scanning calorimetry (DSC), thermomechanical analysis (TMA) and dynamic mechanical analysis (DMA), the glass transition temperature of the precursor fibre material can be approximated graphically before comparing with expected values from the literature. For semicrystalline polymers, the modulus of elasticity is highest at temperatures below the glass transition temperature and decreases rapidly throughout the glass transition temperature range until the melting temperature is reached. By performing a series of tensile tests at various constant temperatures, a plot of the modulus of elasticity as a function of temperature can be developed that can be used to approximate the glass transition temperature.

To achieve this, a sample of 25 lb break strength nylon-6 monofilament was cut to 250 mm in length and secured to two paperclips. Both ends of the paper clips were attached to either ends of the aluminum rods following the eccentric experimental setup. Starting at room temperature, the precursor fibre is stretched to 5% strain at 2 mm per minute under isothermal conditions while the stress and strain data were recorded. At 5 degree increments, the experiment was repeated and the precursor fibre modulus of elasticity was calculated from the slope of the elastic region of the stress-strain diagram for temperatures ranging from 20°C to 80°C. Figure 21 plots the precursor fibre modulus of elasticity as a function of temperature. The modulus of elasticity decreased rapidly between 30°C and 50°C as the material transitioned from a stiffer glassy state to a softer rubbery state throughout this region. These results indicate that the precursor fibre glass transition temperature falls within the range of 30°C to 50°C, which is consistent with values reported in the literature [58]. Furthermore, Haines et al., reported that the glass transition temperature of the fully

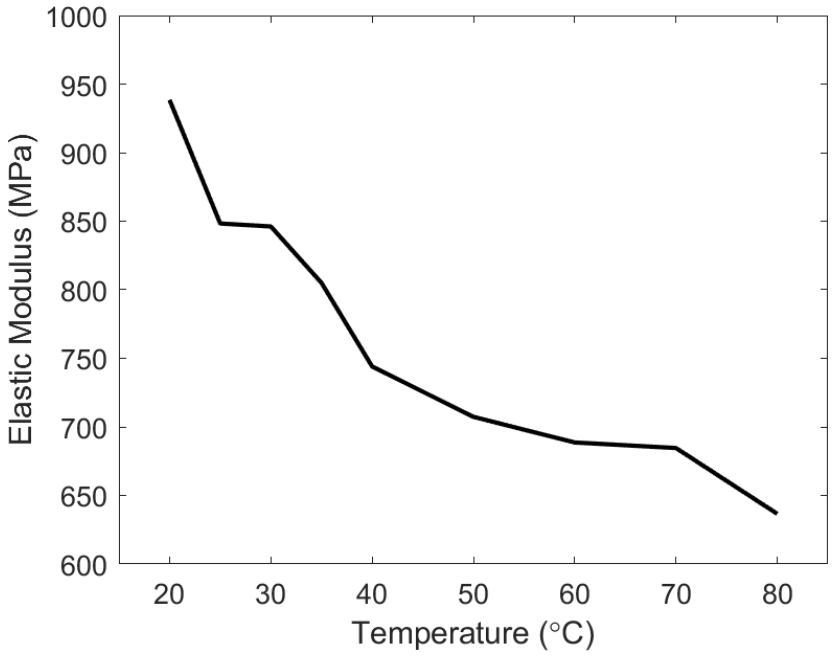

Figure 21: Elastic modulus of nylon-6 precursor fibre measured as a function of temperature

coiled TCP is slightly higher than the measured glass transition temperature of the precursor fibre, meaning a larger thermal stimulus is required to enhance the mobility of the polymer chains [29], [31].

While the glass transition temperature relates to the region of greatest mechanical response from the actuators, TCPs should not be operated near or above the polymer melting temperature because the strength of the precursor fibre material deteriorates with increasing temperature. For the nylon-6 material investigated in this work, melting temperatures are reported in the range of 210°C to 225°C [58]. To ensure the samples do not fail prematurely, operating temperatures should not exceed 200°C throughout the actuator's use. The operating range is from room temperature to 200°C, with the largest actuator response expected to fall within the glass transition temperature region of the fully coiled TCP, in this case slightly above 50°C.

Since the driving mechanism behind tensile actuation arises from the precursor fibre material anisotropy in thermal expansion, the linear coefficients of thermal expansion (CTE) in the longitudinal and transverse directions should be determined. For extruded nylon-6, the longitudinal CTE is reported in the range of 19.8-110 μm/m°C, while the transverse CTE is reported in the range of 70.0-140 μm/m°C [58]. The degree of anisotropy in thermal expansion

can be found by taking the ratio of transverse CTE to longitudinal CTE. In this case, the degree of anisotropy in thermal expansion is expected be within 1.27 and 3.54 for extruded nylon-6.

The precursor fibre material's capacity to store and transfer thermal energy are directly related to the actuator response. These properties are known as the material's specific heat capacity and the thermal conductivity. Specific heat capacity refers to the amount of thermal energy required to increase the temperature of the material by a degree, while thermal conductivity refers to the material's ability to conduct thermal energy throughout its volume. For extruded nylon-6, the specific heat capacity is reported in the range of 1.55-2.55 J/g°C, while the thermal conductivity is reported in the range of 0.230-0.320 W/mK [58]. These metrics help illustrate the slow response times of TCP actuators, and consequently why these actuators are being investigated solely under static or quasi-static applications.

Chapter 4
Experimental Evaluation, Analysis, and Discussion

With the mechanical and thermal properties of the precursor fibre material better understood, it is important to evaluate the effects of various design considerations on the final actuator performance. This step involves isolating and varying a design parameter during either fabrication or operation, and experimentally evaluating the effects of each parameter according to the experimental setups outlined in Chapter 3. Several performance metrics were investigated including the actuating stroke measured as a function of temperature during isotonic contractions, the actuating force measured as a function of temperature during isometric contractions, and the change in tensile modulus captured during eccentric contractions at constant ambient temperature. Throughout this chapter, the fabrication procedure will be presented for each parameter investigated, followed by the isotonic, isometric, and eccentric contraction test results. The results are discussed in the context of optimizing the TCP actuator performance, while reducing the negative effects of trade-offs from additional design parameters.

4.1 – Effects of Operating Conditions

4.1.1 – Fabrication and Initial Properties

The first parameters investigated were the operating conditions during each of the three experimental test setups. This involved altering the external actuating load during isotonic tests, adjusting the preload through initial extensions during isometric tests, and varying the strain rate during eccentric tests. For these conditions, two 300 mm samples of nylon-6 precursor fibre were fabricated, annealed, and trained with consistent properties following the manufacturing setup outlined in Chapter 3. Table 2 shows the measured properties of the samples.

Table 2: Measured properties of TCP samples for varying operating conditions

Sample Number	1	2
Precursor Fibre Length (mm)	297	300
Final Coiled Length, L_0 (mm)	87.14	88.38
Length Contraction Factor (LCF)	3.41	3.39
Coil Diameter D (mm)	0.98	0.98
Spring Index (C = D/d)	2.04	2.04
Average Motor Speed (rpm)	244	250
Number of Twists to Induce Coiling	170	172
Number of Twists to Fully Coil	277	287
Load Used During Coiling (g)	261.92	261.92
Final Length After Annealing, L_i (mm)	89.11	89.62

4.1.2 – Isotonic Test Results

To adjust the operating conditions during isotonic testing, different external loads were applied at the end of the TCP samples while the actuation stroke was measured as a function of temperature. Masses of 0.2 lb, 0.5 lb, 0.7 lb, 1.0 lb, and 1.5 lb were suspended from the lower ends of the TCP samples following the isotonic experimental setup. The samples were then heated from 45°C to 200°C, while actuator contraction was measured by the LVDT. Figure 22 shows the results of the isotonic tests under various external loads.

From these graphs, the actuation stroke increases from a minimum of 10.11% when actuating against the 0.2 lb external load, to a maximum of 15.91% actuating against the 0.7 lb external load while heating from 45°C to 200°C. As additional mass is added, the actuation stroke decreases from approximately 10.50% at 1.0 lb to a minimum of 6.21% at 1.5 lb. This indicates that the actuation stroke of TCPs depends on the external loading conditions, where an optimal stroke was observed when actuating against the 0.7 lb load for these specific TCP samples.

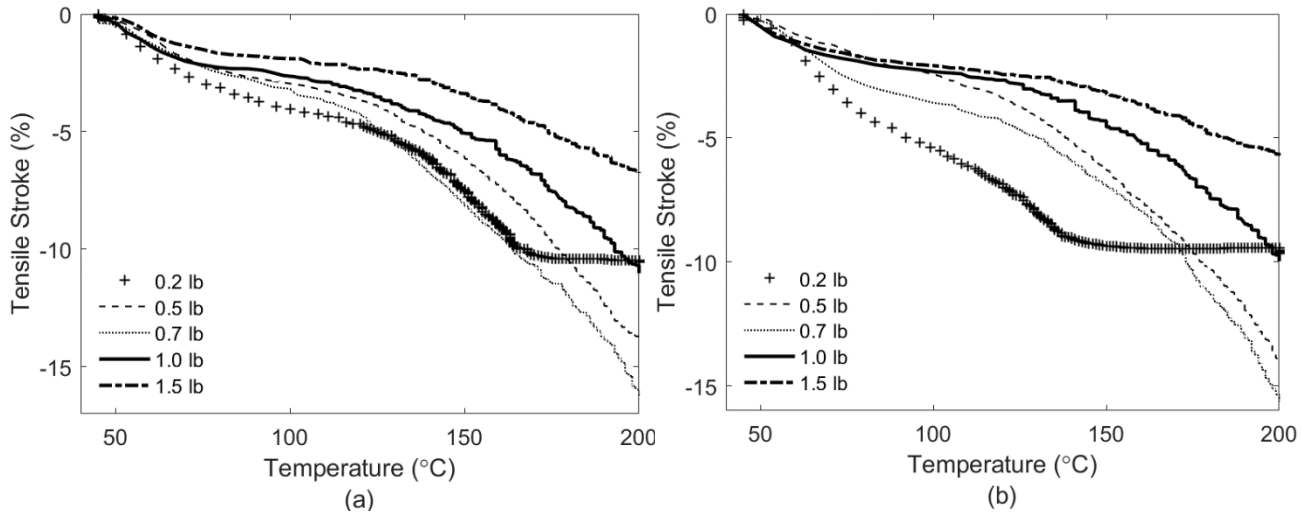

Figure 22: Results of isotonic tests when varying operating loads for a) Sample 1; b) Sample 2

Selecting the proper actuating load is an important factor for designers that must be taken into account. If too much weight is used, the external load exceeds the generated load capacity of the TCP samples, and actuation stroke is limited to the equilibrium position between the external tensile force and the internal contraction force of the muscle. Conversely if too little weight is used during actuation, the external load will not introduce enough space in between coils for the sample to contract and the actuator contraction will saturate before the final temperature has been reached. This is evident in the samples tested at 0.2 lb from Figure 22a), where the stroke increases up until approximately 170°C then remains constant for the remainder of the test. These results illustrate the importance of selecting the proper load during actuation, where optimal stroke can be achieved depending on the initial loading conditions.

4.1.3 – Isometric Test Results

Adjusting the operating conditions during isometric testing involved introducing different amounts of initial extension into the TCP sample, and consequently different magnitudes of external preloading, followed by measuring the generated actuation force as a function of temperature. Following the isometric experimental test setup, the Instron machine was used to introduce initial extensions into the samples until preloads of 0.5 N, 0.75 N, 1.0 N, 1.25 N, and 1.5 N were reached. The samples were also tested with no initial extension or preload, and the force being measured is referred to as the blocked force. Once the initial extensions were introduced, the samples were then heated from 45°C to 200°C, while the generated actuator force was measured

by the Instron load cell. Figure 23 shows the results of the isometric tests under various initial extensions.

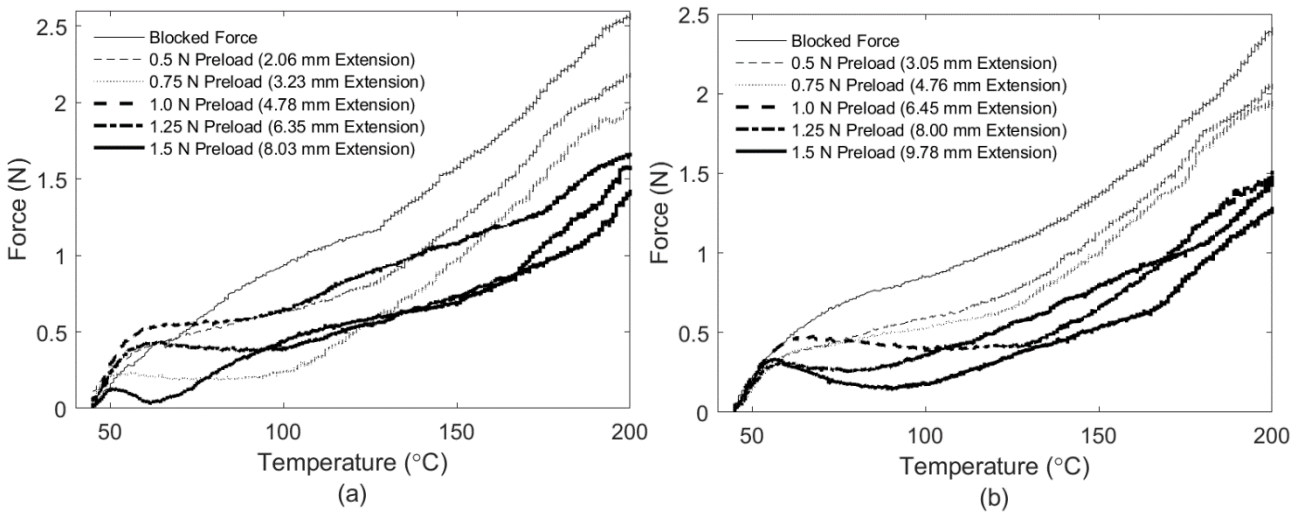

Figure 23: Results of isometric tests when varying initial extensions for a) Sample 1; b) Sample 2

The generated actuation force decreased with increasing initial extension or preload. When the samples were extended to the maximum elongation required to obtain 1.5 N of preload, the maximum actuator force for both samples ranged between 1.25 N and 1.40 N. In contrast, the samples with the lowest amount of extension and a preload of 0.5 N to the sample achieved maximum actuation forces between 2.06 N to 2.19 N. The maximum forces generated in either sample were recorded when no initial extension or preload was introduced, where the samples generated blocked forces in the range of 2.4 N to 2.6 N.

Consistent with the results from the isotonic testing, there is a trade-off in performance between the generated actuator force, and the amount of initial extension introduced to the sample. While introducing additional space between neighbouring coils is critical to achieving higher tensile strokes, it comes at the expense of reduced force generation. Depending on the force and stroke requirements of the actuators during operation, designers must take into account this trade-off in performance to meet the specific needs of the design.

4.1.4 – Eccentric Test Results

When testing under the eccentric experimental setup, strain rates were varied to capture the hysteretic effects in the loading and unloading cycles, along with the effects on the actuator variable stiffness properties. To start, Sample 1 from Table 2 was secured to the ends of the

aluminum rods and aligned inside the Instron environmental chamber. At four constant temperatures starting at 25℃, 50℃, 80℃, and up to 110℃, loading and unloading cycles were performed with the Instron machine at strain rates of 2 mm per minute, 5 mm per minute, and 10 mm per minute from 0% to 5% strain. Force and elongation data were recorded by the Instron sensors and were converted to its corresponding stress and strain. Figures 25-26 present the stress-strain diagrams for the sample tested at various strain rates.

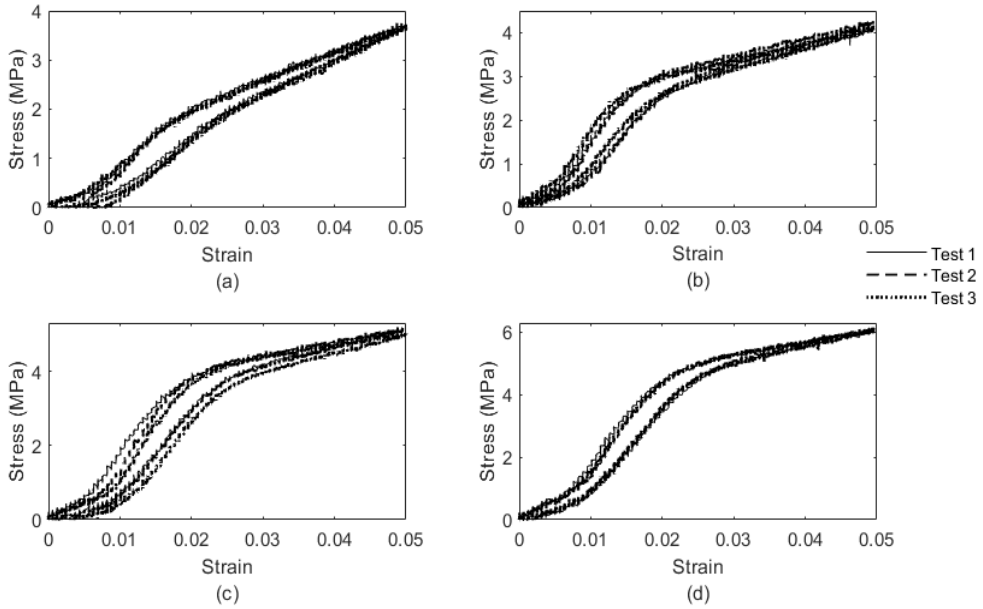

Figure 25: Results of eccentric tests of Sample 1 loaded and unloaded at 2 mm per minute at temperatures of a) 25℃; b) 50℃; c) 80℃; and d) 110℃

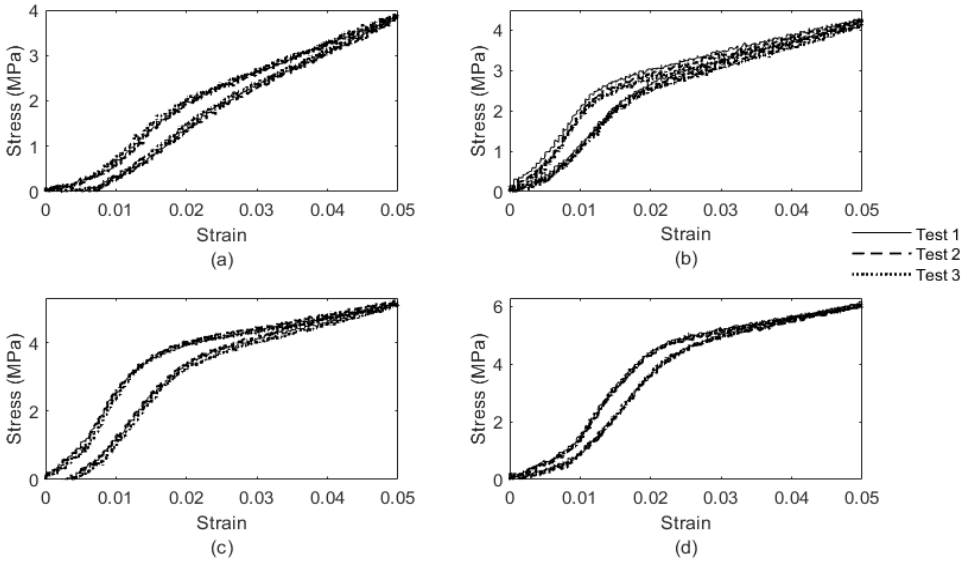

Figure 24: Results of eccentric tests of Sample 1 loaded and unloaded at 5 mm per minute at temperatures of a) 25℃; b) 50℃; c) 80℃; and d) 110℃

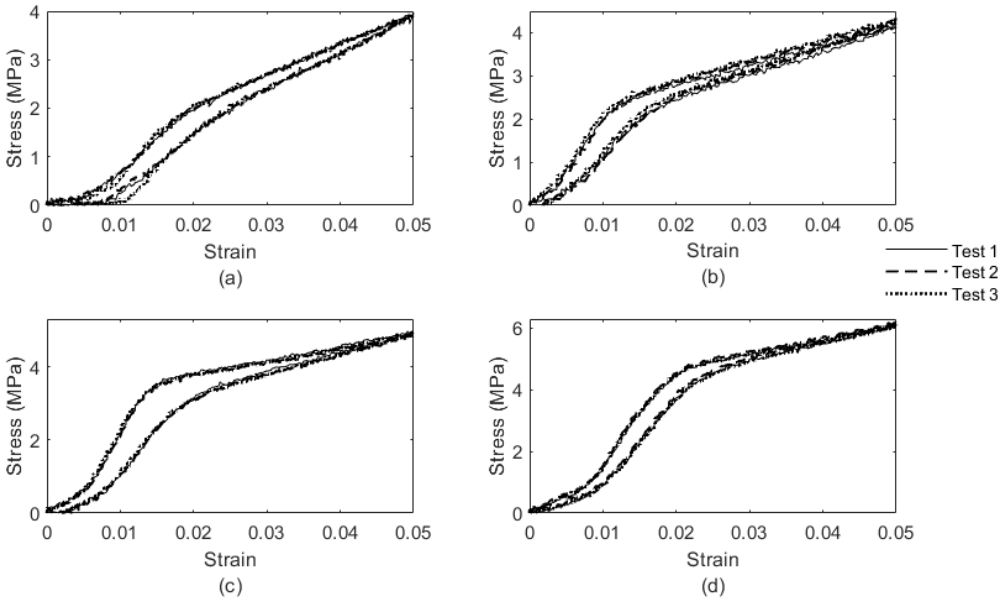

Figure 26: Results of eccentric tests of Sample 1 loaded and unloaded at 10 mm per minute at temperatures of a) 25°C; b) 50°C; c) 80°C; and d) 110°C

From these results, the magnitude of the hysteresis appears to decrease with increasing temperature in all cases when tested within the ranges of 25°C to 110°C. When comparing the results of Figures 25-26, the magnitude of the hysteresis does not appear to be influenced by the strain rates used during experiments, and no clear trend was observed between the different test conditions. These results are consistent with those obtained for the precursor fibre testing presented in Chapter 3.3.1. Hysteresis in the loading and unloading cycles can be quantified as the maximum offset in stress values for a given strain, divided by the full span of stress values. For all strain rates, the magnitude of the hysteresis peaked at a temperature of 80°C where hysteresis was in the range of 27.72% to 30.33%. Measured hysteresis values were minimal at a temperature of 110°C for all test conditions, with values calculated in the range of 12.12% to 15.59%.

Next, the tensile moduli for all samples were calculated and compared between the different strain rates. Looking at the curves of Figures 25-26, the typical loading curve of a TCP during eccentric testing exhibits an initial low stiffness region at the start as the sample is aligned with the direction of the force. The curve then exhibits a steep, almost linear region, as the external load attempts to separate the neighbouring coils apart. Once all the coils have been separated, continued loading of the sample produces a third, near linear region of lower stiffness. This region of the curve is where the stiffness of the sample transitions to being governed by the elastic modulus of the underlying precursor fibre material, which is known to decrease with increasing

temperature. This is evident in all samples where the final region of the loading curve exhibits a decreasing slope once all neighbouring coils have been separated. To measure the modulus of the samples, lines were inserted manually using MATLAB to follow the slope of the linear portion of the second region of the curve as shown in Figure 27. The modulus was calculated for each test at every temperature, and the average of the moduli were calculated and presented in Table 3.

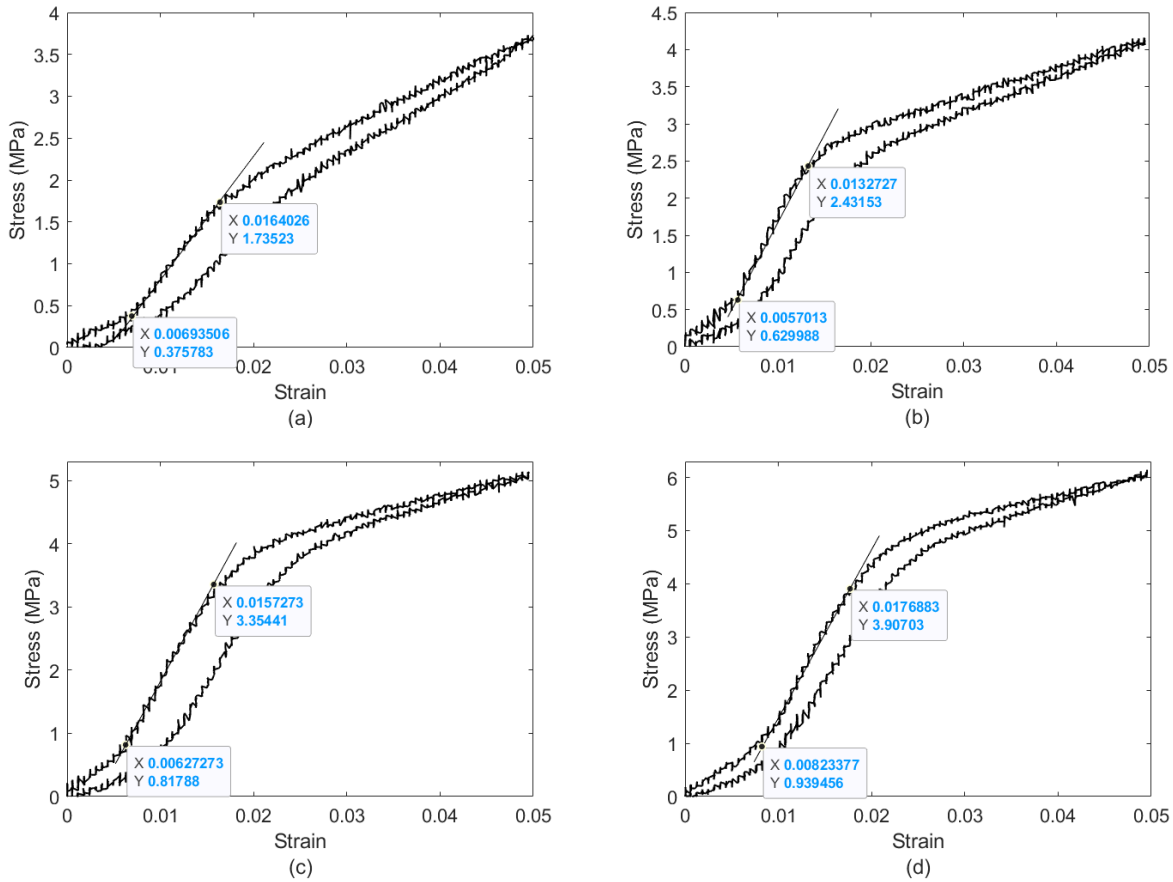

Figure 27: Example of tensile modulus at a) 25°C; b) 50°C; c) 80°C; and d) 110°C

Table 3: Average elastic modulus values for samples tested at different strain rates

Test Condition	Average Modulus at 25°C (MPa)	Average Modulus at 50°C (MPa)	Average Modulus at 80°C (MPa)	Average Modulus at 110°C (MPa)	Range in Stiffness (Max./Min.)
2 mm/minute	142.32	235.58	286.77	303.46	2.13

5 mm/minute	146.00	240.20	304.71	321.45	2.20
10 mm/minute	147.04	241.03	330.03	340.24	2.31

The results show that the actuator stiffness increased in all cases when heating from 25°C to 110°C. Furthermore, consistent with the results obtained when testing the precursor fibre in Chapter 3.3.1, the actuator stiffness increased with increasing strain rate. This is evident as the variation in stiffness achieved is largest at a factor of 2.31 when testing 10 mm per minute, and lowest at a factor of 2.13 when testing 2 mm per minute.

Although testing at higher strain rates yields greater variation in stiffness, the load cell and displacement sensor are recording less data for the same given strain interval and as a result leave behind jagged, discontinuous curves. While this effect cannot be completely eliminated, it can be mitigated by using a lower strain rate. For these reasons, as higher strain rates may produce unreliable data, and lower strain rates are impractical for time considerations, all remaining eccentric tests were performed at a rate of 5 mm per minute.

4.2 – Effects of Precursor Fibre Diameter

4.2.1 – Fabrication and Initial Properties

To investigate the effects of the precursor fibre diameter on the coiled muscle performance, four TCP samples were fabricated using nylon-6 monofilaments with diameters of 0.21 mm, 0.38 mm, 0.48 mm, and 0.71 mm. To ensure the coiling stress was constant throughout fabrication, a coiling stress of 14.1 MPa was selected, and the coiling load was determined by multiplying the coiling stress by the original precursor fibre cross-sectional area. Table 4 shows the measured initial properties of the TCP samples made with different fibre diameters.

Table 4: Measured properties of TCP samples with different precursor fibre diameters

Sample Number	**1**	**2**	**3**	**4**
Precursor Fibre Diameter (mm)	0.21	0.38	0.48	0.71
Precursor Fibre Length (mm)	298	298	299	297
Final Coiled Length, L_0 (mm)	80.13	82.05	80.21	80.78

Length Contraction Factor (LCF)	3.72	3.63	3.73	3.68
Coil Diameter D (mm)	0.47	0.79	1.03	1.48
Spring Index (C = D/d)	2.24	2.08	2.15	2.08
Average Motor Speed (rpm)	249	249	251	244
Number of Twists to Induce Coiling	260	219	175	127
Number of Twists to Fully Coil	398	353	276	195
Load Used During Coiling (g)	49.78	163.01	260.09	569.06
Final Length After Annealing, L_i (mm)	90	99	98	92
Load Used During Actuation (g)	65	205	326	714

4.2.2 – Isotonic Test Results

The four samples made with different fibre diameters were prepared to be tested following the isotonic experimental test setup. In these tests, static masses were suspended off the lower ends of the TCP samples and the samples were placed inside the environmental chamber. The loads used during actuation were once again normalized to the precursor fibre cross-sectional area, such that the actuation stress remained constant between samples. The magnitude of the loads used during actuation is shown in Table 4. Starting at 45°C and heating until 200°C, the actuator displacement was recorded by the LVDT as a function of temperature. Figure 28 shows the results of the isotonic tests for the samples made with different precursor fibre diameters.

Results show that for each sample, regardless of the precursor fibre diameter, actuation stroke reached an average between 15.74% and 16.63% over all tests when heating from 45°C to 200°C. This indicates that the tensile stroke of the TCP actuators is independent of the precursor fibre diameter used, as long as the stresses used during coiling and actuation remains constant between samples. These results are similar to those observed by Aziz et al. when testing the torsional performance of twisted, non-coiled bundles [32]. This is an important effect for the scalability of TCP actuators, where actuators of all sizes can achieve consistent and repeatable actuation strokes when actuating against constant external stresses.

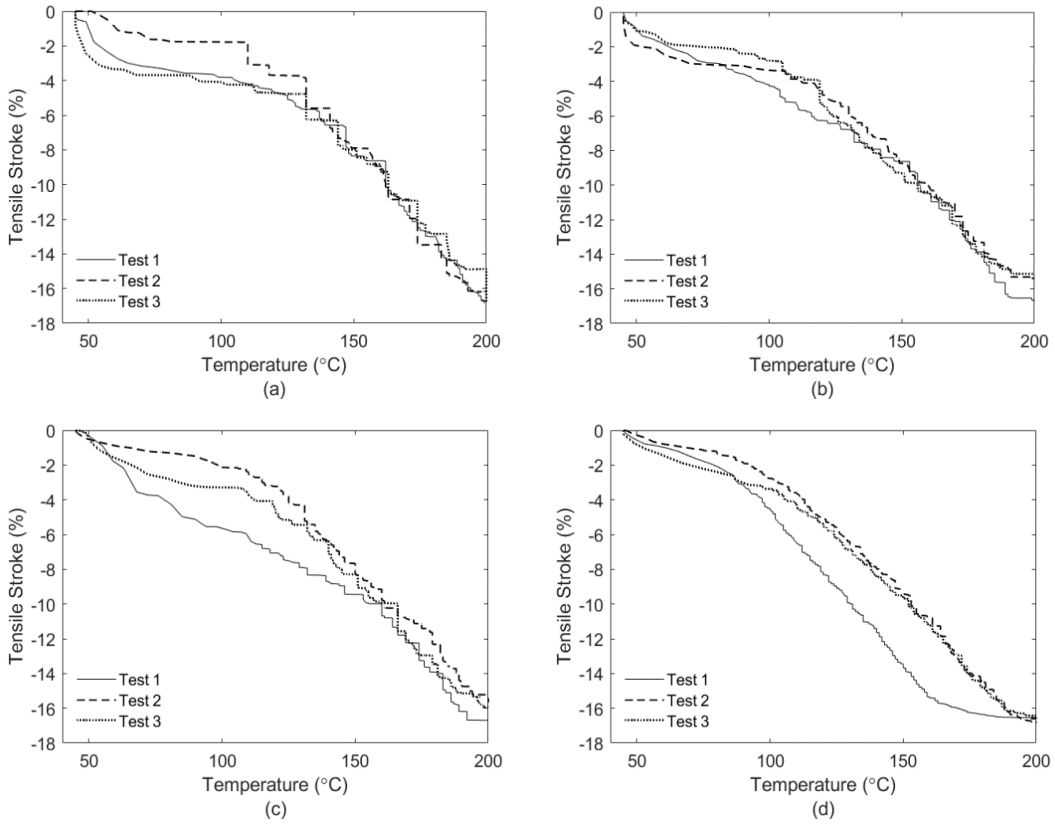

Figure 28: Results of isotonic tests for samples fabricated with precursor fibre diameters of a) 0.21 mm; b) 0.38 mm; c) 0.48 mm; d) 0.71 mm

4.2.3 – Isometric Test Results

The samples were fixed to both ends of the aluminum rods following the isometric experimental test setup. The Instron machine was used to reposition the end fixtures such that all slack or tension was removed from the sample prior to testing. Once the samples were aligned vertically with the aluminum rods, they were heated from 45°C to 200°C while the blocked force of the samples were measured by the Instron load cell. Figure 29 shows the results from the isometric tests for samples made with different precursor fibre diameters.

From these figures, a clear trend was observed between the precursor fibre diameter and the magnitude of the blocked force generated. For the samples fabricated with the smallest fibre diameter of 0.21 mm, measured blocked forces of the samples were recorded in the range of 0.67 N to 0.83 N. In contrast, for the samples fabricated with the largest fibre diameter of 0.71 mm,

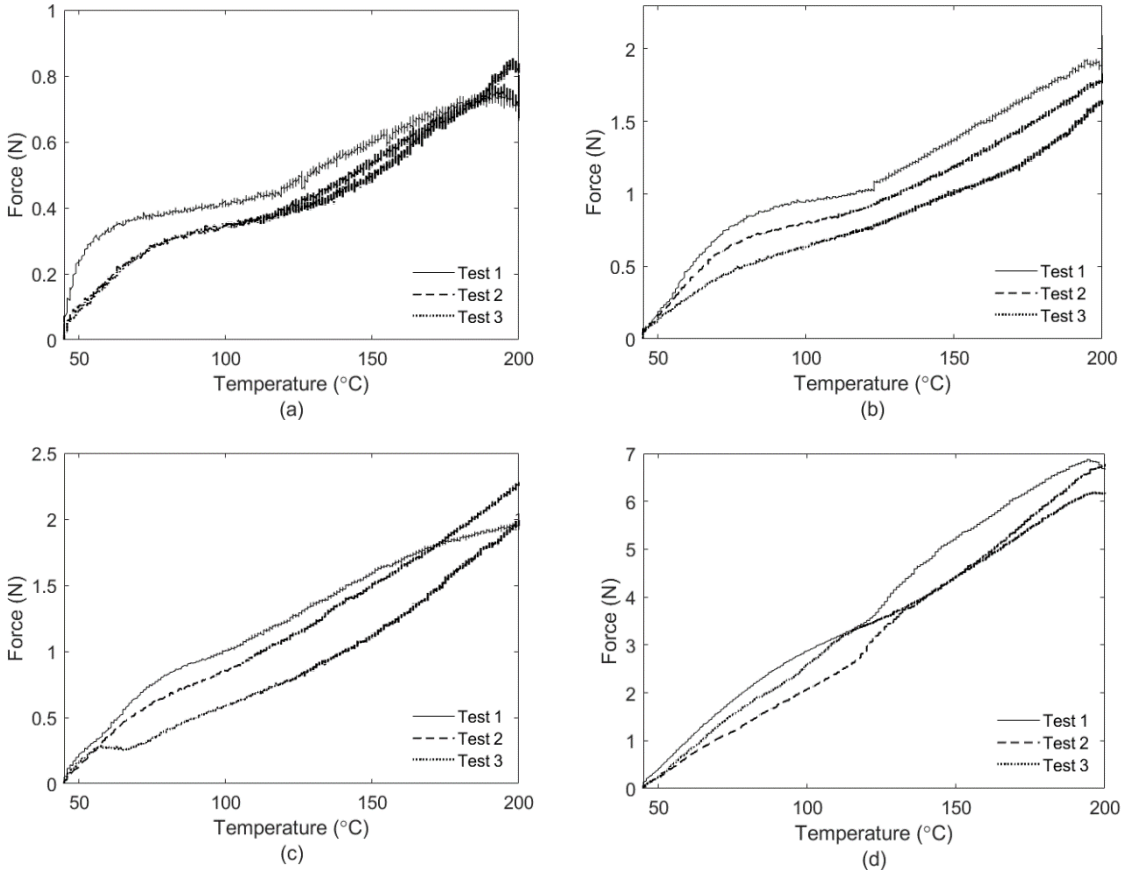

Figure 29: Results of isometric tests for samples fabricated with precursor fibre diameters of a) 0.21 mm; b) 0.38 mm; c) 0.48 mm; d) 0.71 mm

blocked forces were measured between 6.16 N and 6.78 N. These results show that the precursor fibre diameter has a considerable influence on the force generation capacity of TCP actuators and should be considered when designing for high force requirements within a set temperature range.

When designing TCP actuators, considering the effects of the precursor fibre diameter, designers should focus on the force requirements of the actuator when selecting an appropriate fibre diameter. While the effects of the precursor fibre diameter were minimal on the actuator tensile stroke, the effects had large influence on the sample force generation capacity. The selection of the precursor fibre diameter should account for the final force requirements of the actuator, such that the proper magnitude of force can be reached within a given temperature range.

4.2.4 – Eccentric Test Results

To investigate the effects of the precursor fibre diameter on the variation in stiffness properties of the actuator, the prepared samples were tested following the eccentric experimental

test setup. First, samples were secured to the aluminum rods inside the environmental chamber. At steady temperatures of 25°C, 50°C, 80°C, and 110°C, the samples are loaded and unloaded at a rate of 5 mm per minute while force and elongation data were recorded by the Instron load cell and displacement sensor. Figures 30-33 present the results of the eccentric tests for samples made with different precursor fibre diameters.

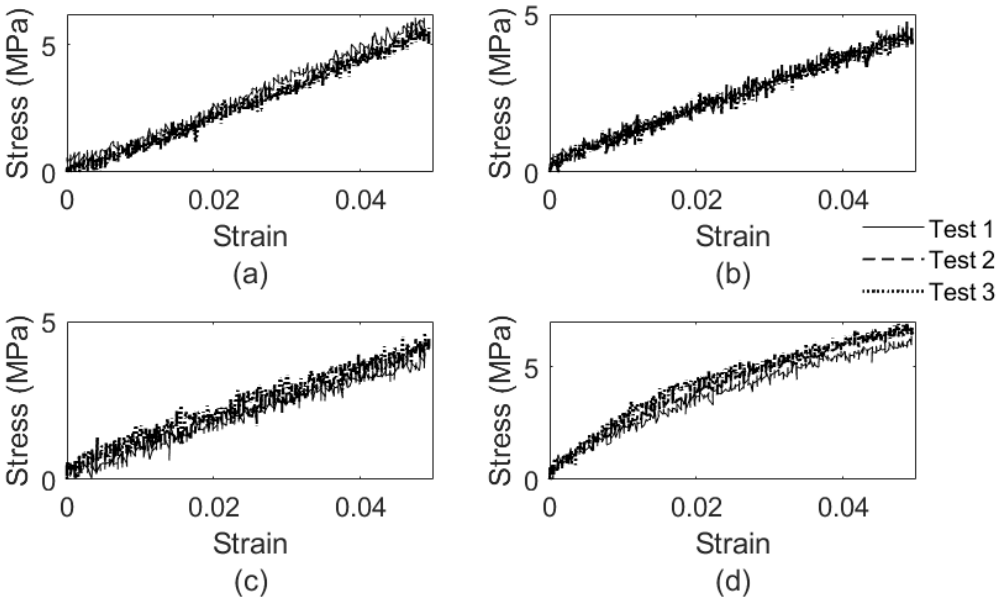

Figure 30: Results of the eccentric tests for sample fabricated with a 0.21 mm precursor fibre diameter at temperatures of a) 25°C; b) 50°C; c) 80°C; and d) 110°C

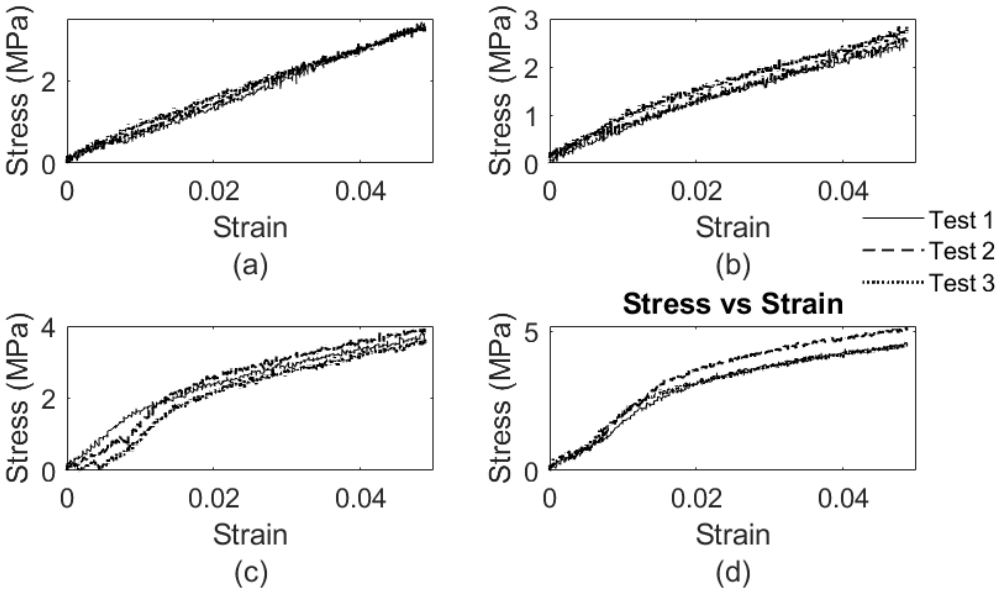

Figure 31: Results of the eccentric tests for sample fabricated with a 0.38 mm precursor fibre diameter at temperatures of a) 25°C; b) 50°C; c) 80°C; and d) 110°C

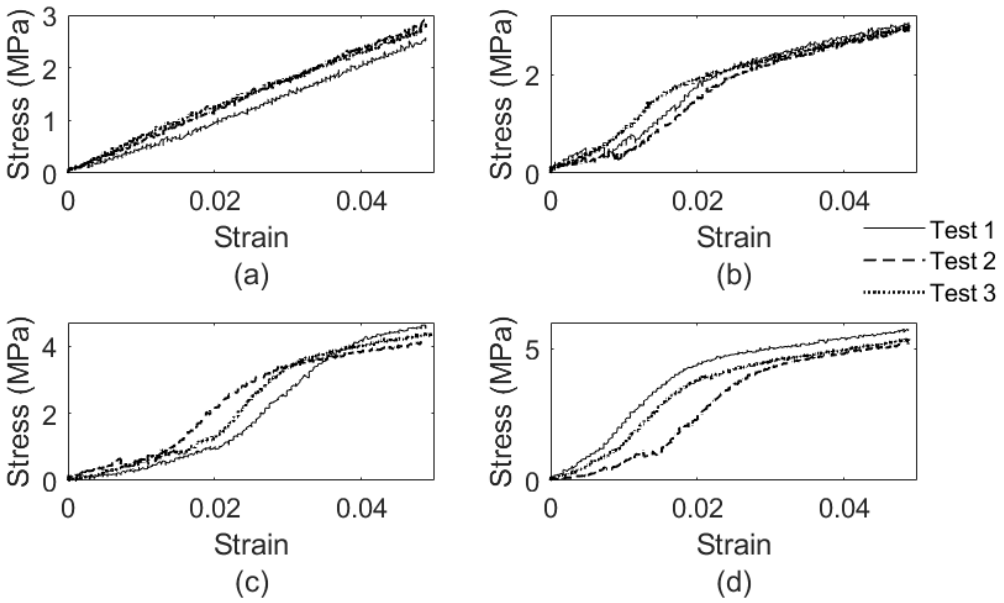

Figure 32: Results of the eccentric tests for sample fabricated with a 0.48 mm precursor fibre diameter at temperatures of a) 25°C; b) 50°C; c) 80°C; and d) 110°C

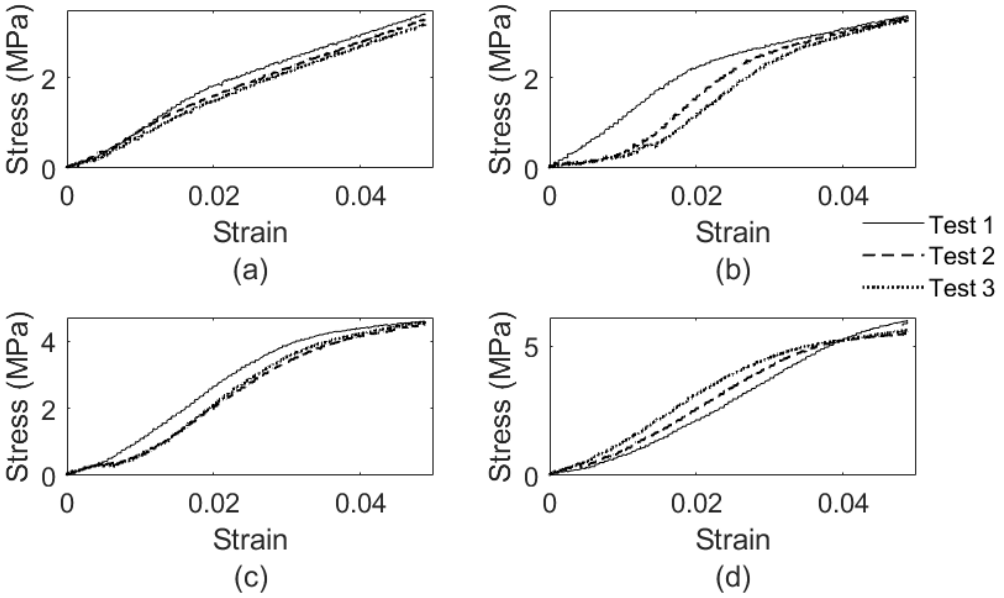

Figure 33: Results of the eccentric tests for sample fabricated with a 0.71 mm precursor fibre diameter at temperatures of a) 25°C; b) 50°C; c) 80°C; and d) 110°C

Next, the force and elongation data were converted to corresponding stress and strain data, and the tensile moduli were calculated for each test. The average modulus at all temperatures for samples made with varying precursor fibre diameters is presented in Table 5.

Table 5: Average elastic modulus values for samples with varying precursor fibre diameters

Test Condition	**Average Modulus at 25°C (MPa)**	**Average Modulus at 50°C (MPa)**	**Average Modulus at 80°C (MPa)**	**Average Modulus at 110°C (MPa)**	**Range in Stiffness (Max./Min.)**
d = 0.21 mm	117.85	88.23	87.09	220.67	2.53
d = 0.38 mm	67.33	69.41	188.13	227.57	3.38
d = 0.48 mm	56.59	131.37	204.09	276.69	4.89
d = 0.71 mm	84.55	124.06	150.74	168.75	2.00

From these results, the magnitude of the change in stiffness increased with increasing fibre diameter, however this trend breaks down for the highest fibre diameter of 0.71 mm. The maximum change in stiffness was observed for the sample fabricated with 0.48 mm diameter, where the modulus increased by a factor of 4.89 from room temperature to 110°C. However, the lowest magnitude of variation in stiffness was recorded for the sample with the largest fibre diameter of 0.71 mm, increasing its stiffness by a factor of 2.00 between room temperature and 110°C.

It remains unclear if the trend observed in these experiments represents improved variable stiffness properties for increasing precursor fibre diameters, or if there is an optimal diameter that can be selected to achieve the highest variation in stiffness. For the sample fabricated with the precursor fibre diameter of 0.21 mm, the forces required to elongate the samples during eccentric contraction were very small in contrast to the other samples. For those tests, the error of the load cell during operation represented a much greater percentage of the overall span, and as a result the loading curves feature even larger fluctuations between data points. This makes it increasingly difficult to predict the true stress and strain values, along with the corresponding modulus for those samples. Future experiments should examine the variation in stiffness of samples prepared with smaller precursor fibre diameters using a load cell with a lower capacity and higher sensitivity to validate the trend observed in these results.

4.3 – Effects of Spring Index

4.3.1 – Fabrication and Initial Properties

The next parameter investigated was the effects of the spring index, *C*, on the actuator performance. The spring index can be tuned either by varying the load used during coiling, or by wrapping the twisted fibre bundle around a mandrel of predetermined diameter allowing for wide ranges of spring indices to be achieved. In this work, the spring index was varied by selecting three different coiling loads during fabrication. To start, 300 mm samples of 0.48 mm nylon-6 precursor fibre were cut to length and secured to the fabrication rig. Using loads of 200 g, 300 g, and 400 g, the fibres were twisted and coiled to create TCP samples with different spring indices. Table 6 shows the measured initial properties of the samples made with varying spring indices.

Table 6: Measured properties of TCP samples with different spring index, C

Sample Number	**1**	**2**	**3**
Precursor Fibre Length (mm)	300	300	300
Final Coiled Length, L_0 (mm)	82.74	82.97	81.67
Length Contraction Factor (LCF)	3.63	3.62	3.67
Load Used During Coiling (g)	200.28	300.1	406.00
Coil Diameter D (mm)	1.04	0.97	0.93
Spring Index (C = D/d)	2.17	2.02	1.94
Average Motor Speed (rpm)	230	232	245
Number of Twists to Induce Coiling	161	180	160
Number of Twists to Fully Coil	270	294	265
Final Length After Annealing, L_i (mm)	94	92	86

4.3.2 – Isotonic Test Results

To evaluate the effects of the spring index on the actuator tensile stroke, the samples were prepared for testing following the isotonic experimental test setup. The samples were placed inside

the environmental chamber and coupled to the LVDT, while a static mass of 0.6 lb was suspended from the coupled ends. As the samples were heated from 45℃ to 200℃, the displacement was recorded by the LVDT as a function of temperature. Figure 34 shows the results of the isotonic tests for samples made with different spring indices.

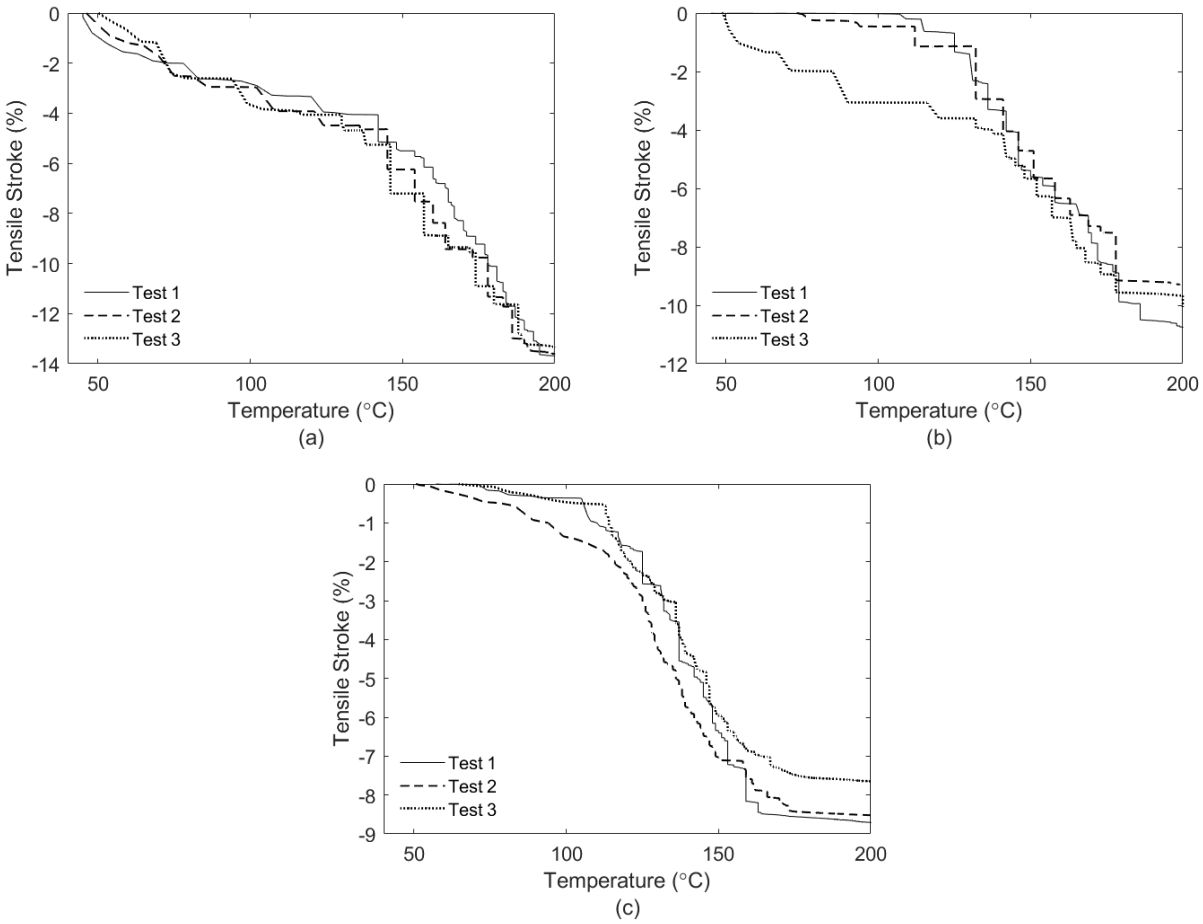

Figure 34: Results of isotonic tests for samples fabricated with a spring index of a) C = 2.17; b) C = 2.02; and c) C = 1.94

For the samples fabricated with the lowest coiling load, the largest spring index of 2.17 was achieved. During actuation from 45℃ to 200℃, the tensile stroke reached between 13.3% and 13.7%. For the samples fabricated with the 300 g coiling load, a spring index of 2.02 was achieved. Tensile strokes were between 9.3% and 10.7% when heated from 45℃ to 200℃. The samples fabricated with the 406 g coiling load produced samples with the lowest spring index of 1.94. These samples showed repeatable actuation strokes between 7.7% and 8.7%, where the actuation stroke was limited upon neighbouring coil contact at approximately 175℃.

From the isotonic test results, it is evident that samples prepared with larger spring indices are able to achieve larger tensile strokes, while samples prepared with lower spring indices suffer

from poor tensile stroke. This is due to the fact that the coils in the TCP become more densely packed with increasing coiling loads during fabrication. The dense packing of the coils reduces the free space between neighbouring coils, and requires larger actuation loads to achieve sufficient coil separation. If the actuating load is kept constant for samples with varying spring indices, inter-coil contact is reached at lower temperatures for the samples with lower spring indices, limiting the effective stroke capacity of the actuator. When designing for higher tensile strokes, actuators should be fabricated with either lower coiling loads or using a mandrel of larger diameter. Additionally, higher operating loads can be used to ensure sufficient space is introduced between neighbouring coils.

4.3.3 – Isometric Test Results

To evaluate the effects of the spring index on the force generation capabilities of TCP actuators, the samples prepared with the three different spring indices were tested under isometric conditions following the experimental setup outlined in Chapter 3. To start, the samples were secured to the aluminum rods and placed inside the environmental chamber. The Instron machine was used to align the sample vertically, ensuring no slack or preload was present in the samples prior to testing. Starting at 45°C and heating until 200°C, the blocked force produced by each sample was recorded by the Instron load cell. Figure 35 shows the results of the isometric testing for each of the three spring indices.

Results of the isometric testing illustrate another clear trend between the spring index of the actuator and the force generation capabilities. Samples made with larger spring indices generated lower forces during actuation, whereas samples made with low spring indices produced larger blocked forces. The samples with the highest spring index of 2.17 generated between 1.71 N and 1.83 N of blocked force. When the coiling load was increased and the spring index of 2.02 was achieved, testing resulted in 2.18 N to 2.33 N of blocked force. For the samples fabricated with the lowest spring index of 1.94, blocked forces were highest in the range of 2.85 N to 3.01 N.

The effects of the spring index on the TCP actuator performance illustrates a noticeable trade-off between stroke and force generation. Tight coils producing samples with low spring indices offer improved force generation at the expense of decreased stroke production, whereas samples prepared with larger spring indices offer increased stroke capacity at the expense of force

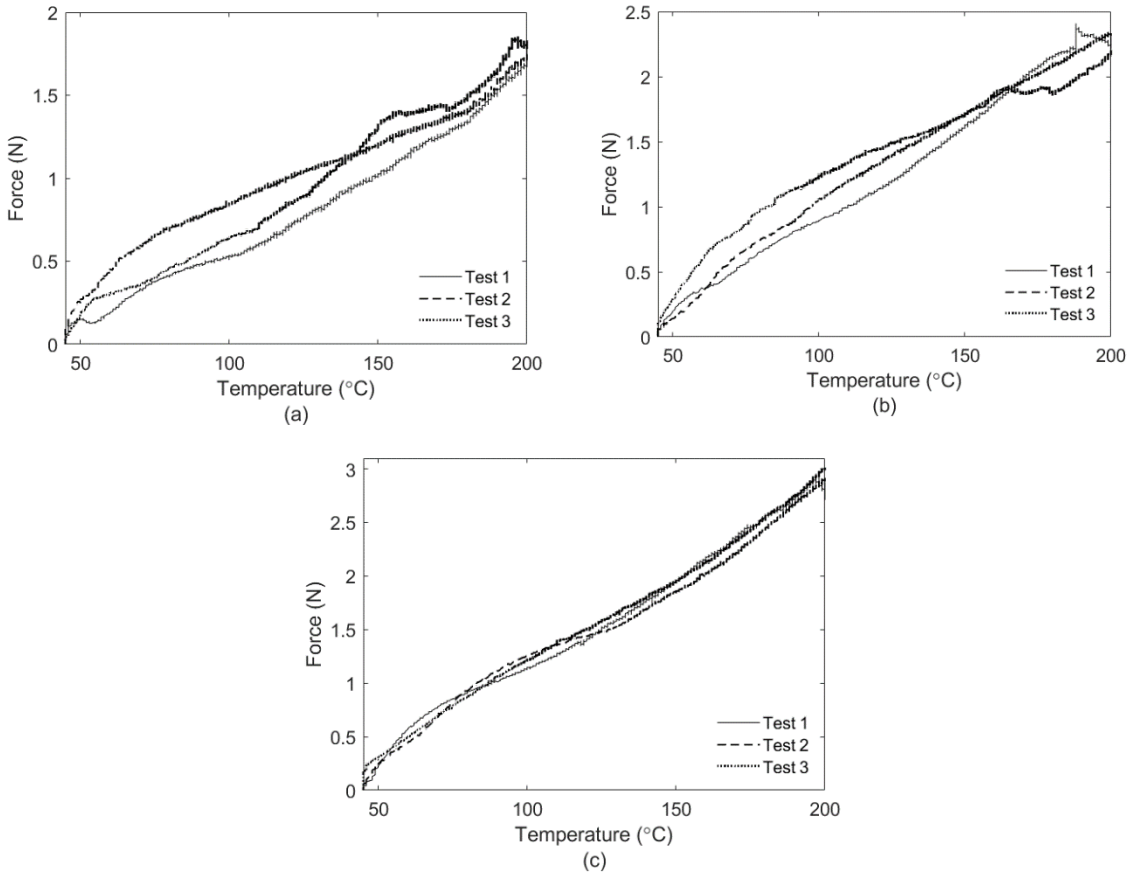

Figure 35: Results of isometric tests for samples fabricated with a spring index of a) C = 2.17; b) C = 2.02; and c) C = 1.94

generation. Depending on the specific needs of the application, TCP actuators must be designed to account for the spring index to ensure the desired stroke and force requirements are met.

4.3.4 – Eccentric Test Results

The effects of the spring index on sample stiffness were investigated. Samples were secured to the aluminum rods and aligned vertically inside the environmental chamber. At temperatures of 25°C, 50°C, 80°C, and 110°C, the samples were loaded to 5% strain and unloaded at a rate of 5 mm per minute. Figures 36-38 show the results of the eccentric tests for samples fabricated with spring indices of 2.17, 2.02, and 1.94. The modulus of elasticity was calculated for each test, and the average modulus for each temperature is presented in Table 7, along with the magnitude of the variation in stiffness for each test condition.

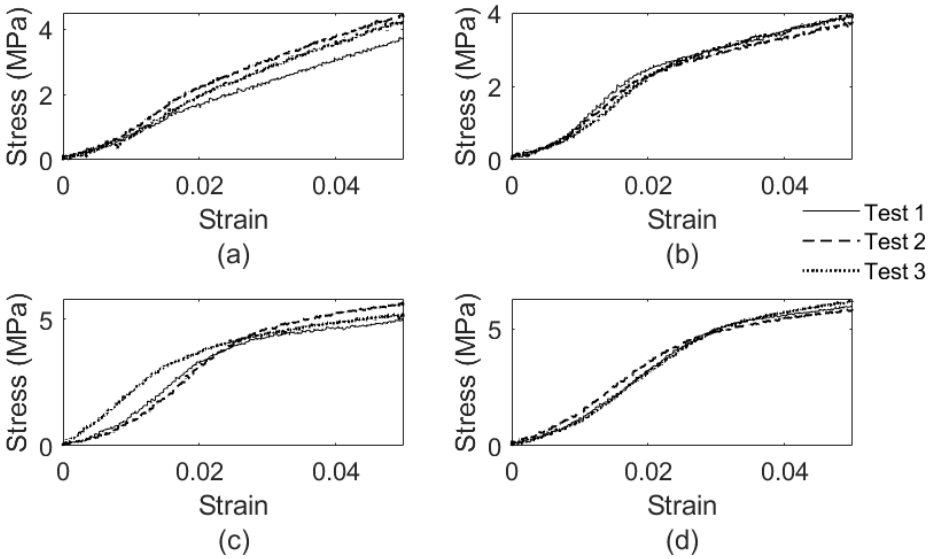

Figure 36: Results of the eccentric tests for sample fabricated with a spring index of 2.17 at temperatures of a) 25°C; b) 50°C; c) 80°C; and d) 110°C

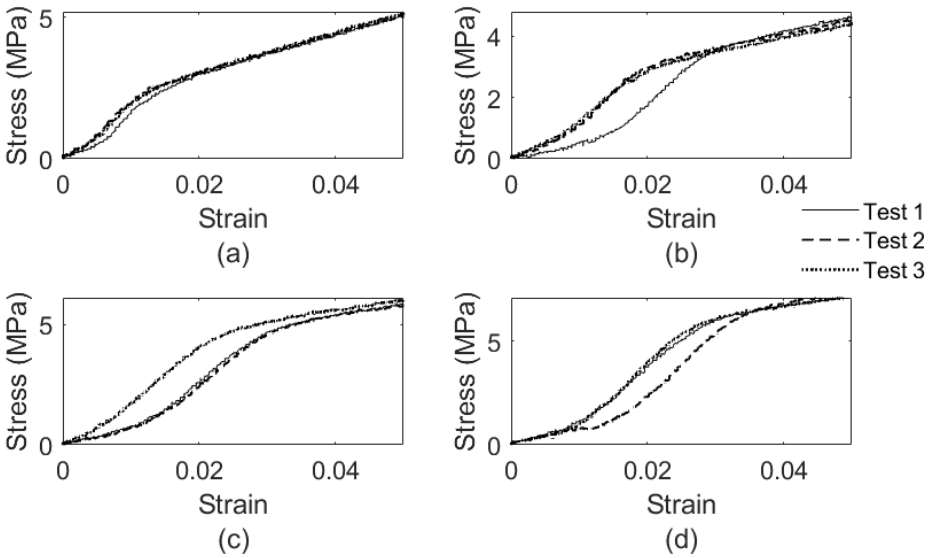

Figure 37: Results of the eccentric tests for sample fabricated with a spring index of 2.02 at temperatures of a) 25°C; b) 50°C; c) 80°C; and d) 110°C

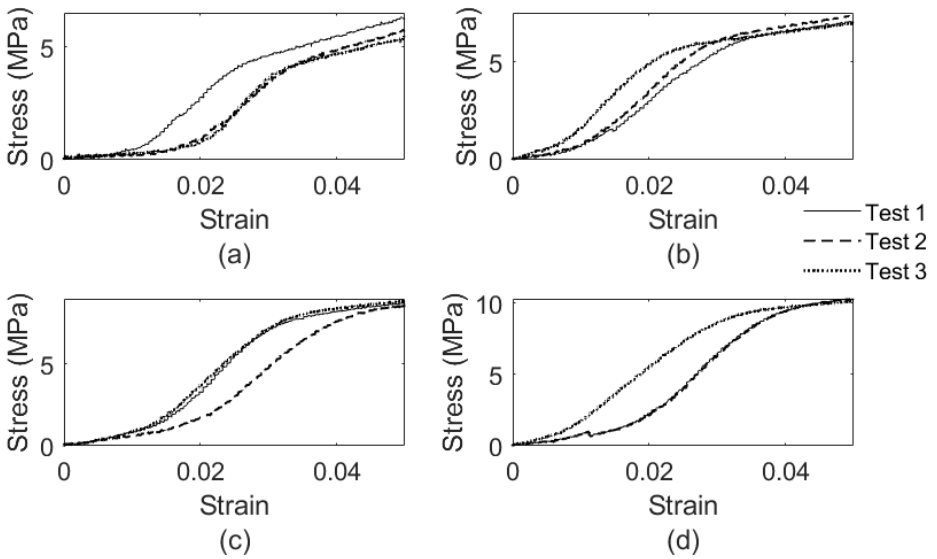

Figure 38: Results of the eccentric tests for sample fabricated with a spring index of 1.94 at temperatures of a) 25°C; b) 50°C; c) 80°C; and d) 110°C

Table 7: Average elastic modulus values for samples with different spring indices

Test Condition	**Average Modulus at 25°C (MPa)**	**Average Modulus at 50°C (MPa)**	**Average Modulus at 80°C (MPa)**	**Average Modulus at 110°C (MPa)**	**Range in Stiffness (Max./Min.)**
C = 2.17	128.08	162.46	202.30	216.78	1.69
C = 2.02	207.04	199.74	242.99	330.46	1.65
C = 1.94	282.12	320.38	384.20	459.84	1.63

These results also show a clear trend between the spring index and the range in stiffness. The variation in stiffness was found to be highest at a factor of 1.69 for the samples made with the highest spring index of 2.17, increasing in stiffness from 128.08 MPa at room temperature to 216.78 MPa at 110°C. For the samples with the intermediate spring index of 2.02, the variation in stiffness reduced to a factor of 1.65. The lowest magnitude of variation in stiffness was observed for the sample with the lowest spring index of 1.94, increasing in stiffness from 282.12 MPa at room temperature to 459.84 MPa at 110 °C.

The effects of the spring index on the actuator stiffness properties are additional factors to consider when designing TCP actuators. The samples fabricated with the lowest spring index required the highest magnitude of stress to separate the coils; however, they are inherently stiffer

at room temperature and so the variation in stiffness is not as prominent. In contrast, the samples fabricated with the highest spring index required the lowest magnitude of stress to separate the coils, yet the range in stiffness factor was largest since the actuators are more compliant at room temperature. For samples prepared with spring indices in the range of 1.94 to 2.17, the difference between the range in stiffness was not as broad as other parameters explored, and future investigations should examine these effects using a wider range of spring indices.

4.4 – Effects of Twist Density and Coil Bias Angle

4.4.1 – Fabrication and Initial Properties

To investigate the effects of the twist density and coil bias angle on the TCP actuator performance, samples were prepared with three ranges of inserted twist. 300 mm samples of 0.48 mm diameter nylon-6 were cut to length and attached to the fabrication rig. The twisting and coiling processes were performed automatically, up until the sample had fully coiled along its length. At this point, additional twists were manually inserted to the samples as the coils became more densely packed. This typically resulted in a decrease in sample length, along with an increase in the coil diameter. The initial measured properties of the samples with varying twist densities are presented in Table 8.

Table 8: Measured properties of TCP samples with varying twist densities

Sample Number	**1**	**2**	**3**
Precursor Fibre Length (mm)	296	300	301
Final Coiled Length, L_0 (mm)	89.74	88.95	86.21
Length Contraction Factor (LCF)	3.30	3.37	3.49
Load Used During Coiling (g)	261.36	261.36	261.36
Coil Diameter D (mm)	0.92	0.99	1.06
Spring Index (C = D/d)	1.92	2.06	2.21
Average Motor Speed (rpm)	235	230	234
Number of Twists to Induce Coiling	169	167	170
Number of Twists to Fully Coil	280	280	285

Final Number of Twists	280	290	305
Coil Bias Angle (degrees)	30	25	21
Final Length After Annealing, L_i (mm)	92	89	88

To measure the coil bias angle, α_c, a microscope with 200 times magnification was used to capture images of the coiled samples. The coil bias angles were measured manually from a plane perpendicular to the longitudinal axis of the samples, up to the line parallel to the individual coils. Microscope images of the samples along with the associated measured angles are presented in Figure 39.

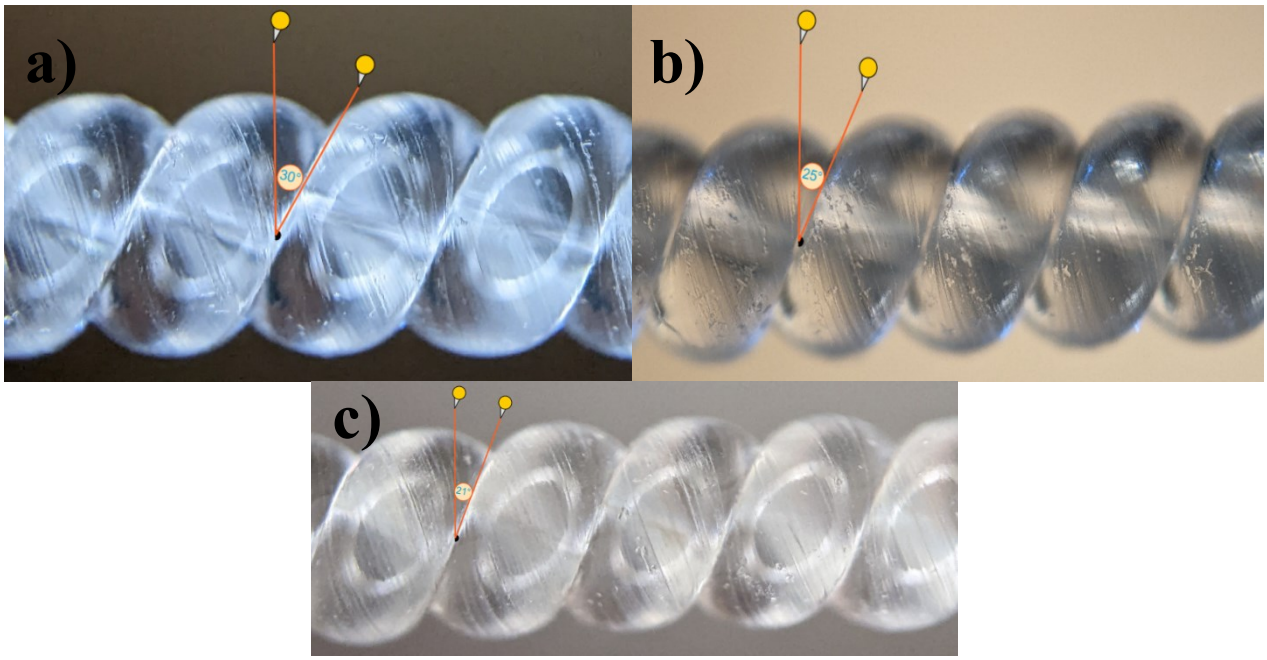

Figure 39: Microscopic images of TCP samples with measured coil bias angles of a) 30°; b) 25°; c) 21°

For the samples with additional inserted twists after the samples had fully coiled, they exhibited much greater twist liveliness due to the built-up internal torsion. For these reasons, the standard annealing procedure outlined in Chapter 3 had to be adjusted to ensure all residual stresses were removed. Instead of the standard 2 hours at 160°C, it was determined experimentally that 3 hours at 170°C was sufficient in retaining the coiled structure of the samples and removing any residual stresses that were present.

4.4.2 – Isotonic Test Results

To investigate the effects of twist density and coil bias angle on the tensile stroke of the actuator, the TCP samples were fixed to the LVDT according to the isotonic experimental setup. A static mass of 0.6 lb was suspended from the coupled ends, introducing an initial extension to the sample. The samples were then heated from 45℃ to 200℃ while the actuation stroke was recorded. Figure 40 shows the isotonic test results for the samples with coil bias angles of 30°, 25°, and 21°.

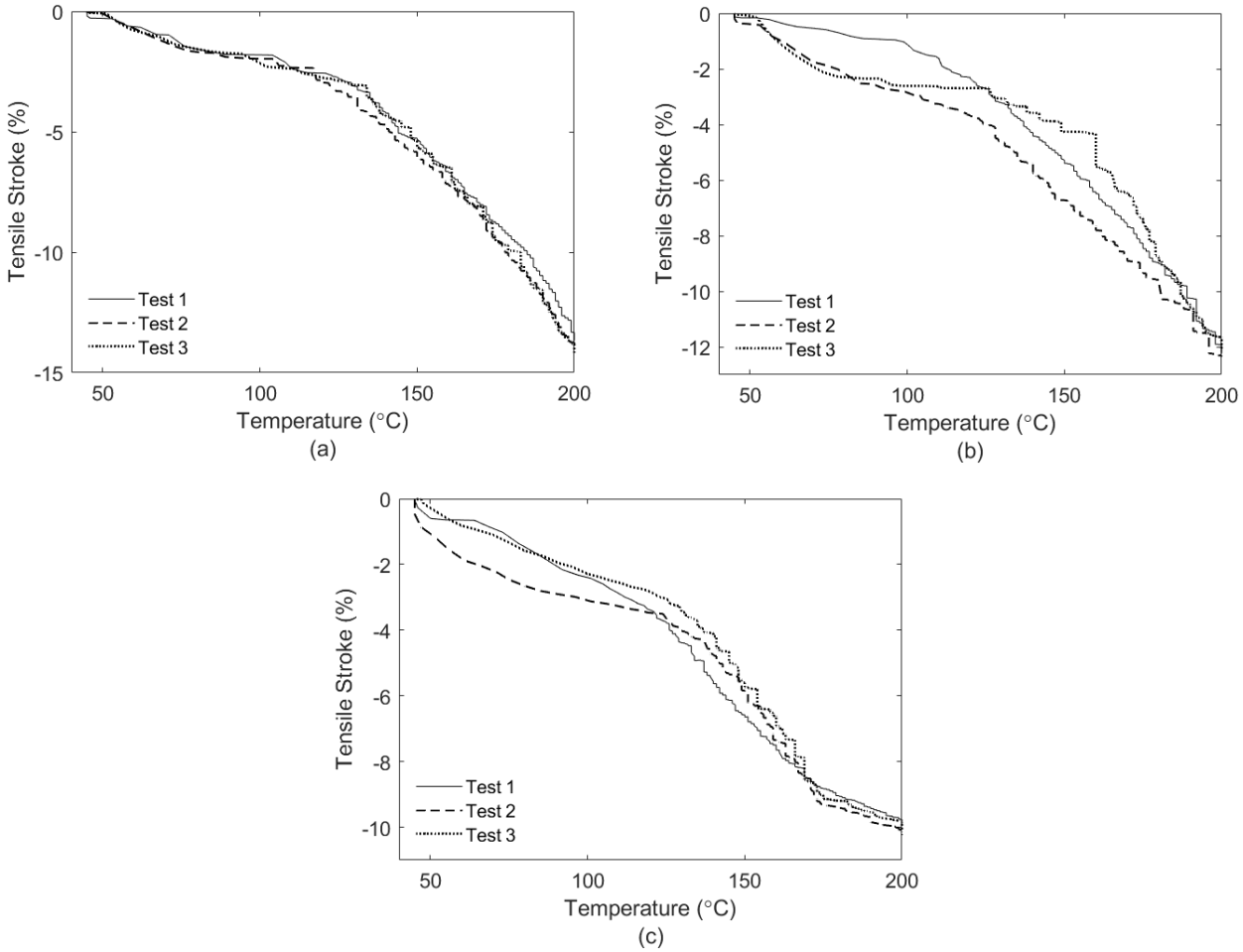

Figure 40: Results of isotonic tests for samples fabricated with varying levels of twist density and measured coil bias angles of a) 30°; b) 25°; and c) 21°

From these results, the actuator tensile stroke decreased with increasing amounts of inserted twists. For the samples made with no additional inserted twists and a measured α_c of 30°, the samples were able to contract between 13.8% and 14.2% when heating up to 200℃. For the samples made with 10 additional twists and a measured α_c of 25°, actuation stroke decreased

slightly, and repeatable contractions were measured between 11.6% and 12.3%. For the samples made with 20 additional twists and a measured α_c of 21°, tensile stroke was reduced even further and measured between 9.8% and 10.2%.

Furthermore, for all tests conducted on the samples with the highest amount of inserted twist, the slope of the actuation curve appears to decrease at a temperature of approximately 175°C. This pattern typically arises when neighbouring coils are near or in contact with one another, restricting any additional tensile stroke. These observations are consistent with the fact that as additional twists are inserted, the coil bias angle decreases as the coils reorient themselves to an angle closer to perpendicular to the longitudinal axis of the actuator. This causes the actuator to behave like a stiff extension spring, where additional force is required to introduce space between the coils for the actuator to contract. The samples made with larger coil bias angles naturally have more space between neighbouring coils, and as a result can generate larger actuation strokes. When designing TCP actuators for large tensile stroke, additional twist insertion should be avoided beyond what is required to fully coil the sample, to ensure that the range of coil bias angles remains sufficiently large for the application.

4.4.3 – Isometric Test Results

Next, the effects of the twist density and coil bias angle on the generated actuator force were investigated. Samples were secured to either ends of the aluminum rods following the isometric experimental setup, and the Instron machine was used to align the sample vertically while removing any slack or tension. Starting at 45°C and heating until 200°C, the generated actuator force was recorded by the Instron load cell as a function of temperature. Figure 41 shows the results for the isometric tests for the samples made with coil bias angles of 30°, 25°, and 21°.

The isometric test results also show a clear trend between the twist density and the magnitude of the generated force. Samples made with fewer inserted twists and larger coil bias angles generated smaller contraction forces than those made with greater inserted twists and smaller coil bias angles. For the samples with a coil bias angle of 30°, the generated actuator force measured between 1.44 N and 1.51 N. For the samples with a coil bias angle of 25°, the generated actuator force increased to values between 1.76 N and 1.88 N. For the samples with the highest

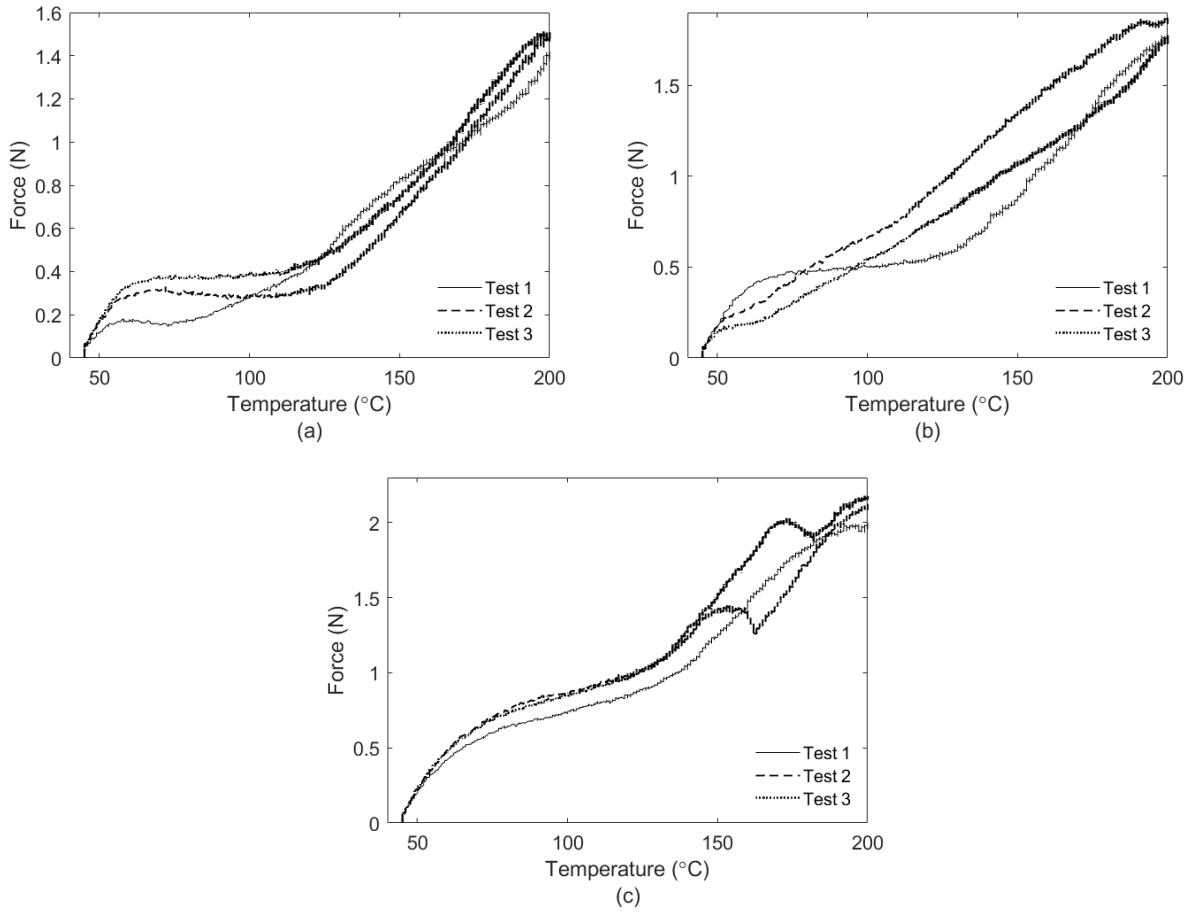

Figure 41: Results of isometric tests for samples fabricated with varying levels of twist density and measured coil bias angles of a) 30°; b) 25°; and c) 21°

amount of inserted twist and a coil bias angle of 21°, the generated actuator force reached a peak between 2.09 N and 2.18 N.

While increasing the twist density hinders the stroke capacity of the actuator, it can be beneficial in applications where larger forces are required. This occurs due to the increasingly dense packing of the underlying fibres within the coil structure, increasing the stored torsional energy within the actuator. As the TCP is heated, samples with higher twist densities have a higher tendency to untwist. When the ends of the actuator are constrained, this enhanced torsional capacity of the highly twisted fibres is translated to larger tensile forces in the coiled actuator as the fibres attempt to untwist during heating. As a result, in high force applications, designers should consider increasing the twist density within the TCP to achieve larger force generation capacities. In addition, further investigation is required to determine the limits of inserting additional twists

to the actuators, since the samples eventually failed during fabrication beyond a critical amount of inserted twists.

4.4.4 – Eccentric Test Results

The samples were then tested under eccentric contraction to capture the effects of the twist density and coil bias angle on the variation in stiffness of the actuators. At temperatures of 25°C, 50°C, 80°C, and 110°C, the samples were loaded at a rate of 5 mm per minute while the force and elongation data were recorded. Figures 42-44 show the corresponding stress and strain data of the loading curves for samples made with varying levels of twist density.

Using these figures, the slope of the loading curves was determined and the tensile moduli for each test was calculated. The average moduli at each temperature for the samples fabricated with varying levels of twist density, along with the magnitudes of the variation in stiffness, are presented in Table 9. From these results, it can be seen that the magnitude of the variation in stiffness decreases with increasing twist density. The sample with the lowest twist density and a coil bias angle of 30° exhibited an increase in stiffness from 115.77 MPa at room temperature to 365.32 MPa at 110°C, yielding a variation in stiffness by a factor of 3.16. For the sample with the intermediate twist density, the stiffness of the actuator increased by a factor of 1.53 from 236.70 MPa at room temperature to 361.57 MPa at 110°C. The magnitude of the variation in stiffness was

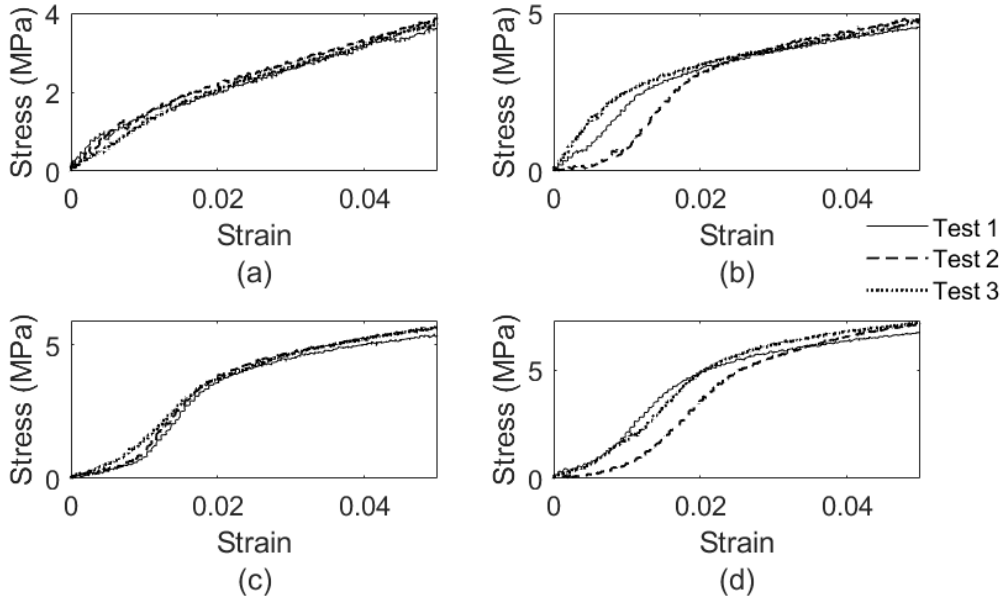

Figure 42: Results of the eccentric tests for sample fabricated with a measured coil bias angle of 30° at temperatures of a) 25°C; b) 50°C; c) 80°C; and d) 110°C

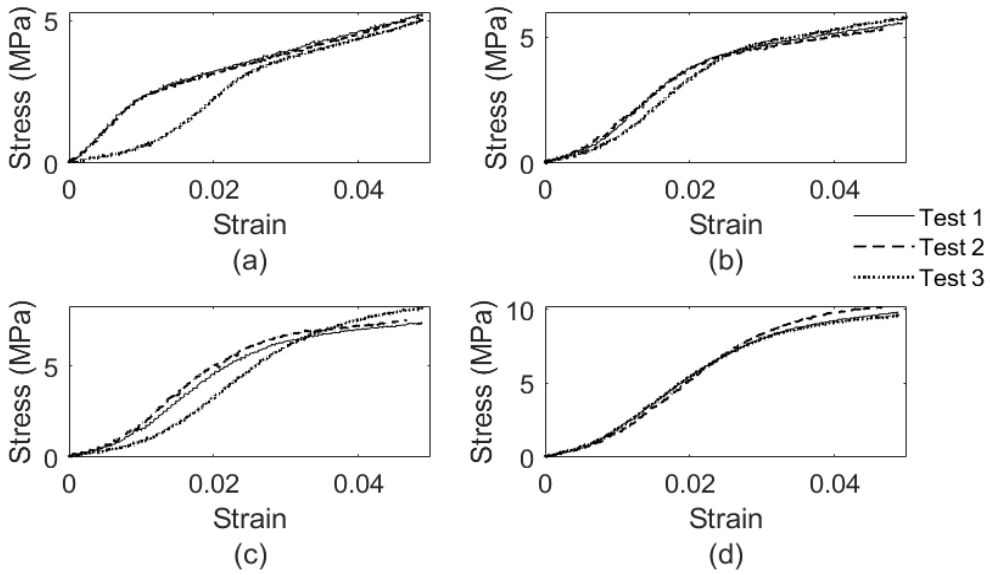

Figure 43: Results of the eccentric tests for sample fabricated with a measured coil bias angle of 25° at temperatures of a) 25°C; b) 50°C; c) 80°C; and d) 110°C

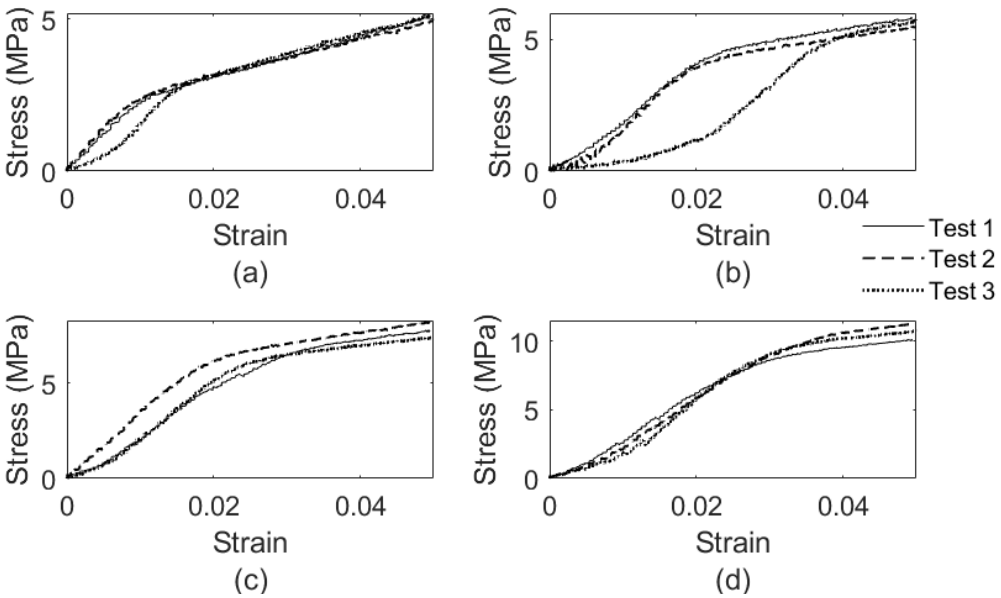

Figure 44: Results of the eccentric tests for sample fabricated with a measured coil bias angle of 21° at temperatures of a) 25°C; b) 50°C; c) 80°C; and d) 110°C

lowest for the sample with the highest twist density and coil bias angle of 21°, with the tensile modulus increasing by a factor of 1.44 from room temperature to 110°C.

While the samples with higher twist densities required larger magnitudes of stress to elongate the muscles, they are also inherently stiffer at room temperature so the effect of the

variation in stiffness is diminished. The average modulus at 110°C for the samples with the largest coil bias angle of 30° is only an average of 23.6 MPa less than the samples with the lowest coil bias angle of 21°, while the average modulus at room temperature is considerably lower by a factor of 2.34. If a wider range of variable stiffness is desired for a specific application, designers should avoid increasing the twist density of the actuators solely for its negative impact on the possible range of achievable stiffness.

Table 9: Average elastic modulus values for samples with varying levels of twist density

Test Condition	**Average Modulus at 25°C (MPa)**	**Average Modulus at 50°C (MPa)**	**Average Modulus at 80°C (MPa)**	**Average Modulus at 110°C (MPa)**	**Range in Stiffness (Max./Min.)**
α_C = 30°	115.77	243.55	319.70	365.32	3.16
α_C = 25°	236.70	241.52	321.77	361.57	1.53
α_C = 21°	270.96	269.31	314.92	388.92	1.44

4.5 – Effects of Twist Insertion Speed

4.5.1 – Fabrication and Initial Properties

The next parameter investigated is the twist insertion speed and its effects on the final actuator performance. In this case, all fabrication parameters were controlled while the twisting and coiling speed was changed using the rotary potentiometer. Precursor fibres were cut to approximately 300 mm in length and secured to the fabrication rig. Four arbitrary twisting and coiling speeds were chosen to fabricate the samples: 60 rpm, 240 rpm, 480 rpm, and 720 rpm. Table 10 presents the measured initial properties of the TCP samples made with different twist insertion speeds.

Table 10: Measured properties of TCP samples with varying twist insertion speeds

Sample Number	**1**	**2**	**3**	**4**
Precursor Fibre Length (mm)	299	299	298	300
Final Coiled Length, L_0 (mm)	84.75	84.38	84.07	85.12

Length Contraction Factor (LCF)	3.53	3.54	3.54	3.52
Load Used During Coiling (g)	261.92	261.92	261.92	261.92
Coil Diameter D (mm)	0.97	0.98	0.97	0.98
Spring Index (C = D/d)	2.02	2.04	2.02	2.04
Average Motor Speed (rpm)	63	244	485	725
Number of Twists to Induce Coiling	167	170	171	175
Number of Twists to Fully Coil	280	283	282	287
Final Length After Annealing, L_i (mm)	87	88	86	88

4.5.2 – Isotonic Test Results

When testing the samples under isotonic conditions, a static mass of 0.6 lb was suspended from the coupled ends of the TCP sample and the LVDT. The samples were heated from 45°C to

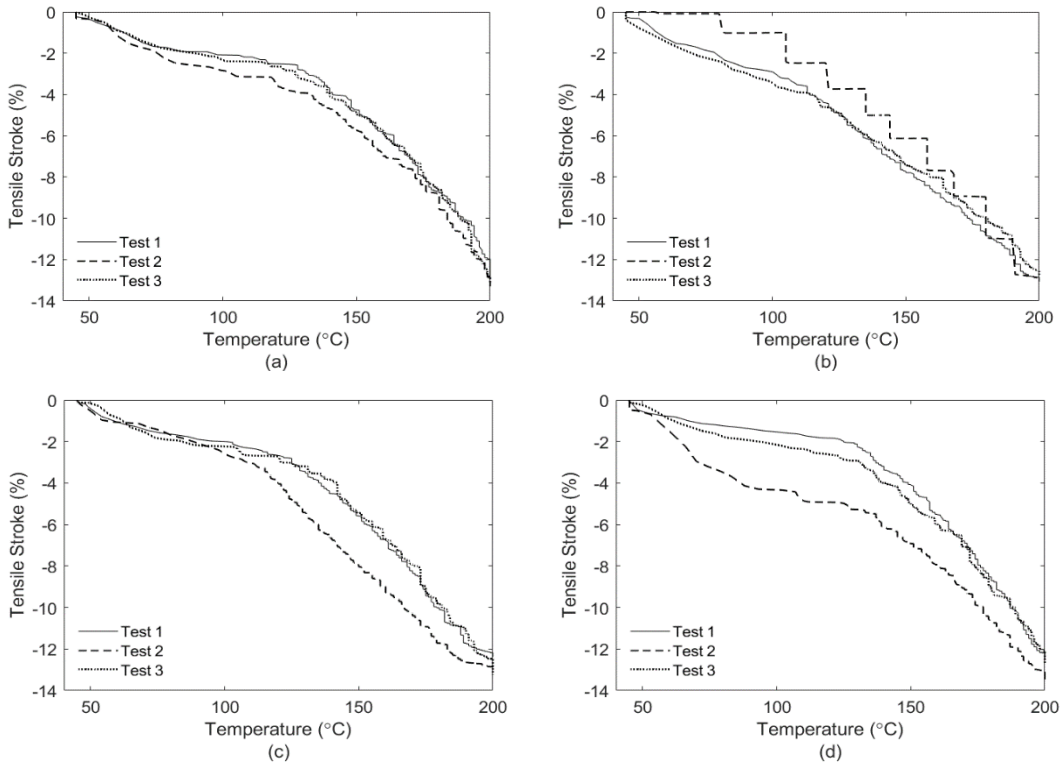

Figure 45: Results of isotonic tests for samples fabricated with twist insertion speeds of a) 60 rpm; b) 240 rpm; c) 480 rpm; and d) 720 rpm

200°C, while the actuator stroke was recorded by the LVDT as a function of temperature. Figure 45 shows the results of the isotonic testing for samples made with varying twist insertion speeds.

Results show that in all cases, when actuating against the same external load, the tensile stroke of the samples was recorded between 12.2% and 13.6% contraction. The samples were able to achieve consistent and repeatable actuation strokes regardless of if the twisting and coiling was performed slowly or sped up by a factor of 12. These results indicate that the twist insertion speed has a negligible effect on the actuator tensile stroke.

4.5.3 – Isometric Test Results

Next, the samples were tested under isometric conditions, where the Instron machine was used to align the samples and remove any slack or tension. The samples were heated from 45°C to

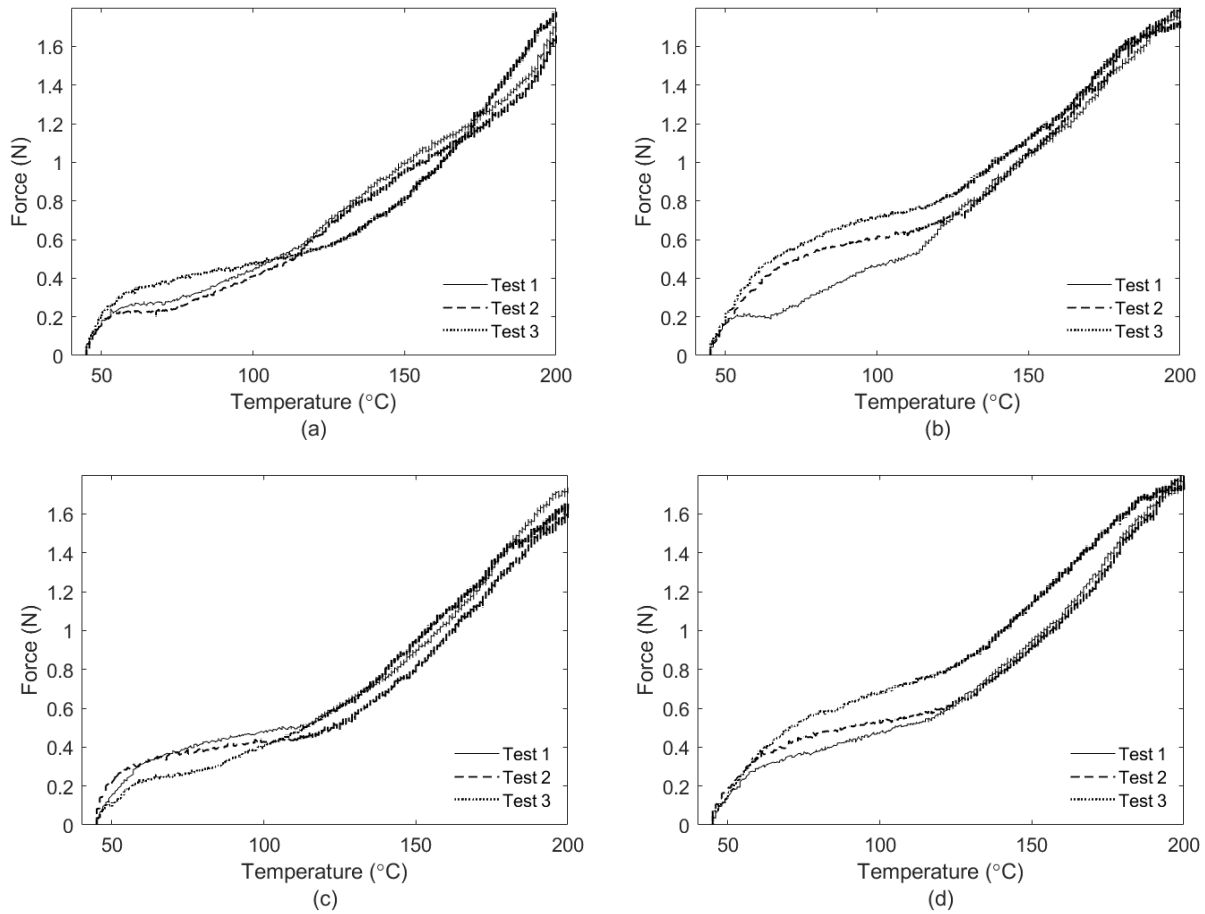

Figure 46: Results of isometric tests for samples fabricated with twist insertion speeds of a) 60 rpm; b) 240 rpm; c) 480 rpm; and d) 720 rpm

200°C, while the generated actuator force was measured by the Instron load cell. Figure 46 shows the results of the isometric testing for samples made with different twist insertion speeds.

For samples prepared at 60 rpm, 240 rpm, 480 rpm, and 720 rpm, all samples achieved repeatable blocked forces between 1.61 N and 1.80 N. While some discrepancy exists between tests and samples, the magnitude of these discrepancies was generally within ±0.1 N, similar to the fluctuation expected with the Instron load cell. Increasing the twist insertion speed by a factor of 12 does not appear to account for these fluctuations, and as such the effects of the twist insertion speed on the force generation capabilities of the actuators can also be said to be negligible. When considering the tensile stroke and force generation capabilities of the actuator, twist insertion speeds can be varied at the discretion of the designer as long as the fabrication setup has been validated to produce consistent and repeatable actuators.

4.5.4 – Eccentric Test Results

To capture the effects of the twist insertion speed on the variable stiffness properties, the samples were tested following the eccentric experimental test setup. First, the samples were secured to the aluminum rods inside the environmental chamber, while the Instron machine was used to load and unload the samples at a rate of 5 mm per minute. The corresponding loading curves for all samples tested at 25°C, 50°C, 80°C, and 110°C are presented in Figure 47-50.

For each test, the tensile modulus was determined from the slope of the second, steepest region of the loading curves. The average modulus for each temperature was calculated for all

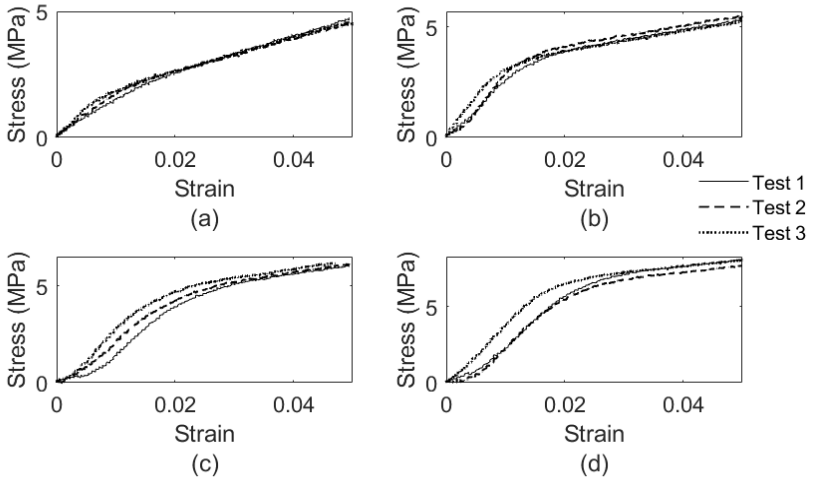

Figure 47: Results of the eccentric tests for sample fabricated at 60 rpm at temperatures of a) 25°C; b) 50°C; c) 80°C; and d) 110°C

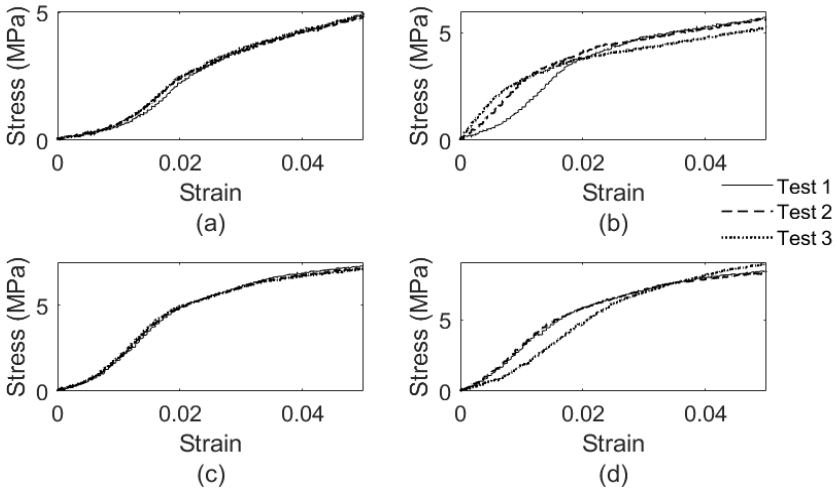

Figure 48: Results of the eccentric tests for sample fabricated at 240 rpm at temperatures of a) 25°C; b) 50°C; c) 80°C; and d) 110°C

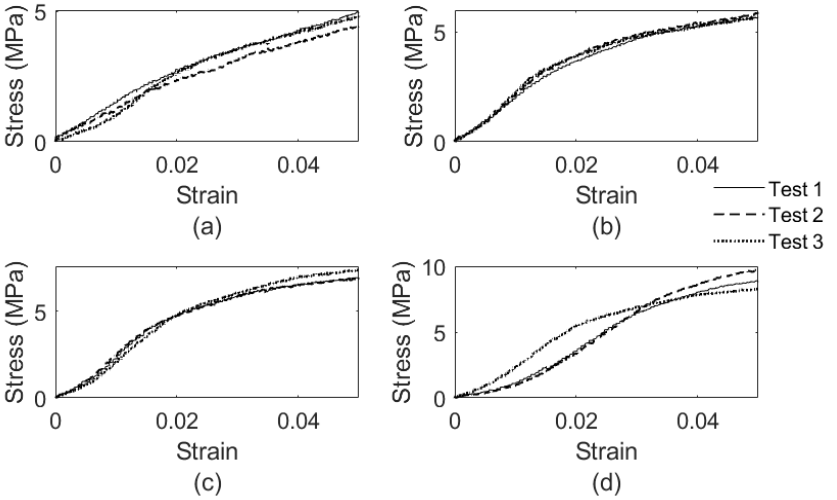

Figure 49: Results of the eccentric tests for sample fabricated at 480 rpm at temperatures of a) 25°C; b) 50°C; c) 80°C; and d) 110°C

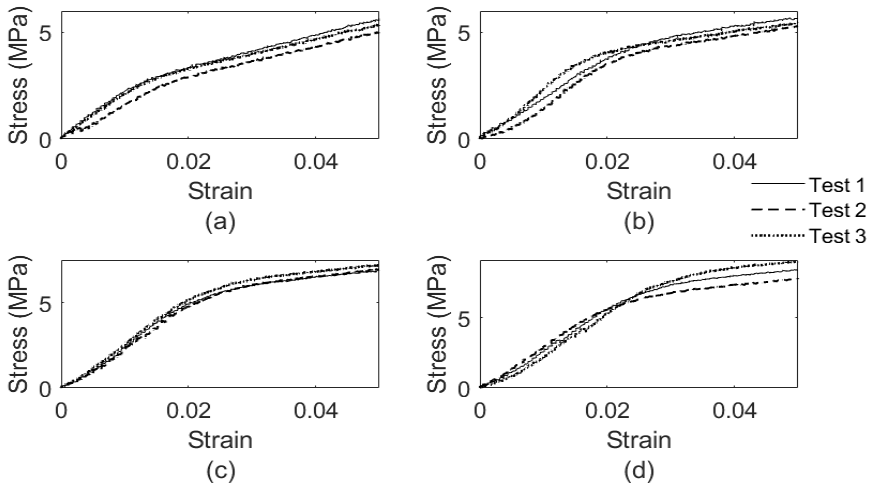

Figure 50: Results of the eccentric tests for sample fabricated at 720 rpm at temperatures of a) 25°C; b) 50°C; c) 80°C; and d) 110°C

samples, and the magnitude of the variation in stiffness was quantified from these results. Table 11 presents the average tensile moduli and variation in stiffness for samples fabricated with different twist insertion speeds.

Table 11: Average elastic modulus values for samples with different twist insertion speeds

Test Condition	**Average Modulus at 25°C (MPa)**	**Average Modulus at 50°C (MPa)**	**Average Modulus at 80°C (MPa)**	**Average Modulus at 110°C (MPa)**	**Range in Stiffness (Max./Min.)**
60 rpm	162.46	314.96	328.78	413.72	2.55
240 rpm	206.16	311.61	332.69	416.29	2.02
480 rpm	136.46	275.24	343.97	362.86	2.66
720 rpm	224.74	245.64	318.12	377.15	1.68

From these results, all samples exhibited a range in stiffness from room temperature to 110°C between factors of 1.68 and 2.66, however no discernible trend is visible between the different samples. While there are some large discrepancies between the results, it remains unclear the effects of increasing the twist insertion speed on the magnitude of the variation in stiffness. Variance in the results could be a result of a relationship between the twist insertion speed and the tensile modulus of the samples, however it could also arise from any variance between fabricated

samples as well as the thermomechanical history from the previous testing conducted. Further experiments should be carried out using carefully controlled twist insertion speeds to verify the relationship, if any, between the twist insertion speed and the magnitude of the variation in stiffness.

4.6 – Effects of Training Load

4.6.1 – Fabrication and Initial Properties

The effects of the training load on the actuator final performance were investigated by fabricating samples with consistent initial properties and altering the training load used prior to testing. First, five 300 mm samples of nylon-6 were cut to length and secured to the fabrication rig. The samples were twisted and coiled following the same procedure and annealed in the environmental chamber under the same conditions. After removing the samples from the environmental chamber, the samples were individually trained using one of five selected training conditions. Three samples were trained against static masses of 0.3 lb, 0.7 lb, and 1.0 lb, while the remaining two samples were trained dynamically against extension springs with spring constants of 0.0319 N/mm and 0.0929 N/mm. Table 12 shows the measured initial properties of the samples trained under different conditions.

Table 12: Measured properties of TCP samples with varying training conditions

Sample Number	**1**	**2**	**3**	**4**	**5**
Precursor Fibre Length (mm)	299	300	301	302	300
Final Coiled Length, L_0 (mm)	81.56	82.00	81.68	82.22	81.49
Length Contraction Factor (LCF)	3.67	3.66	3.69	3.67	3.68
Load Used During Coiling (g)	261.92	261.92	261.92	261.92	261.92
Coil Diameter D (mm)	0.98	0.98	0.99	0.99	0.98
Spring Index (C = D/d)	2.04	2.04	2.06	2.06	2.04

Average Motor Speed (rpm)	246	244	258	235	245
Number of Twists to Induce Coiling	172	170	165	173	169
Number of Twists to Fully Coil	287	281	280	282	282
Final Length After Annealing, L_i (mm)	83	84	83	84	86
Training Conditions	Static (0.3 lb)	Static (0.7 lb)	Static (1.0 lb)	Dynamic (k = 0.0319 N/mm)	Dynamic (k = 0.0929 N/mm)

Training of each sample involved heating from 45°C to 200°C until repeatable actuation strokes were observed. Figure 51a-e) shows the results of the training steps for each sample. In each case, consistent actuation strokes were observed after approximately 3 training cycles. Training of the actuators is typically accompanied by a change in length of the sample after the first or second training cycle. This was evident in Figure 51a-c), where both the sample lengths and tensile strokes increased between the first and second tests. As larger training loads were used, more space was introduced between the coils after each training cycle and the initial length of the muscle was increased further. When training against static masses, this change in length should be accounted for in the design of the final actuator.

Interestingly, when training against dynamic loads such as extension springs, the change in length typically accompanied with training was less prominent if present at all. Repeatable actuation strokes were still obtained after 3 training cycles, however the sample length remained fairly consistent throughout the process. This could be due to the fact that when actuating against an extension spring, the external load from the spring never exceeds the generated actuator force and instead exhibits a plateau once the actuator force and spring force are in equilibrium. An example of this is seen in Figure 51d). When cooling the sample, the spring force gradually returns the TCP sample back to its original length. In contrast, during cooling of the samples trained against static masses, the external load is often enough to extend the sample past its initial length as the sample softens with the number of training cycles. Dynamic training against extension springs presents an opportunity to train the actuator without the accompanied changes in length,

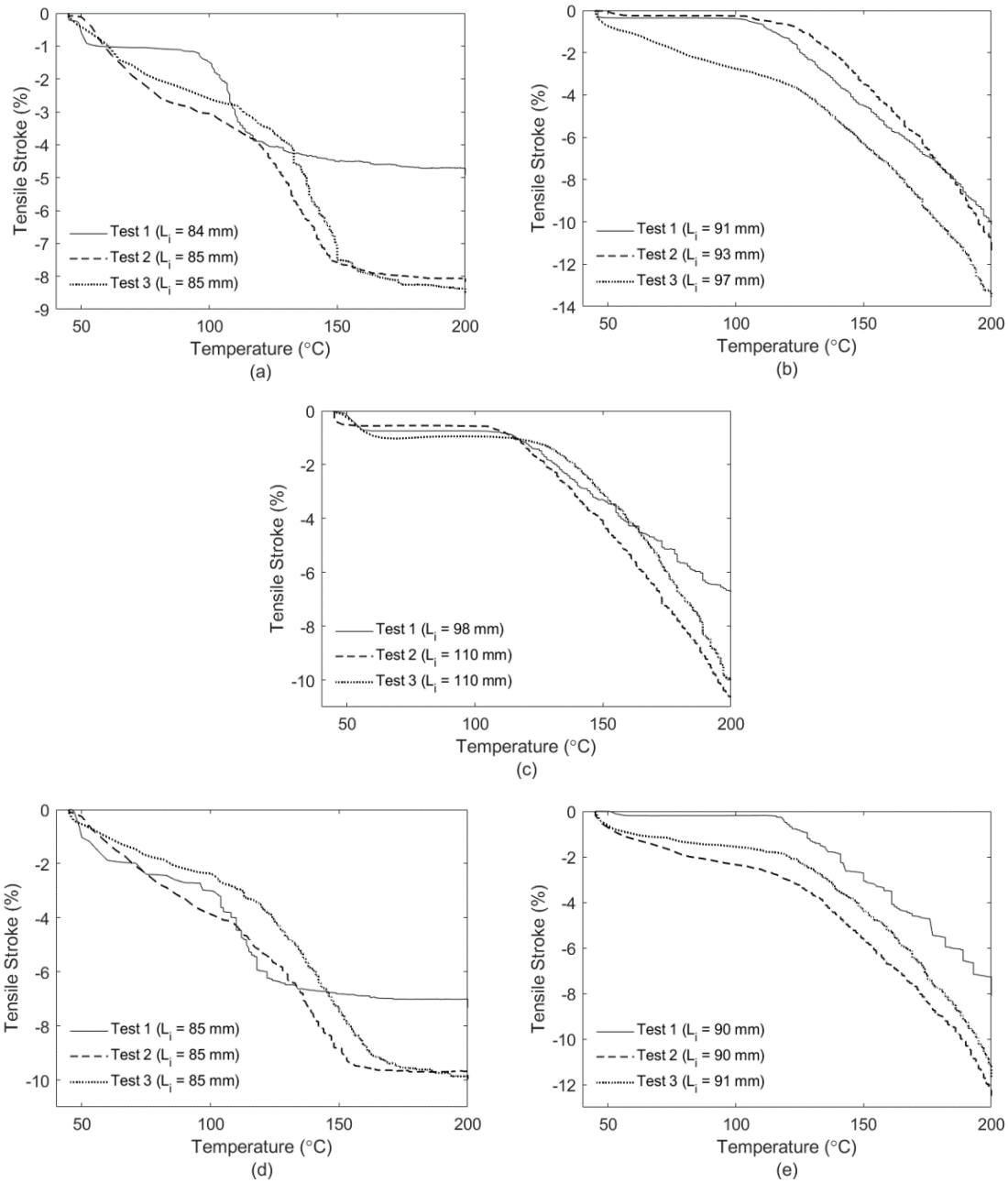

Figure 51: Results during training cycles at a) 0.3 lb (Static); b) 0.7 lb (Static); c) 1.0 lb (Static); d)Spring constant of k = 0.0319 N/mm (Dynamic); e) Spring constant of k = 0.0929 N/mm (Dynamic)

however more research is required to find the optimal spring stiffness and initial conditions during training.

4.6.2 – Isotonic Test Results

When investigating the effects of the training conditions on the actuator stroke generation, the five samples were tested following the isotonic experimental setup. During these experiments,

the external actuating load was kept constant between samples with a static mass of 0.6 lb suspended from the coupled ends of the TCP sample and the LVDT. The samples were heated from 45℃ to 200℃, while the actuator stroke was recorded as a function of temperature. Figure 52a-e) show the results of the isotonic testing for samples fabricated with varying training conditions.

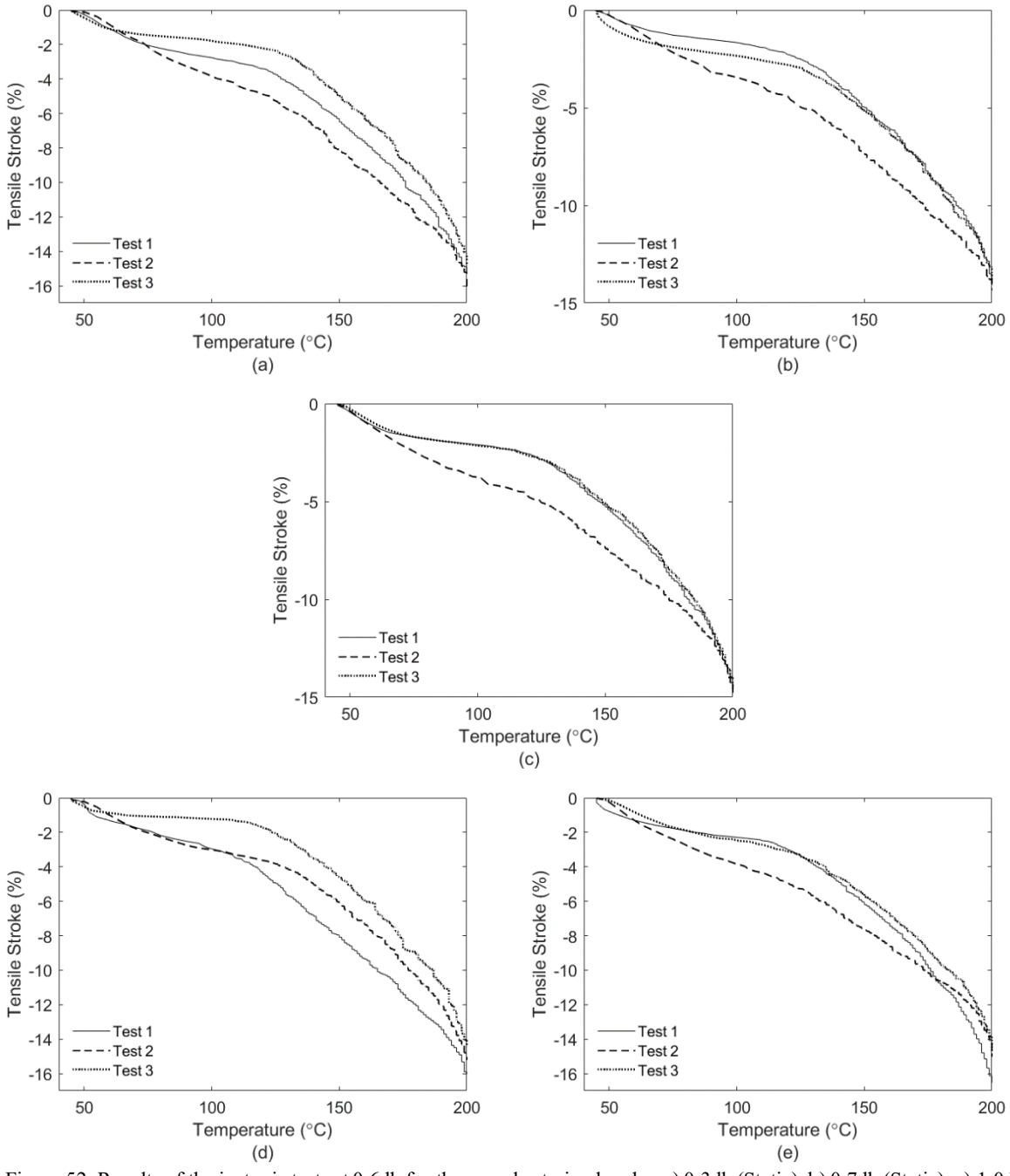

Figure 52: Results of the isotonic tests at 0.6 lb for the samples trained under: a) 0.3 lb (Static); b) 0.7 lb (Static); c) 1.0 lb (Static); d) Spring constant of k = 0.0319 N/mm (Dynamic); and e) Spring constant of k = 0.0929 N/mm (Dynamic), conditions

Results show that in all cases, actuation stroke settled between 14.13% stroke and 15.42% stroke on the third test of each sample when actuating against the same external load. For the samples trained using static masses, if the training load used was less than the actuating load during testing (as was the case with Sample 1), larger tensile strokes were observed during the first two tests of the experiment ranging between 15.2% and 16.2% stroke. Similarly, for the samples trained using dynamic loads, the first two tests of the experiments produced larger strokes before settling at its repeatable strokes between 14.4% and 14.7%.

These observations are similar in effect to the changes in stroke seen when training the samples for the first time, indicating a minor retraining step may be needed when adjusting the load used. If the actuating load is increased from the standard load used throughout the thermomechanical history of the actuator, additional viscoelastic strain is released within the sample leading to a small change in length during the first couple sets of heating and cooling cycles. This is accounted for during continued testing, where eventually the actuators achieve consistent and repeatable stroke. If the actuation load is kept constant, the training load does not appear to have a large effect on the tensile stroke of the actuator, except for the initial changes in tensile stroke observed during the first set of tests.

4.6.3 – Isometric Test Results

Next, the effects of the training conditions on the actuator force production were investigated. Samples were secured to the aluminum rods following the isometric experimental setup, and the Instron machine was used to align the samples vertically ensuring no initial extensions or preloads were introduced to the samples. Heating from 45°C to 200°C, the blocked forces of the samples were recorded as a function of temperature and are presented in Figure 53a-e).

From these experiments, it is evident that the training load has a considerable effect on the actuator force generation capabilities. For the samples trained with static masses, the blocked force of the samples showed to increase with increasing training load. The sample trained with the lowest static mass of 0.3 lb generated the smallest forces, ranging between 1.66 N and 1.73 N. When training against a static mass of 0.7 lb, the actuator produced a blocked force between 2.01 N and

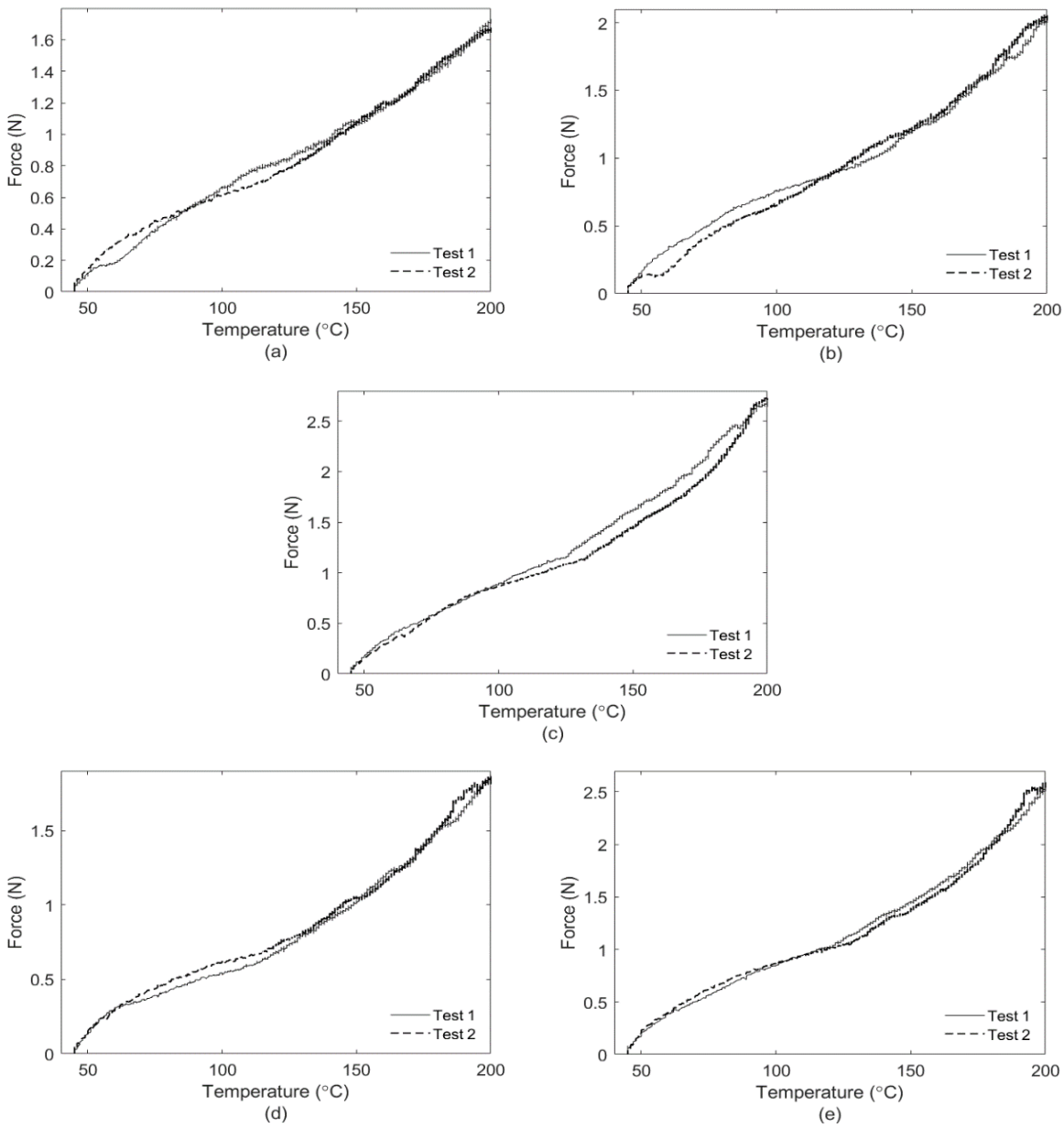

Figure 53: Results of the isometric tests for the samples trained under a) 0.3 lb (Static); b) 0.7 lb (Static); c) 1.0 lb (Static); d) Spring constant of k = 0.0319 N/mm (Dynamic); and e) Spring constant of k = 0.0929 N/mm (Dynamic), conditions

2.05 N. The sample trained against the largest static mass of 1.0 lb produced the largest blocked forces ranging from 2.71 N to 2.73 N. When training against a dynamic load, the sample trained with the lower spring constant of 0.0319 N/mm generated blocked forces between 1.81 N and 1.86 N, while the sample trained with the stiffer spring constant of 0.0929 N/mm generated between 2.54 N and 2.58 N of blocked force.

Regardless of the training method selected (static or dynamic), the training process should be tailored to the final force requirements of the actuator. When samples are trained against heavier

static loads or stiffer extension springs, the generated viscoelastic response within the material is enhanced. This thermomechanical history is stored within the material, so when ends are constrained from rotation or contraction, the increased viscoelastic strain energy is released during heating and translates to higher blocked forces. These results suggest that when designing TCP actuators for high force applications, training should be performed using heavier static masses or stiffer extension springs.

4.6.4 – Eccentric Test Results

The next stage of experiments involved capturing the effects of the training conditions on the variation in stiffness capacity of the actuators. These effects were investigated independently for the samples trained with static masses, and those trained dynamically against bias springs. In all cases, samples were secured to the aluminum rods inside the environmental chamber and kept at constant temperatures of 25°C, 50°C, 80°C, and 110°C. The samples were loaded and unloaded at a rate of 5 mm per minute, and force and elongation data were recorded through the Instron load cell and displacement sensor, respectively. Figures 54-56 present the results of the eccentric tests for the samples trained with static masses of 0.3 lb, 0.7 lb, and 1.0 lb, respectively, while Figures 57-58 present the results for the samples trained under dynamic conditions.

With this set of experimental data, the tensile modulus was determined for each test by calculating the slope of the steepest region of the loading curves. Table 13 presents the results for the average tensile moduli at all temperatures along with the associated magnitude of the variation in stiffness, for samples trained under both static and dynamic conditions.

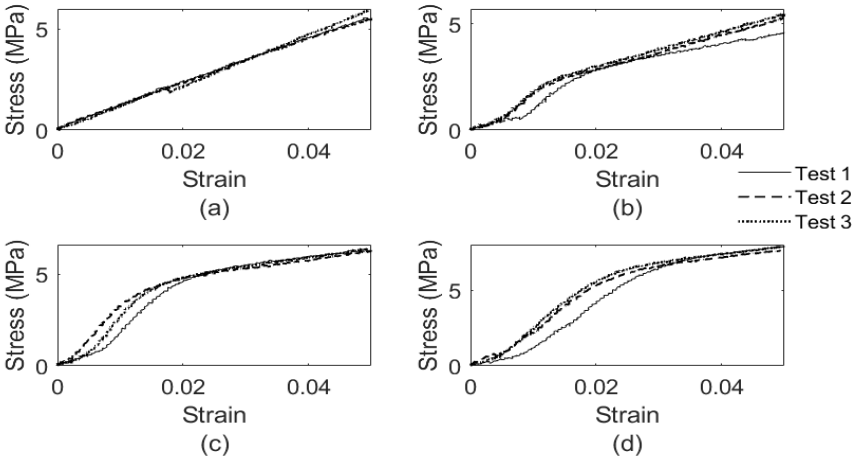

Figure 54: Results of the eccentric tests for sample trained under static conditions at 0.3 lb at temperatures of a) 25°C; b) 50°C; c) 80°C; and d) 110°C

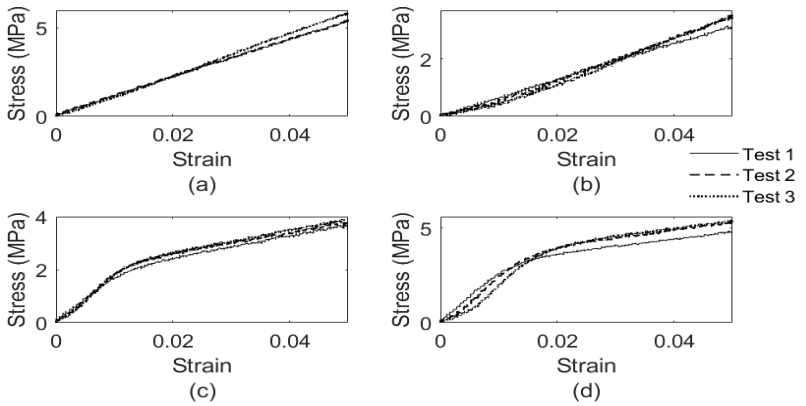

Figure 55: Results of the eccentric tests for sample trained under static conditions at 0.7 lb at temperatures of a) 25℃; b) 50℃; c) 80℃; and d) 110℃

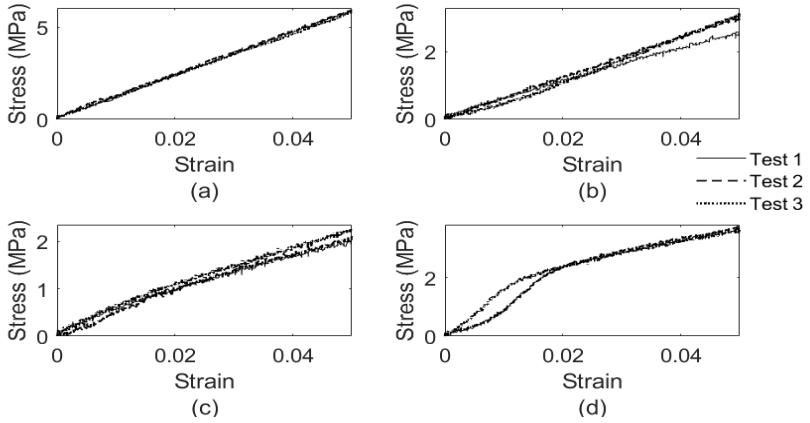

Figure 56: Results of the eccentric tests for sample trained under static conditions at 1.0 lb at temperatures of a) 25℃; b) 50℃; c) 80℃; and d) 110℃

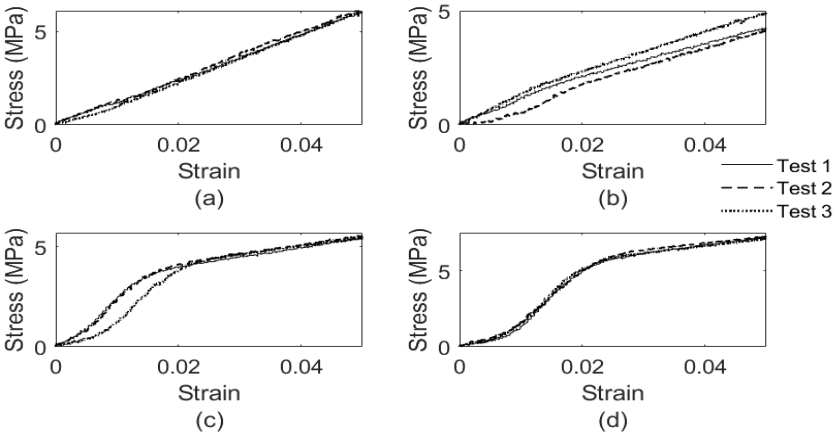

Figure 57: Results of the eccentric tests for sample trained under dynamic conditions with a spring constant of k = 0.0319 N/mm at temperatures of a) 25℃; b) 50℃; c) 80℃; and d) 110℃

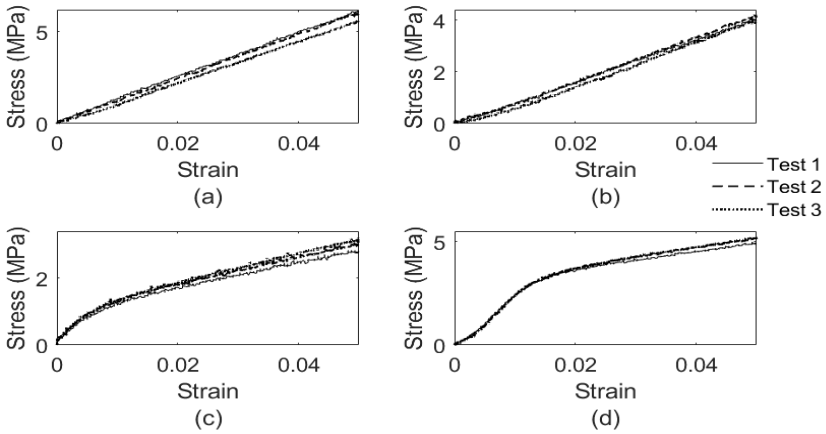

Figure 58: Results of the eccentric tests for sample trained under dynamic conditions with a spring constant of k = 0.0929 N/mm at temperatures of a) 25°C; b) 50°C; c) 80°C; and d) 110°C

Table 13: Average elastic modulus values for samples with different training conditions

Training Condition	**Average Modulus at 25°C (MPa)**	**Average Modulus at 50°C (MPa)**	**Average Modulus at 80°C (MPa)**	**Average Modulus at 110°C (MPa)**	**Range in Stiffness (Max./Min.)**
0.3 lb (Static)	115.67	263.35	380.19	386.17	3.34
0.7 lb (Static)	112.91	71.72	203.92	288.79	4.03
1.0 lb (Static)	119.02	59.65	64.50	180.76	3.03
k = 0.0319 N/mm (Dynamic)	123.96	145.07	301.34	398.21	3.21
k = 0.0929 N/mm (Dynamic)	122.41	87.87	181.78	287.09	3.27

From these results, the largest range in stiffness was observed for the samples trained against a static mass of 0.7 lb, where the stiffness increased by a factor of 4.03 between 50°C and 110°C. For the samples trained against static masses, there appears to be an optimal training load that yields the largest variation in stiffness. As previously mentioned, when higher training loads are used, additional space is introduced between the coils when the samples are in their relaxed state. The key to achieving larger magnitudes of stiffness in TCP actuators requires inter-coil contact. If more space is present between neighbouring coils, a higher magnitude of thermal stimulus is needed to achieve inter-coil contact. This is evident in the shape of the curves in Figures

54-56, where the steepest secondary region of the curve only appears at higher temperatures as the training load increased. When neighbouring coils are not in contact, the governing stiffness of the actuator is closer to the elastic modulus of the precursor fibre material, which is known to degrade with increasing temperature. This relationship presents another trade-off in performance where inter-coil contact may not be achieved if too much space is introduced between coils, whereas having minimal space between neighbouring coils leads to inherently stiffer actuators where the effect of the variation in stiffness is reduced.

For the samples trained under dynamic conditions, similar effects were observed to those seen when training under static conditions. While higher stresses were required to separate the coils and elongate the actuator at 110°C for the sample trained against the low stiffness spring, additional space was present between neighbouring coils for the sample trained against the high stiffness spring. This required a higher thermal stimulus to achieve inter-coil contact, as the modulus was reduced at a temperature of 50°C. When considering the minimum stiffness at 50°C instead of room temperature, the magnitude of the variation in stiffness is greater for the sample trained against the stiffer spring compared with the sample trained against the lower stiffness spring. When designing TCPs for use as variable stiffness actuators, testing should be performed at various training loads to find the optimal mass or spring constant specific to those samples, which yields the largest range of possible stiffness.

4.7 – Effects of Pre-Stretching Precursor Fibre

4.7.1 – Fabrication and Initial Properties

` The next parameter investigated were the effects of pre-stretching the precursor fibre, and subsequently increasing the anisotropy in thermal expansion, on the TCP actuator final performance. To achieve this, three strain values were selected around the yield point of the precursor fibre, attempting to reach approximately 2.5%, 5%, and 7.5% strain. Samples were cut to appropriate lengths, with the final length for all samples selected as 210 mm. The samples were tied to steel fishing rigs and connected to metal supports, which were then secured to either ends of the aluminum rods inside the Instron machine as shown in Figure 59. Using the Instron machine, the samples were stretched from their initial lengths to 210 mm and held in place inside the

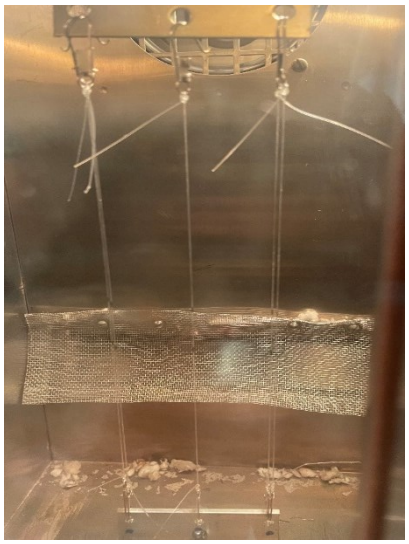

Figure 59: Inside view of Instron environmental chamber with precursor fibres being stretched to 5% and annealed

environmental chamber. The precursor fibres were then annealed at 80°C, with the samples retaining their length after approximately 4 hours. The fibres were left to cool for 24 hours and were later twisted and coiled using the fabrication rig. Since pre-stretching the fibre along its longitudinal axis also reduces the cross-sectional area, the coiling loads were adjusted accordingly to ensure the coiling stress was consistent between all samples. Table 14 presents the measured initial properties of the precursor fibres and associated final TCP actuators.

Table 14: Measured properties of TCP samples with pre-stretch introduced to precursor fibres

Sample Number	**1**	**2**	**3**
Precursor Fibre Initial Length (mm)	205	200	195
Precursor Fibre Final Length (mm)	210	210	210
Precursor Fibre Diameter (mm)	0.48	0.47	0.45
Measured Pre-Stretch in Precursor Fibre (%)	2.44	5.00	7.69
Final Coiled Length, L_0 (mm)	59.68	61.09	58.78
Length Contraction Factor (LCF)	3.45	3.40	3.57
Load Used During Coiling (g)	229.96	220.73	202.04

Coil Diameter D (mm)	0.99	0.99	0.98
Spring Index (C = D/d)	2.06	2.11	2.18
Average Motor Speed (rpm)	182	178	172
Number of Twists to Induce Coiling	118	111	105
Number of Twists to Fully Coil	191	184	178
Final Length After Annealing, L_i (mm)	59	59	57

4.7.2 – Isotonic Test Results

The TCP samples were placed inside the environmental chamber and coupled with the LVDT, and a static mass of 0.6 lb was suspended from the coupled ends. Starting at a temperature of 45°C and heating until 200°C, the tensile strokes of the actuators were measured as a function of temperature and plotted in Figure 60.

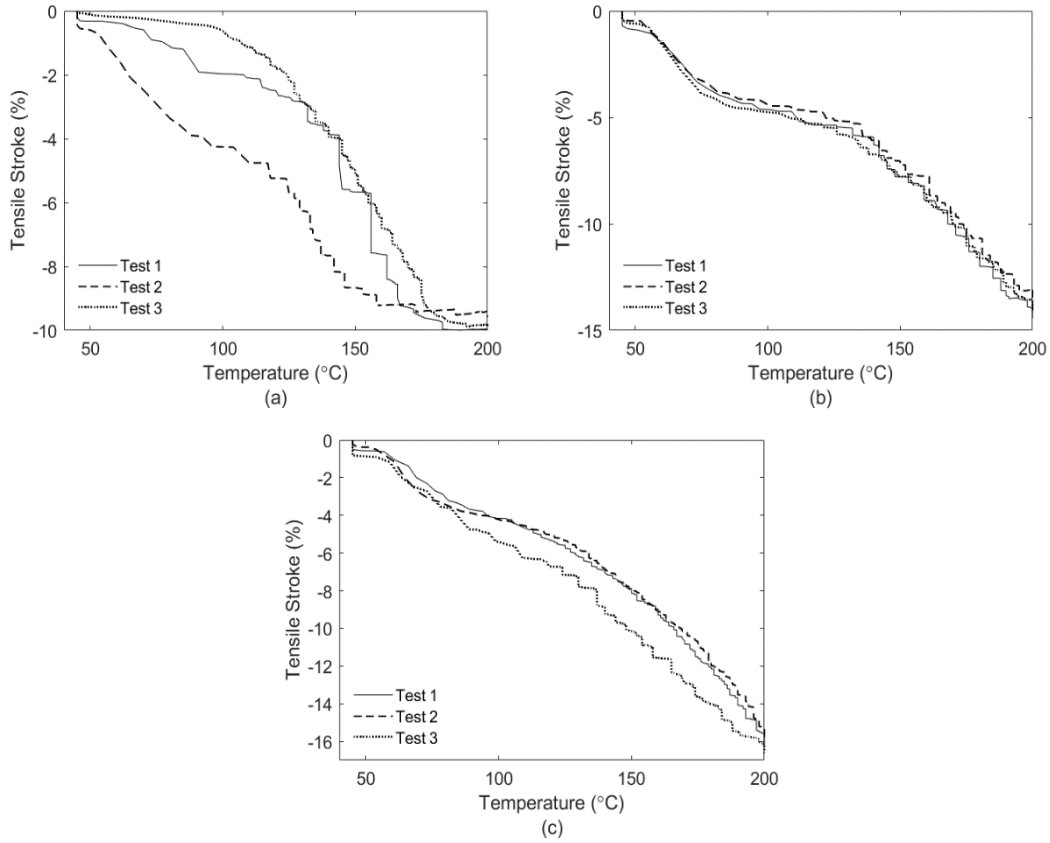

Figure 60: Results of isotonic tests for samples fabricated with a) 2.5%; b) 5%; and c) 7.5% pre-stretch in the precursor fibre

From these results, there is a clear trend between the amount of pre-stretch introduced in the precursor fibres and the tensile stroke of the final TCP actuators. For the samples stretched minimally to 2.44%, repeatable actuation strokes were observed in the range of 9.41% to 9.98%. In addition, all samples reached saturated contraction between approximately 175°C and 185°C as contact between neighbouring coils restricted any further contraction. For the samples stretched near the yield point to 5%, tensile stroke of the actuators increased to the range of 14.00% and 14.42%. When the precursor fibres were stretched further to 7.69%, tensile strokes of the TCP actuators also improved to between the ranges of 16.14% and 16.60%.

The results of the isotonic tests showed that improved tensile strokes can be achieved by introducing pre-stretch into the precursor fibres and annealing the samples. It is well understood that the degree of mismatch between the longitudinal and radial thermal expansion coefficients is a driving force behind tensile actuation of coiled muscles, where precursor fibre materials with the highest degree of mismatch between the coefficients are expected to produce the largest tensile strokes when coiled if other fabrication parameters are kept consistent. In this work, the degree of mismatch between the axial and radial thermal expansion coefficients were improved through pre-stretching the precursor fibre and annealing to set the shape of the extended tie chains within the material. This method proved effective at improving the anisotropy in thermal expansion, which was demonstrated in the improved tensile stroke of the coiled samples upon increased fibre pre-stretching.

4.7.3 – Isometric Test Results

Following the isotonic testing, the TCP samples were tested under isometric conditions. All slack was removed using the Instron machine and no preload was introduced to the samples. Starting at 45°C and heating to 200°C, the blocked force of the actuators was recorded as a function of temperature and is plotted in Figure 61.

Similar to the isotonic test results, there is a clear trend between the amount of pre-stretch introduced in the precursor fibres and the force generation capabilities of the TCP actuator. The fibres with the lowest amount of pre-stretch generated the largest blocked forces in the actuators between 1.94 N and 1.99 N. The precursor fibres that were stretched to 5% near the yield point, produced TCP actuators with reduced force generation between the ranges of 1.70 N and 1.74 N.

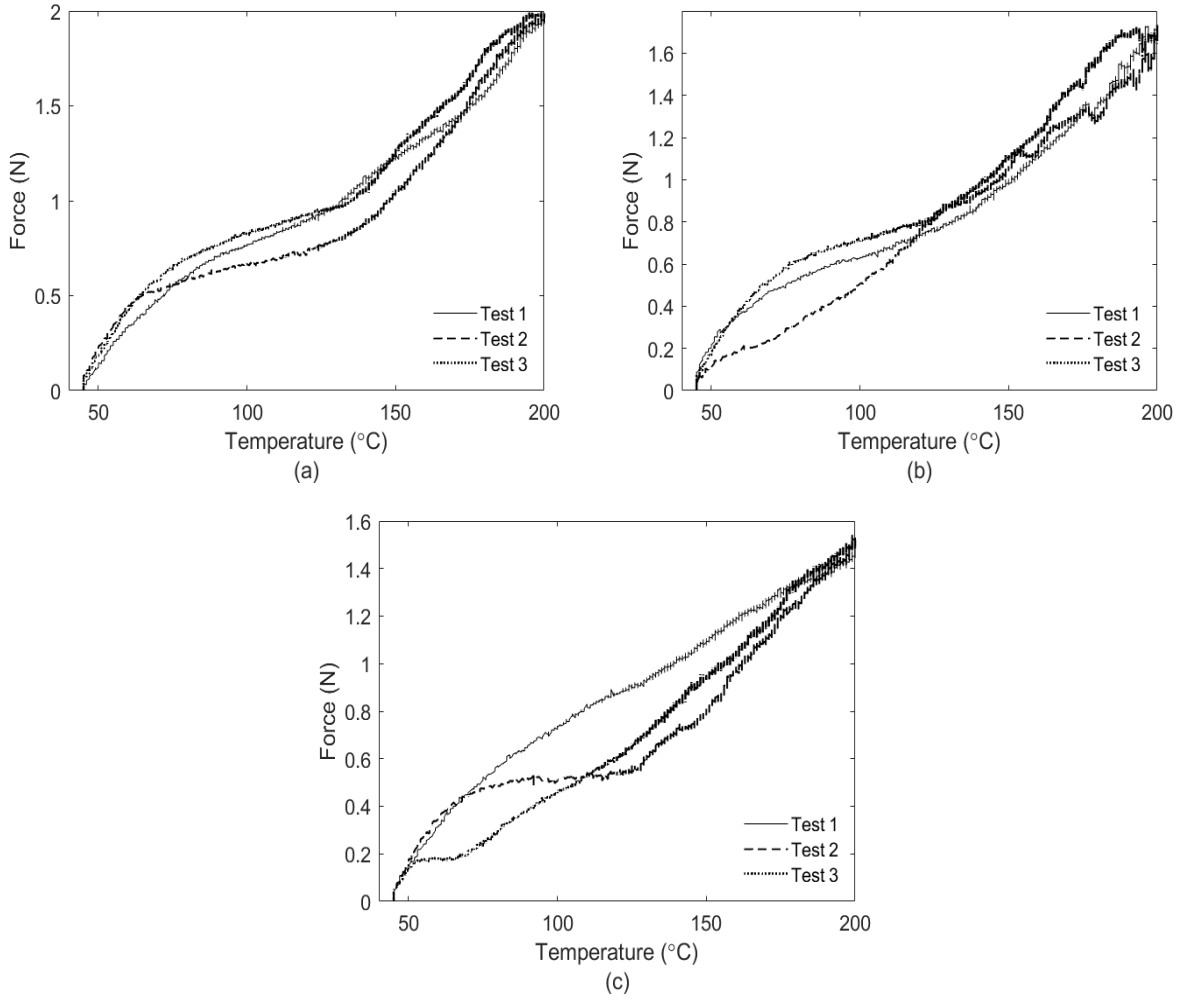

Figure 61: Results of isometric tests for samples fabricated with a) 2.5%; b) 5%; and c) 7.5% pre-stretch in the precursor fibre

When the fibres were stretched even further to 7.69%, the TCP actuators exhibited the lowest force generation capabilities with blocked forces between 1.52 N and 1.54 N.

These results show that as further stretch is introduced in the precursor fibre, especially in cases beyond the yield point of the fibre, the force generation capacity of the final TCP actuators quickly deteriorates. One explanation for these results is from the permanent plastic deformation resulting from chain slippage at higher magnitudes of pre-stretch. With increasing amounts of pre-stretch, both elastic deformation and viscous flow are generated within the precursor fibre. The high strength and force properties of the precursor fibre material and associated TCP actuator arises from the high degree of alignment between the constituent elements and the longitudinal axis of the fibre. If the fibre is stretched beyond its yield point, permanent deformation is expected to occur in the form of chain slippage which reduces this alignment and degrades the strength of the material. This results in a decreased force generation capacity when the pre-stretched fibres are

fabricated as TCP actuators and tested under isometric contractions. While pre-stretching the precursor fibres improves the anisotropy in thermal expansion and the tensile stroke of the TCP actuators, it comes at the expense of reduced force generation. Designers should weigh this trade-off in tensile stroke and force when manufacturing TCP actuators, such that the specific requirements of the application are met.

4.7.4 – Eccentric Test Results

Next, the effects of the amount of pre-stretch introduced in the precursor fibre, and its corresponding anisotropy in thermal expansion, on the variation in stiffness of the actuators was investigated. At steady temperatures of 25°C, 50°C, 80°C, and 110°C, the samples were loaded and unloaded at a rate of 5 mm per minute. Figures 62-63 show the loading curves for the samples made with varying levels of pre-stretch in the precursor fibre. From these curves, the slopes of the steepest region of the stress-strain diagrams were determined for each test. The average tensile moduli and magnitude of the variation in stiffness was calculated at all temperatures for each sample, and the results are presented in Table 15.

From these results, the magnitude of the variation in stiffness was lowest for the sample with the least amount of pre-stretch, increasing in stiffness by a factor of 1.92 from room temperature to 110°C. For the precursor fibres stretched to 5% and annealed, the variation in stiffness of the TCP actuator was measured as a factor of 2.12 between room temperature and

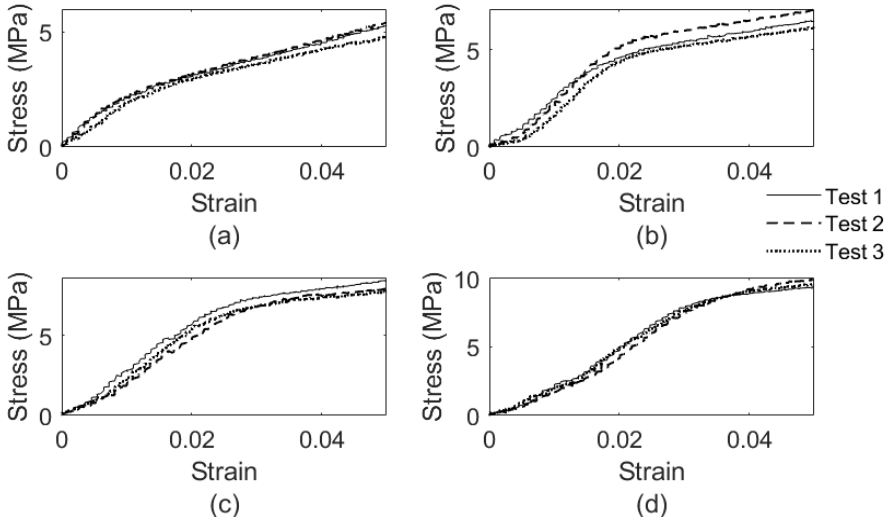

Figure 62: Results of the eccentric tests for sample fabricated with 2.5% pre-stretch in precursor fibre at temperatures of a) 25°C; b) 50°C; c) 80°C; and d) 110°C

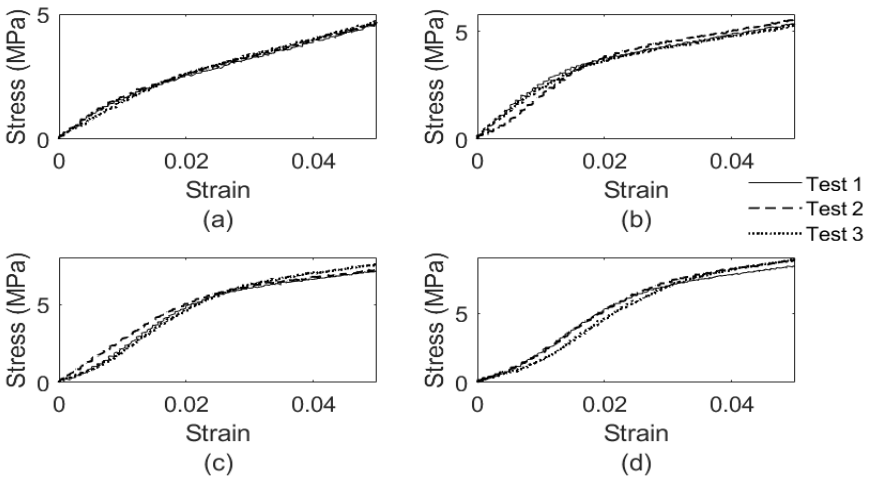

Figure 64: Results of the eccentric tests for sample fabricated with 5% pre-stretch in precursor fibre at temperatures of a) 25℃; b) 50℃; c) 80℃; and d) 110℃

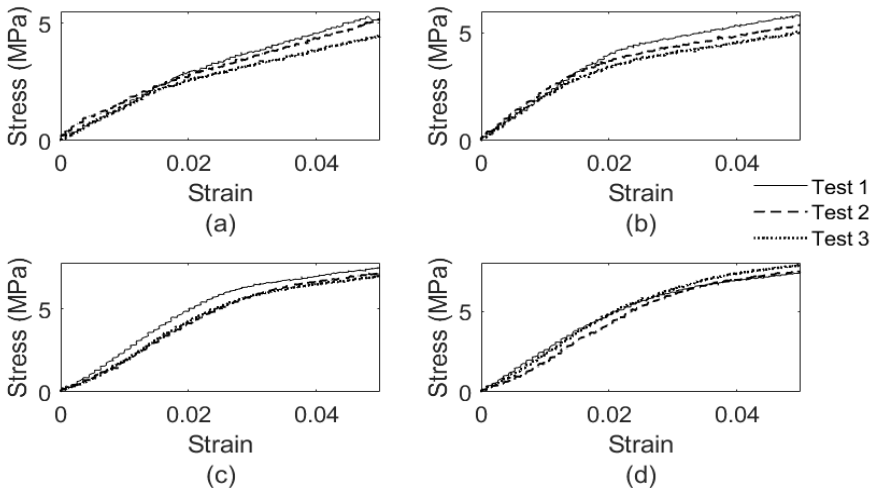

Figure 63: Results of the eccentric tests for sample fabricated with 7.5% pre-stretch in precursor fibre at temperatures of a) 25℃; b) 50℃; c) 80℃; and d) 110℃

110℃. The magnitude of the variation in stiffness increased further with increasing levels of precursor fibre pre-stretch, however the variation in stiffness for the samples with approximately 7.5% pre-stretch is not significantly higher than the range of achievable stiffnesses for the sample stretched to 5%, increasing only by a factor of 2.13 throughout the full temperature range.

Table 15: Average elastic modulus values for samples with different levels of pre-stretch in precursor fibre

Test Condition	Average Modulus at 25°C (MPa)	Average Modulus at 50°C (MPa)	Average Modulus at 80°C (MPa)	Average Modulus at 110°C (MPa)	Range in Stiffness (Max./Min.)
2.5% Pre-Stretch	203.05	325.28	346.96	390.69	1.92
5% Pre-Stretch	160.76	271.75	308.13	340.27	2.12
7.5% Pre-Stretch	140.55	215.62	256.45	298.67	2.13

This indicates there may be an optimal level of pre-stretch to be introduced in the sample to obtain the largest magnitude of variation in stiffness, where the strength of the actuator may degrade with increasing amounts of precursor fibre pre-stretch. This is also apparent when comparing the moduli at constant temperatures for different levels of pre-stretch in Table 15. In all cases, when comparing at the same ambient temperature, the tensile modulus of the samples tends to decrease with increasing levels of pre-stretch. This is consistent with the observations made during the isometric testing, where increased pre-stretching of the precursor fibre had a negative impact on the force generation capacity of the coiled muscles. Additional experiments should be conducted using a wider range of precursor fibre pre-stretch values to investigate what optimal levels of pre-stretch are necessary to achieve the widest range of stiffness for a given actuator.

4.8 – Effects of Stretching Coiled Samples During Annealing

4.8.1 – Fabrication and Initial Properties

The final parameter investigated was the effects of stretching the coiled samples during annealing on the final actuator performance. First, samples of 0.48 mm diameter nylon-6 were cut to approximately 300 mm in length and attached to the fabrication rig. All parameters during twisting and coiling were controlled during this set of experiments. Once the samples had fully coiled, they were placed on the oven rack with varying levels of pre-stretch, as shown in Figure

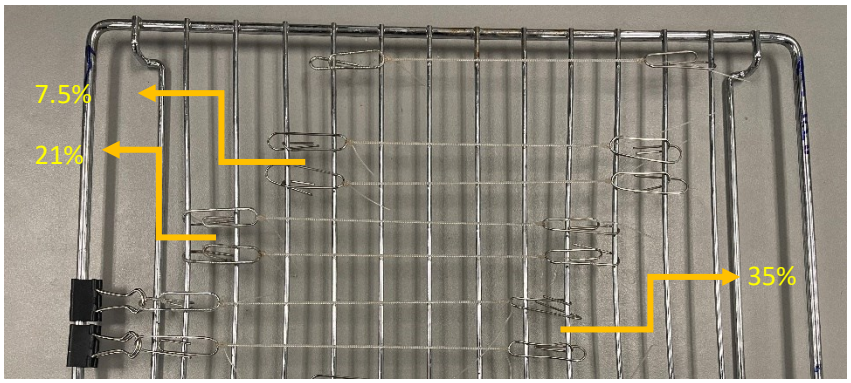

Figure 65: Oven rack with samples stretched to desired lengths in preparation for annealing

65. Three magnitudes were selected and approximated to reach 7.5%, 21%, and 35% pre-stretch of the coiled samples, with the goal to introduce space between neighbouring coils after annealing. It was found that annealing the samples for 3 hours at 170℃ was sufficient in retaining the structure of the coiled samples and removing any residual stresses. Table 16 presents the measured initial properties of the TCP samples made with varying levels of pre-stretch during annealing. While most of the strain of the samples was elastically recovered after removing them from the wire rack, some of the strain remained in the form of plastic deformation as neighbouring coils had additional space between them.

Table 16: Measured properties of TCP samples with pre-stretch introduced during annealing

Sample Number	**1**	**2**	**3**
Precursor Fibre Initial Length (mm)	301	298	300
Final Coiled Length, L_0 (mm)	88.21	88.02	88.77
Length Contraction Factor (LCF)	3.41	3.39	3.38
Coil Diameter D (mm)	0.97	0.98	0.98
Spring Index (C = D/d)	2.02	2.04	2.04
Average Motor Speed (rpm)	231	235	248
Number of Twists to Induce Coiling	170	177	177
Number of Twists to Fully Coil	284	286	285
Load Used During Coiling (g)	261.92	261.92	261.92

Measured Length During Annealing (mm)	95.21	107.02	119.77
Measured Pre-Stretch During Annealing (%)	7.94	21.59	34.92
Final Length After Annealing, L_i (mm)	90	92	94

4.8.2 – Isotonic Test Results

To investigate the effects of pre-stretching the TCP samples during annealing, and consequently introducing additional space between neighbouring coils, the samples were tested following the isotonic experimental setup. Samples were secured to the LVDT inside the environmental chamber, and a static mass of 0.6 lb was suspended off the coupled ends as the actuating load. The TCP samples were heated from 45°C to 200°C, while the LVDT recorded the

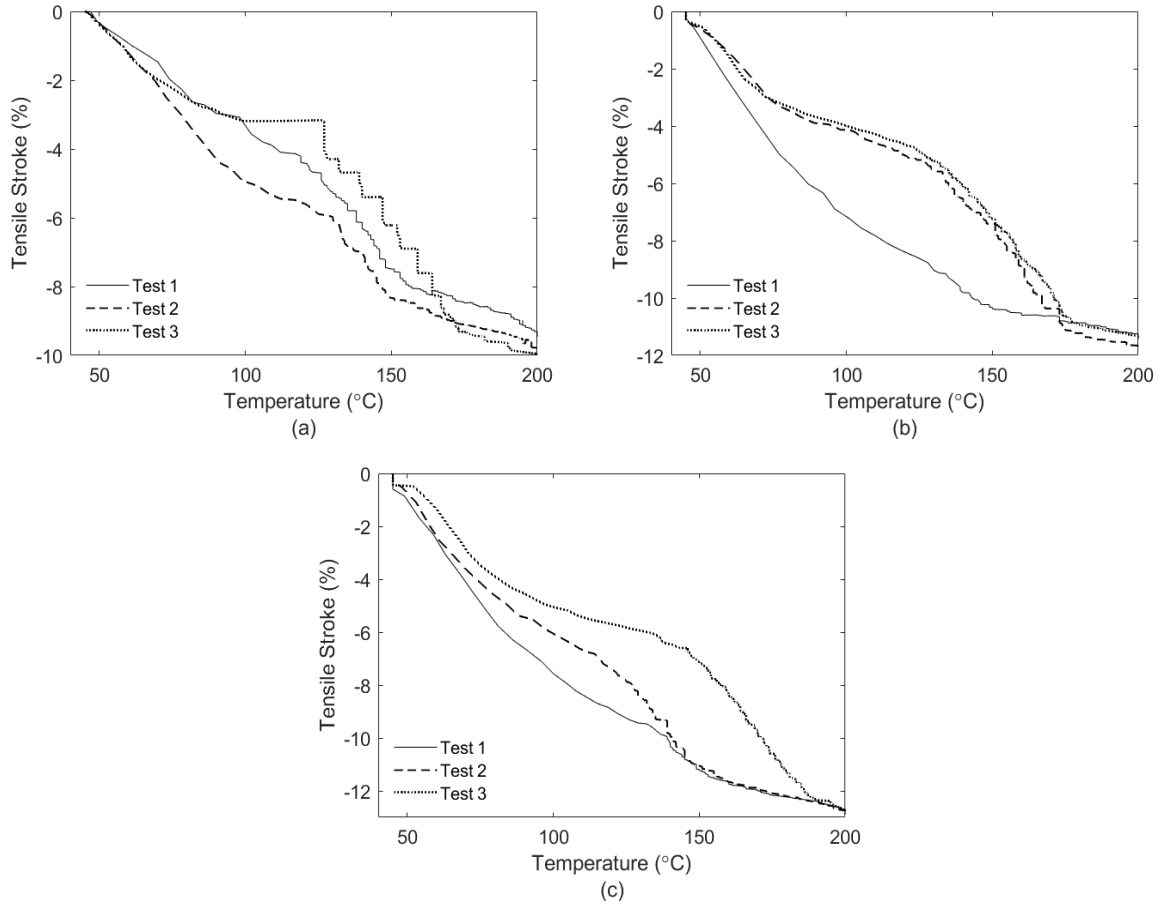

Figure 66: Results of isotonic tests for samples fabricated with a) 7.5%; b) 21%; and c) 35% pre-stretch in the coiled samples during annealing

tensile stroke. Figure 66 shows the results of the isotonic tests for samples made with varying levels of pre-stretch during the annealing process.

From these experiments, there is a noticeable trend between the level of pre-stretch introduced in the TCP samples during annealing, and the tensile stroke capacity during isotonic testing. For the samples with 7.94% pre-stretch during annealing, repeatable tensile strokes were observed in the range of 9.42% to 9.99%. For the samples with moderate pre-stretch of 21.59%, tensile stroke improved to between 11.37% and 11.78%. As the pre-stretch increased to 34.92% and additional space was present between neighbouring coils, the tensile stroke of the TCP samples improved once more to the range of 12.80% to 12.83%.

These results show that when actuating against the same external load, coiled samples fabricated with increased pre-stretching in the annealing process are able to achieve higher tensile strokes. When fabricating the TCP samples, if all properties are kept consistent including the amount of inserted twist, the primary change occurring as the samples are pre-stretched during annealing is the amount of space introduced between neighbouring coils. After the samples have been annealed and cooled to their initial resting length, the samples with the largest amount of pre-stretch were measured to be the longest before commencing actuation tests due to the increased space between neighbouring coils. Once the external actuating load was applied, the samples with higher pre-stretch were also able to extend further when loaded, allowing the actuator to access a wider range of coil bias angles throughout the temperature range of the tests. One limiting factor to the tensile stroke of any TCP actuator is the point of inter-coil contact between neighbouring coils which saturates any further contraction. This negative effect can be mitigated by introducing different magnitudes of pre-stretch into the coiled samples during the annealing process.

4.8.3 – Isometric Test Results

The next stage of this investigation involves capturing the effects of the pre-stretch during annealing on the force generation capacity of the TCP samples. This is achieved through testing the samples under isometric conditions. First, the samples are secured to the aluminum rods inside the environmental chamber, and the Instron machine is used to align the samples such that any slack is removed, and no initial preload is present in the sample. Next, the samples are heated from 45°C to 200°C as the blocked force of the actuator is recorded by the load cell. Figure 67 presents

the results of the isometric tests for samples made with varying levels of pre-stretch during annealing.

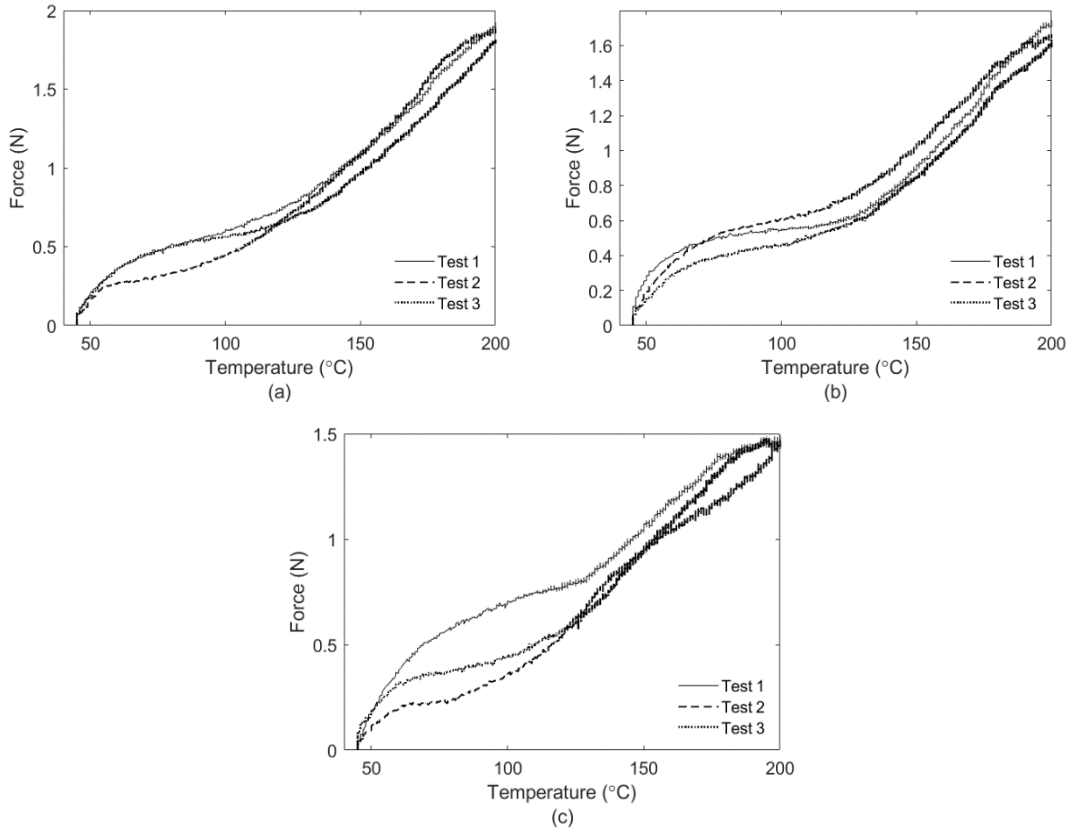

Figure 67: Results of isometric tests for samples fabricated with a) 7.5%; b) 21%; and c) 35% pre-stretch in the coiled samples during annealing

Similar to the isotonic results, there is a clear trend between the level of pre-stretch in the TCP samples and the force generation capabilities of the actuator during isometric contraction. For the samples with the lowest pre-stretch during annealing, blocked forces were measured in the range of 1.80 N to 1.92 N. When the pre-stretch in the TCP samples was increased to 21.59%, the measured blocked forces decreased to between 1.64 N and 1.75 N. Finally, for the samples with the maximum pre-stretch during annealing of 34.92%, the blocked forces generated were reduced even further to between 1.47 N and 1.49 N.

These results illustrate that another trade-off is present between the tensile stroke and force generation capacities for samples made with varying levels of pre-stretch during annealing, where TCP samples annealed with higher levels of pre-stretch are able to achieve larger tensile strokes at the expense of decreased force generation. When fabricating TCP actuators, it is critical to ensure enough space is introduced between the coils for the actuator to achieve sufficient

contraction for the application. However, if too much space is introduced, the force generation capacity of the muscle begins to diminish. One explanation for this result is that as the coil length is extended, the underlying twisted bundle within the coil begins to untwist. This reduces the torsional capacity of the twisted bundle, which ultimately limits the tensile performance of the coiled structure. Depending on the specific requirements of the final application of the actuators, designers should carefully consider the magnitude of pre-stretch in the samples during annealing to ensure the stroke and force requirements are both met, while minimizing the negative impacts of the trade-off.

4.8.4 – Eccentric Test Results

Finally, the effects of the levels of pre-stretch introduced to the TCP during annealing on the variation in stiffness properties of the actuator were investigated. Samples were secured to the aluminum rods following the eccentric experimental setup, and were kept at constant temperatures of 25°C, 50°C, 80°C, and 110°C inside the environmental chamber during testing. At a rate of 5 mm per minute, the samples were loaded and unloaded, and the force and elongation data were recorded through the LabVIEW software. Figures 68-70 show the results of the loading curves for samples annealed with different levels of pre-stretch.

For each test, the tensile modulus of the actuator was determined by calculating the slope of the steepest region of the curves in Figures 68-70. The average modulus for each temperature was calculated for all samples, along with the magnitude of the variation in stiffness. These results are presented in Table 17.

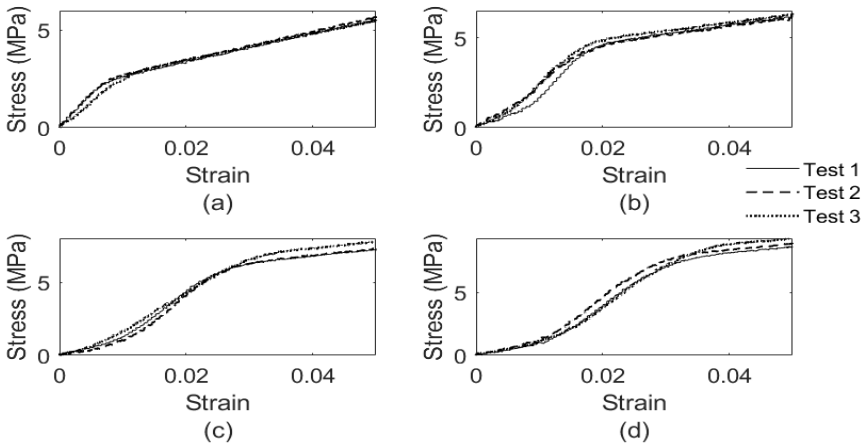

Figure 68: Results of the eccentric tests for sample fabricated with 7.5% pre-stretch in coiled sample during annealing at temperatures of a) 25°C; b) 50°C; c) 80°C; and d) 110°C

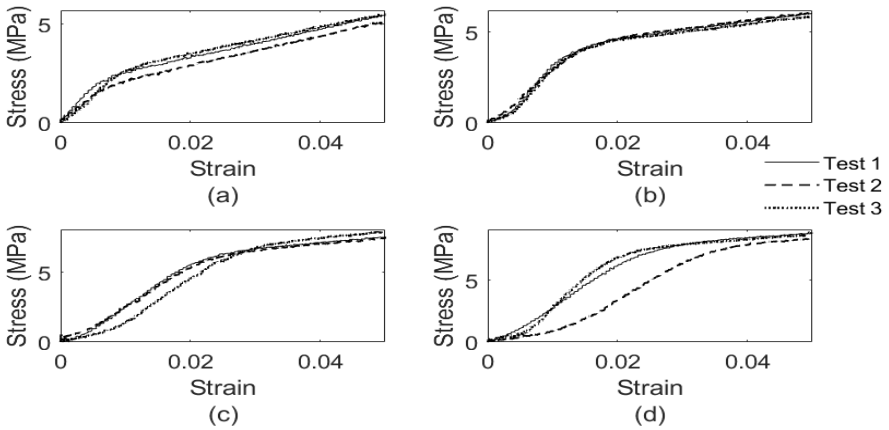

Figure 69: Results of the eccentric tests for sample fabricated with 21% pre-stretch in coiled sample during annealing at temperatures of a) 25°C; b) 50°C; c) 80°C; and d) 110°C

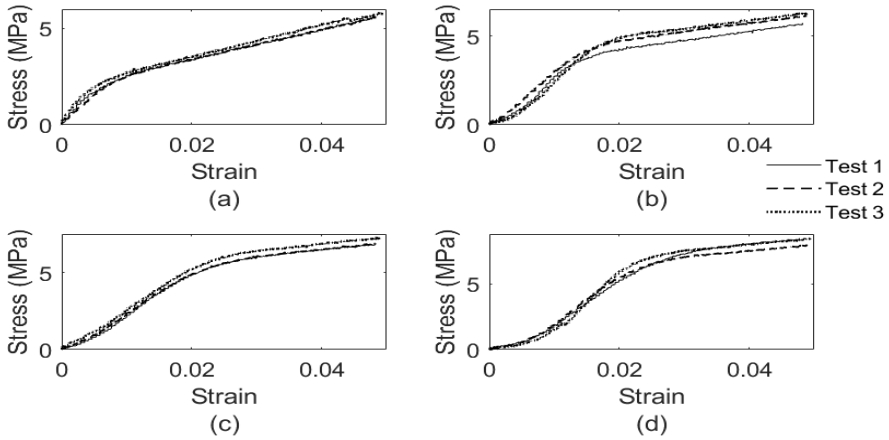

Figure 70: Results of the eccentric tests for sample fabricated with 35% pre-stretch in coiled sample during annealing at temperatures of a) 25°C; b) 50°C; c) 80°C; and d) 110°C

Table 17: Average elastic modulus values for samples with different levels of TCP pre-stretch during annealing

Test Condition	**Average Modulus at 25°C (MPa)**	**Average Modulus at 50°C (MPa)**	**Average Modulus at 80°C (MPa)**	**Average Modulus at 110°C (MPa)**	**Range in Stiffness (Max./Min.)**
7.5% Pre-Stretch	293.44	378.30	396.34	425.95	1.45
21% Pre-Stretch	284.63	327.84	352.21	391.52	1.38
35% Pre-Stretch	281.18	317.37	324.45	374.54	1.33

Results show another clear trend between the amount of pre-stretch in the coiled samples during annealing and the magnitude of the variation in stiffness achieved. The sample with the lowest amount of pre-stretch had the largest variation in stiffness, increasing by a factor of 1.45 between room temperature and 110°C. In contrast, the sample with the largest amount of pre-stretch had the lowest magnitude of variation in stiffness, increasing by a factor of 1.33 between room temperature and 110°C. In all cases, a temperature of 50°C was sufficient in reaching inter-coil contact between neighbouring coils, as is evident in the shape of the curves in Figures 68-70.

Similar to the observations seen during the isometric testing, increased pre-stretching of the coiled samples prior to annealing tends to reduce the effective force capacity and strength of the actuators once the coiled structure is set. This is clear when comparing the moduli at each temperature for the samples with varying levels of pre-stretch, where the modulus at each temperature showed to decrease with increasing levels of pre-stretch. When considering the actuators for high-force applications, or if a wide range of variable stiffness are desired, designers should avoid introducing additional space between coils during the annealing process beyond what is required to meet the stroke requirements of the actuator.

4.9 – Summary of Experimental Results

Throughout this chapter, eight fabrication and operation parameters were experimentally evaluated to investigate their effects on the final TCP actuator performance including the tensile stroke, the generated force capacity, and the range in stiffness. Each experiment produced consistent data that led to many conclusive, and some inconclusive trends. For convenience, and to serve as guidance in the future design of TCP actuators, a summary of each design parameter and their respective effects on the tensile stroke, force generation capacity, and variable stiffness properties of the actuator is presented in Table 18. It should be noted the quantitative values presented are specific to the material, fabrication, and experimental methodologies employed in this work. Designers should consider these values as qualitative trends and validate the results for each unique experimental setup when designing TCP actuators. Lastly, Appendix A presents the average values and standard deviations for all tests conducted in Chapter 4.

Table 18: Summary of experimental results and relationships between the investigated parameters and the final performance of the TCP actuator

Design Parameter	Change	Effect on Tensile Stroke	Effect on Force Generation	Effect on Range of Variable Stiffness
Operating Conditions	Increase in applied load	Increase from 9.65% to 16.18% (Decrease to 5.65% for maximum applied load)	Decrease from 2.60 N (Blocked Force) to 1.25 N	Increase in variation in stiffness factor from 2.13 to 2.31
	Increase in strain rate			Minimal effect on hysteresis
Precursor Fibre Diameter	Increase in precursor fibre diameter	No change if actuating stress is kept constant	Increase from 0.67 N to 6.78 N	Increase in variation in stiffness factor from 2.53 to 4.89 (decrease to 2.00 for largest fibre diameter)
Spring Index	Increase in spring index	Increase from 7.70% to 13.70%	Decrease from 3.01 N to 1.71 N	Increase in variation in stiffness factor from 1.63 to 1.69
Coil Bias Angle	Increase in coil bias angle	Increase from 9.80% to 14.20%	Decrease from 2.18 N to 1.44 N	Increase in variation in stiffness factor from 1.44 to 3.16
Twist Insertion Speed	Increase in twist insertion speed	Negligible effect	Negligible effect	Inconclusive
Training Conditions	Increase in training load (Static)	Minimal effect if actuating stress is kept constant	Increase from 1.66 N to 2.73 N	Increase in variation in stiffness factor from 3.34 to 4.03 (Decrease to 3.03 for maximum training load)
	Increase in spring constant (Dynamic)		Increase from 1.81 N to 2.58 N	Increase in variation in stiffness factor from 3.21 to 3.27
Pre-Stretching Precursor Fibre	Increase in precursor fibre pre-stretch	Increase from 9.41% to 16.60%	Decrease from 1.99 N to 1.52 N	Increase in variation in stiffness factor from 1.92 to 2.13
Pre-Stretching Coiled Sample During Annealing	Increase in pre-stretch of coiled sample during annealing	Increase from 9.42% to 12.83%	Decrease from 1.92 N to 1.47 N	Decrease in variation in stiffness factor from 1.45 to 1.33

Chapter 5

Conclusions and Recommendations for Future Work

5.1 – Conclusions

The objective of this thesis was to characterize the mechanical and thermal behaviours of TCP actuators to assist with the fabrication of unique actuators that can be designed to satisfy a specific set of design criteria or requirements. A literature review survey was conducted to gain a thorough understanding of the working mechanisms behind TCP actuation, and to identify any design parameters that may influence the final performance of the actuators. This led to the detection of gaps in the current research which required further investigation. Specifically, reported results in the literature lacked consistency and insufficient repeatability in the fabrication process. Eight fabrication and operation parameters were identified for their potential effects on the final performance of the actuator, which included the tensile stroke, generated actuator force, and range in stiffness. These parameters lacked comprehensive characterization collectively and required further investigation to study their effects on the final actuator performance.

With the identification of these critical parameters, a custom fabrication setup was built to enable the independent control of each parameter. Additionally, three experimental setups were designed to mimic isotonic contraction, isometric contraction, and eccentric contraction. The custom fabrication setup was used to create TCP prototypes where all fabrication and operation parameters were controlled except for the target parameter which was varied. Testing of these prototypes following the three experimental setups led to a comprehensive experimental evaluation of the quasi-static behaviour of TCPs, along with identification of several relationships between specific fabrication and operation parameters and the final performance of the actuators.

Analysis of the isotonic tests provided many relationships between individual design parameters and the effect on the tensile stroke of the actuator. First, an optimal actuating load can yield the maximum tensile stroke for a given actuator. To achieve increased tensile stroke, improving the anisotropy in thermal expansion through pre-stretching and annealing the precursor

fibre was effective at improving the stroke of the coiled actuator. Furthermore, coiled samples that had increased amounts of pre-stretching during the annealing process achieved higher tensile strokes as additional space was present between neighbouring coils. Conversely, samples exhibited poorer tensile stroke performance when higher coiling loads were used to create samples with low spring indices, or if the sample twist density was increased, which reduced the coil bias angle. Tensile stroke was independent of the precursor fibre diameter if the coiling and actuating stresses were constant between samples, and the twist insertion speed also had a negligible effect on the tensile stroke. When adjusting the actuator training load, tensile stroke was also not influenced by the change except for minor changes in sample length observed during the first set of tests.

Similarly, the analysis from the isometric contraction tests provided further insight into the relationships between fabrication parameters and the actuator force generation capacity. In all cases, actuation forces of TCPs were highest when no initial preload was introduced, and the forces measured are the blocked forces. To fabricate actuators with larger force generation capacities, designers could use precursor fibres with larger diameters, or employ training techniques using heavier static masses or stiffer extension springs. In contrast, increasing the spring index using a lower coiling load reduced the effective force generation of the actuator, presenting a noticeable trade-off in performance between the tensile stroke and force generation. A similar trade-off was observed for the effects of the twist density and coil bias angle, where samples with lower twist densities and higher coil bias angles produced smaller blocked forces. For both parameters involving pre-stretching, consistent trends were observed where actuators generated weaker forces with increasing levels of pre-stretch. The twist insertion speed during fabrication was determined to have a negligible effect on the force generation of the actuators.

The final performance metric evaluated was the range in stiffness. This effect was found to be largest when using precursor fibre of increasing diameter, however this trend did not hold up for the largest fibre diameter of 0.71 mm. The training conditions also exhibited a noticeable effect on the variation in stiffness, where optimal static loads and spring constants should be determined for each unique actuator. Pre-stretching the precursor fibre also showed an increasing trend in the magnitude of the variation in stiffness, however there may be an optimal level of pre-stretch that yields the widest range of achievable stiffness. When evaluating the samples prepared with different spring indices, the magnitude of the variation in stiffness increased with increasing spring

index. Another trend that was observed but with minimal variance was the amount of pre-stretch introduced to the TCP sample during annealing. Samples with the lowest amount of pre-stretch exhibited the widest range of stiffness, however the magnitude of this range was not as notable as other parameters investigated. Some trends were found to have negative impacts on the variable stiffness attributes, including increasing the twist density beyond what is required to fully coil the sample. If an application requires a wide range of stiffness values, designers should avoid inserting additional twists into the sample. Finally, no detectable trend was observed between the twist insertion speed and the variable stiffness properties, however further analysis is required to validate these observations.

5.2 – Recommendations for Future Work

In this thesis, the scope primarily focused on the characterization of actuator parameters and their effects on the final actuator performance, namely the tensile stroke, force generation, and range in stiffness. While these performance metrics are critical in the design of TCP actuators, analyses of additional performance metrics are required before these materials can be implemented in upscaled soft actuator designs. Since these actuators are to be operated primarily under quasi-static conditions, additional creep and stress relaxation tests should be performed to evaluate how these materials perform when subjected to constant loading over long periods of time. Furthermore, the energy dissipation behaviours of TCPs are of significant importance in the design of variable stiffness actuators and should be further explored to investigate the effects of the individual design parameters on the hysteresis in the activation and relaxation cycles.

While many trends were identified between fabrication and operation parameters and the final actuator performance, the prototypes fabricated for each control parameter were not intended to be compared with one another. The key to adopting these materials in suitable variable stiffness actuator designs is finding the optimal combination of design parameters that would yield the desired set of performance requirements, while minimizing the negative impacts and effects of any trade-offs. Additional research should be conducted to identify what optimal combination of design traits should be used to meet a prescribed range of requirements, along with the determination of any parameters that may be dependent on one another. This will assist future designers in not only knowing which parameters to combine to achieve the desired final actuator

performance, but also which parameters should be avoided to mitigate the effects of any limitations in performance.

Although this work was effective in the primary objective of characterizing the fabrication-performance relationships of specific design parameters, the data obtained is insufficient to obtain an accurate model or simulation of these actuators. This was mainly due to sources of experimental error during both fabrication and testing of the prototypes, which negatively influenced the accuracy of these results. Further improvements to both the fabrication rig and experimental testing setups should be considered to refine the data and validate the observed trends.

To start, the bushings within the slider on the fabrication rig did not fit perfectly relative to the sliding rails, leaving minor gaps in between. During twisting of the precursor fibres, the rope connecting the mass to the slider would occasionally rotate the slider, causing friction between the bushings and the sliding rails. This forced the motor speed to slow down as additional torque was required to continue inserting twists. A similar issue was observed in the bearings that assist in translating the mass vertically during twisting, where occasionally the shaft would stick causing uneven tension in the precursor fibre during twisting and coiling. These effects can be reduced by replacing the bushings, bearings, and sliding rails to minimize the friction between moving components in the fabrication rig. Next, the motor speed was controlled manually with a rotary potentiometer and was difficult to control since the torque on the motor shaft built up with increasing fibre twists. Future iterations of the fabrication rig should include a control system with a feedback loop to accurately account for the changes in motor speed during twist insertion. Lastly, it was observed that a common point of failure during testing of the TCP prototypes was at the attachment point between the fibre and the end connections. This was mitigated by switching the knot type from a standard double knot to a Palomar knot, however additional knot types or use of clamps should be explored when actuating against heavier loads.

All temperatures used in this work were based off the approximated glass transition temperature of the material found in Chapter 3. As specific thermal properties of commercially available precursor fibres are not often available, these critical properties should be determined experimentally through reliable methods such as differential scanning calorimetry, thermomechanical analyses, or dynamic mechanical analyses. When testing the prototypes during the isotonic and isometric contractions, the temperature recorded through LabVIEW was the

ambient temperature within the environmental chamber. While this gives a fair estimation of the current temperature of the actuator, improved methods could be used to measure the temperature of the sample during actuation such as infrared imaging or placing thermocouples at the surface of the actuators along its length. The elevated temperatures during actuation presented additional problems during testing, where the internal components within the load cell were effected at high temperatures when positioned near the environmental chamber. As the temperature increased, components within the load cell would begin to expand, inducing compressive forces in the sensor. The net result was a reduction in the generated force reading of the TCPs in some instances at elevated temperatures. This was alleviated by mounting an air conditioning unit with the experimental setup to regulate the load cell temperature; however, some tests had to be repeated if the ducting was not positioned properly around the load cell. Future experiments should consider using a load cell with a higher operating temperature range or finding more reliable countermeasures to control the internal load cell temperature.

While the magnitudes of the tensile strokes, generated forces, and stiffness values calculated at the end of each test were representative of the true performance of the actuators, the activation and relaxation curves between the start and end points of each test could be improved. This is critical for future implementation of these actuators into upscaled devices, where specific control of these metrics as a function of temperature are necessary. First, when testing under isometric or eccentric contraction, in many cases some slippage occurred between the paperclips and the aluminum rods as the samples were heated or elongated. This caused a near instantaneous drop in the loading curves, effecting the rest of the force values for that test. Similarly, when loading the samples at higher loads, the paperclips in some cases were prone to bending, which negatively effected the force readings. These effects can be resolved by using stronger attachment types at the ends of the samples, and ensuring they are fixed to the ends of the aluminum rods with no space to rotate. Lastly, when testing under isotonic contractions, the LVDT core had some minor curvature and would slide against the core walls of the LVDT. This friction would prevent further actuation stroke, up until the actuation force exceeded the friction force within the core. At this point, large spikes were observed in the actuation curves as the actuator quickly contracts, making it difficult to predict the true stroke within those temperature ranges. Future experiments should ensure that minimal friction is present between the core and the LVDT or employ alternative sensing techniques to measure the actuator displacement.

References

[1] S. C. Government of Canada, "A demographic, employment and income profile of Canadians with disabilities aged 15 years and over, 2017," Nov. 28, 2018. https://www150.statcan.gc.ca/n1/pub/89-654-x/89-654-x2018002-eng.htm (accessed May 16, 2021).

[2] A. S. Gorgey, "Robotic exoskeletons: The current pros and cons," *World J. Orthop.*, vol. 9, no. 9, pp. 112–119, Sep. 2018, doi: 10.5312/wjo.v9.i9.112.

[3] S. M. Mirvakili and I. W. Hunter, "Artificial Muscles: Mechanisms, Applications, and Challenges," *Adv. Mater.*, vol. 30, no. 6, p. 1704407, 2018, doi: https://doi.org/10.1002/adma.201704407.

[4] D. Kongahage and J. Foroughi, "Actuator Materials: Review on Recent Advances and Future Outlook for Smart Textiles," *Fibers*, vol. 7, no. 3, Art. no. 3, Mar. 2019, doi: 10.3390/fib7030021.

[5] T. Mirfakhrai, J. D. W. Madden, and R. H. Baughman, "Polymer artificial muscles," *Mater. Today*, vol. 10, no. 4, pp. 30–38, Apr. 2007, doi: 10.1016/S1369-7021(07)70048-2.

[6] J. Zhang *et al.*, "Robotic Artificial Muscles: Current Progress and Future Perspectives," *IEEE Trans. Robot.*, vol. 35, no. 3, pp. 761–781, Jun. 2019, doi: 10.1109/TRO.2019.2894371.

[7] R. Samatham *et al.*, "Active Polymers: An Overview," in *Electroactive Polymers for Robotic Applications: Artificial Muscles and Sensors*, K. J. Kim and S. Tadokoro, Eds. London: Springer, 2007, pp. 1–36. doi: 10.1007/978-1-84628-372-7_1.

[8] C. Sun, Y. Wang, C. Zhang, E. Zhou, and J. Su, "A modified self-consistent computational model for an electrostrictive graft elastomer," *Smart Mater. Struct.*, vol. 17, no. 2, p. 025007, Feb. 2008, doi: 10.1088/0964-1726/17/2/025007.

[9] F. Bauer, "Review on the properties of the ferrorelaxor polymers and some new recent developments," *Appl. Phys. A*, vol. 107, no. 3, pp. 567–573, Jun. 2012, doi: 10.1007/s00339-012-6831-8.

[10] R. H. Baughman *et al.*, "Carbon Nanotube Actuators," *Science*, vol. 284, no. 5418, pp. 1340–1344, May 1999, doi: 10.1126/science.284.5418.1340.

[11] J. Foroughi *et al.*, "Torsional Carbon Nanotube Artificial Muscles," *Science*, vol. 334, no. 6055, pp. 494–497, Oct. 2011, doi: 10.1126/science.1211220.

[12] M. D. Lima *et al.*, "Electrically, Chemically, and Photonically Powered Torsional and Tensile Actuation of Hybrid Carbon Nanotube Yarn Muscles," *Science*, vol. 338, no. 6109, pp. 928–932, Nov. 2012, doi: 10.1126/science.1226762.

[13] M. D. Lima *et al.*, "Efficient, Absorption-Powered Artificial Muscles Based on Carbon Nanotube Hybrid Yarns," *Small*, vol. 11, no. 26, pp. 3113–3118, 2015, doi: https://doi.org/10.1002/smll.201500424.

[14] J. A. Lee *et al.*, "Electrochemically Powered, Energy-Conserving Carbon Nanotube Artificial Muscles," *Adv. Mater.*, vol. 29, no. 31, p. 1700870, 2017, doi: https://doi.org/10.1002/adma.201700870.

[15] R. H. Baughman, A. A. Zakhidov, and W. A. de Heer, "Carbon Nanotubes--the Route Toward Applications," *Science*, vol. 297, no. 5582, pp. 787–792, Aug. 2002, doi: 10.1126/science.1060928.

[16] J. D. W. Madden *et al.*, "Artificial muscle technology: physical principles and naval prospects," *IEEE J. Ocean. Eng.*, vol. 29, no. 3, pp. 706–728, Jul. 2004, doi: 10.1109/JOE.2004.833135.

[17] T. L. Buckner and R. Kramer-Bottiglio, "Functional fibers for robotic fabrics," *Multifunct. Mater.*, vol. 1, no. 1, p. 012001, Aug. 2018, doi: 10.1088/2399-7532/aad378.

[18] T. J. White and D. J. Broer, "Programmable and adaptive mechanics with liquid crystal polymer networks and elastomers," *Nat. Mater.*, vol. 14, no. 11, Art. no. 11, Nov. 2015, doi: 10.1038/nmat4433.

[19] R. S. Kularatne, H. Kim, J. M. Boothby, and T. H. Ware, "Liquid crystal elastomer actuators: Synthesis, alignment, and applications," *J. Polym. Sci. Part B Polym. Phys.*, vol. 55, no. 5, pp. 395–411, 2017, doi: https://doi.org/10.1002/polb.24287.

[20] J. Naciri, A. Srinivasan, H. Jeon, N. Nikolov, P. Keller, and B. R. Ratna, "Nematic Elastomer Fiber Actuator," *Macromolecules*, vol. 36, no. 22, pp. 8499–8505, Nov. 2003, doi: 10.1021/ma034921g.

[21] D. K. Shenoy, D. Laurence Thomsen III, A. Srinivasan, P. Keller, and B. R. Ratna, "Carbon coated liquid crystal elastomer film for artificial muscle applications," *Sens. Actuators Phys.*, vol. 96, no. 2, pp. 184–188, Feb. 2002, doi: 10.1016/S0924-4247(01)00793-2.

[22] D. J. Leo, *Engineering Analysis of Smart Material Systems*, 1st ed. John Wiley & Sons, Ltd, 2007. doi: 10.1002/9780470209721.

[23] S. Kim, E. Hawkes, K. Choy, M. Joldaz, J. Foleyz, and R. Wood, "Micro artificial muscle fiber using NiTi spring for soft robotics," in *2009 IEEE/RSJ International Conference on Intelligent Robots and Systems*, Oct. 2009, pp. 2228–2234. doi: 10.1109/IROS.2009.5354178.

[24] F. Pilate, A. Toncheva, P. Dubois, and J.-M. Raquez, "Shape-memory polymers for multiple applications in the materials world," *Eur. Polym. J.*, vol. 80, pp. 268–294, Jul. 2016, doi: 10.1016/j.eurpolymj.2016.05.004.

[25] J. Leng, X. Lan, Y. Liu, and S. Du, "Shape-memory polymers and their composites: Stimulus methods and applications," *Prog. Mater. Sci.*, vol. 56, no. 7, pp. 1077–1135, Sep. 2011, doi: 10.1016/j.pmatsci.2011.03.001.

[26] C. Liu, H. Qin, and P. T. Mather, "Review of progress in shape-memory polymers," *J. Mater. Chem.*, vol. 17, no. 16, pp. 1543–1558, Apr. 2007, doi: 10.1039/B615954K.

[27] T. Xie, "Recent advances in polymer shape memory," *Polymer*, vol. 52, no. 22, pp. 4985–5000, Oct. 2011, doi: 10.1016/j.polymer.2011.08.003.

[28] L. Saharan and Y. Tadesse, "Chapter 3 - Novel twisted and coiled polymer artificial muscles for biomedical and robotics applications," in *Materials for Biomedical Engineering*, A.-M. Holban and A. M. Grumezescu, Eds. Elsevier, 2019, pp. 45–75. doi: 10.1016/B978-0-12-816909-4.00003-8.

[29] C. S. Haines *et al.*, "Artificial Muscles from Fishing Line and Sewing Thread," *Science*, vol. 343, no. 6173, pp. 868–872, Feb. 2014, doi: 10.1126/science.1246906.

[30] J. Xiong, J. Chen, and P. S. Lee, "Functional Fibers and Fabrics for Soft Robotics, Wearables, and Human–Robot Interface," *Adv. Mater.*, vol. n/a, no. n/a, p. 2002640, doi: https://doi.org/10.1002/adma.202002640.

[31] C. S. Haines, N. Li, G. M. Spinks, A. E. Aliev, J. Di, and R. H. Baughman, "New twist on artificial muscles," *Proc. Natl. Acad. Sci.*, vol. 113, no. 42, pp. 11709–11716, Oct. 2016, doi: 10.1073/pnas.1605273113.

[32] S. Aziz, S. Naficy, J. Foroughi, H. R. Brown, and G. M. Spinks, "Controlled and scalable torsional actuation of twisted nylon 6 fiber," *J. Polym. Sci. Part B Polym. Phys.*, vol. 54, no. 13, pp. 1278–1286, 2016, doi: https://doi.org/10.1002/polb.24035.

[33] C. Piao and J. W. Suk, "Graphene/silver nanoflower hybrid coating for improved cycle performance of thermally-operated soft actuators," *Sci. Rep.*, vol. 10, no. 1, Art. no. 1, Oct. 2020, doi: 10.1038/s41598-020-74641-5.

[34] S. M. Mirvakili and I. W. Hunter, "Multidirectional Artificial Muscles from Nylon," *Adv. Mater.*, vol. 29, no. 4, p. 1604734, 2017, doi: https://doi.org/10.1002/adma.201604734.

[35] M. C. Yip and G. Niemeyer, "High-performance robotic muscles from conductive nylon sewing thread," in *2015 IEEE International Conference on Robotics and Automation (ICRA)*, May 2015, pp. 2313–2318. doi: 10.1109/ICRA.2015.7139506.

[36] L. Saharan and Y. Tadesse, "Fabrication Parameters and Performance Relationship of Twisted and Coiled Polymer Muscles," presented at the ASME 2016 International Mechanical Engineering Congress and Exposition, Feb. 2017. doi: 10.1115/IMECE2016-67314.

[37] S. Kianzad *et al.*, "Nylon coil actuator operating temperature range and stiffness," in *Electroactive Polymer Actuators and Devices (EAPAD) 2015*, Apr. 2015, vol. 9430, p. 94301X. doi: 10.1117/12.2085601.

[38] D. Kongahage, G. M. Spinks, and J. Foroughi, "Twisted and coiled multi-ply yarns artificial muscles," *Sens. Actuators Phys.*, vol. 318, p. 112490, Feb. 2021, doi: 10.1016/j.sna.2020.112490.

[39] L. Saharan and Y. Tadesse, "A Novel Design of Thermostat Based on Fishing Line Muscles," presented at the ASME 2016 International Mechanical Engineering Congress and Exposition, Feb. 2017. doi: 10.1115/IMECE2016-67298.

[40] L. Li, W. Ma, Q. Zhang, G. Yuan, H. Li, and Y. Tian, "Research on the mechanism of variable stiffness of the twisted and coiled polymer actuator during saturated contraction," *Smart Mater. Struct.*, vol. 29, no. 6, p. 065014, May 2020, doi: 10.1088/1361-665X/ab85a0.

[41] F. Karami, L. Wu, and Y. Tadesse, "Modeling of One-Ply and Two-Ply Twisted and Coiled Polymer Artificial Muscles," *IEEEASME Trans. Mechatron.*, vol. 26, no. 1, pp. 300–310, Feb. 2021, doi: 10.1109/TMECH.2020.3014931.

[42] C. L. Choy, F. C. Chen, and K. Young, "Negative thermal expansion in oriented crystalline polymers," *J. Polym. Sci. Polym. Phys. Ed.*, vol. 19, no. 2, pp. 335–352, 1981, doi: https://doi.org/10.1002/pol.1981.180190213.

[43] M. Hiraoka *et al.*, "Power-efficient low-temperature woven coiled fibre actuator for wearable applications," *Sci. Rep.*, vol. 6, no. 1, Art. no. 1, Nov. 2016, doi: 10.1038/srep36358.

[44] L. Wu, I. Chauhan, and Y. Tadesse, "A Novel Soft Actuator for the Musculoskeletal System," *Adv. Mater. Technol.*, vol. 3, no. 5, p. 1700359, 2018, doi: https://doi.org/10.1002/admt.201700359.

[45] S. Y. Yang *et al.*, "High performance twisted and coiled soft actuator with spandex fiber for artificial muscles," *Smart Mater. Struct.*, vol. 26, no. 10, p. 105025, Sep. 2017, doi: 10.1088/1361-665X/aa84e4.

[46] J. Zhang, K. Iyer, A. Simeonov, and M. C. Yip, "Modeling and Inverse Compensation of Hysteresis in Supercoiled Polymer Artificial Muscles," *IEEE Robot. Autom. Lett.*, vol. 2, no. 2, pp. 773–780, Apr. 2017, doi: 10.1109/LRA.2017.2651401.

[47] L. Saharan and Y. Tadesse, "Robotic hand with locking mechanism using TCP muscles for applications in prosthetic hand and humanoids," in *Bioinspiration, Biomimetics, and Bioreplication 2016*, Apr. 2016, vol. 9797, p. 97970V. doi: 10.1117/12.2219535.

[48] S. Liu, X. Tang, D. Zhou, and Y. Liu, "Fascicular module of nylon twisted actuators with large force and variable stiffness," *Sens. Actuators Phys.*, vol. 315, p. 112292, Nov. 2020, doi: 10.1016/j.sna.2020.112292.

[49] S. Kianzad, M. Pandit, J. Lewis, A. Berlingeri, K. Haebler, and J. Madden, "Variable stiffness and recruitment using nylon actuators arranged in a pennate configuration," *Proc. SPIE - Int. Soc. Opt. Eng.*, vol. 9430, Apr. 2015, doi: 10.1117/12.2086799.

[50] A. Simeonov *et al.*, "Bundled Super-Coiled Polymer Artificial Muscles: Design, Characterization, and Modeling," *IEEE Robot. Autom. Lett.*, vol. 3, no. 3, pp. 1671–1678, Jul. 2018, doi: 10.1109/LRA.2018.2801469.

[51] S. Y. Yang *et al.*, "Soft Fabric Actuator for Robotic Applications," in *2018 IEEE/RSJ International Conference on Intelligent Robots and Systems (IROS)*, Oct. 2018, pp. 5451–5456. doi: 10.1109/IROS.2018.8594275.

[52] D. Kongahage, G. M. Spinks, C. J. Richards, D. J. Shepherd, and J. Foroughi, "A new approach to develop, characterise and model actuating textiles," *Smart Mater. Struct.*, vol. 30, no. 2, p. 025019, Jan. 2021, doi: 10.1088/1361-665X/abd58d.

[53] "Certification of Test." Instron Corporation, Dec. 05, 1987.

[54] "The Series 96 User's Manual," *Watlow*. https://www.watlow.com/resources-and-support/Technical-Library/User-Manuals?keyw=Series%2096 (accessed Jun. 17, 2022).

[55] "The TransTek, Inc. Series 240 General Purpose DC-DC LVDTs," *Trans-Tek Inc.* https://transtekinc.com/products/series-240/ (accessed Aug. 07, 2022).

[56] "Standard type M36N-4E | DC Brush motors," *Mitsumi Product DataBase*. https://www.mitsumi.co.jp/latest/Catalog/compo/motorav/m36n4eseries_e.html (accessed May 22, 2022).

[57] "Trilene® Big Game™," *Berkley® Fishing*. https://www.berkley-fishing.com/products/trilene-big-game-1285546 (accessed Aug. 27, 2022).

[58] "Overview of materials for Nylon 6, Extruded," *MatWeb - Material Property Data*. https://www.matweb.com/search/DataSheet.aspx?MatGUID=726845c457b94b7cafe31d2e65739e1d&ckck=1 (accessed Jul. 21, 2022).

[59] J. T. Cheung and M. Zhang, "7 - Mechanics of the human skin and underlying soft tissues," in *Biomechanical Engineering of Textiles and Clothing*, Y. Li and X.-Q. Dai, Eds. Woodhead Publishing, 2006, pp. 111–124. doi: 10.1533/9781845691486.2.111.

Appendix A: Mean and Standard Deviation Results for Isotonic, Isometric, and Eccentric Tests

Isotonic Results:

Test Condition	Mean Stroke (%) [Standard Deviation]
Operating Load	
0.2 lb	-10.11 [0.62]
0.5 lb	-13.84 [0.16]
0.7 lb	-15.91 [0.39]
1.0 lb	-10.50 [0.74]
1.5 lb	-6.21 [0.78]
Precursor Fibre Diameter	
0.21 mm	-16.55 [0.33]
0.38 mm	-15.74 [0.84]
0.48 mm	-16.09 [0.54]
0.71 mm	-16.63 [0.13]
Spring Index	
C = 2.17	-13.55 [0.19]
C = 2.02	-10.04 [0.71]
C = 1.94	-8.31 [0.57]
Coil Bias Angle	
21°	-10.10 [0.15]
25°	-12.25 [0.11]
30°	-13.94 [0.25]
Twist Insertion Speed	
60 rpm	-13.11 [0.15]
240 rpm	-12.93 [0.13]
480 rpm	-12.85 [0.44]
720 rpm	-12.92 [0.58]
Training Conditions	
0.3 lb (Static)	-15.42 [0.69]
0.7 lb (Static)	-14.13 [0.18]
1.0 lb (Static)	-14.72 [0.15]
k = 0.0319 N/mm (Dynamic)	-15.23 [0.80]
k = 0.0929 N/mm (Dynamic)	-15.42 [0.98]
Pre-Stretch in Precursor Fibre	
2.5%	-9.82 [0.21]
5.0%	-14.20 [0.21]
7.5%	-16.28 [0.29]
Pre-Stretch in Coiled Sample	
7.5%	-9.75 [0.28]
21%	-11.52 [0.20]
35%	-12.83 [0.03]

Isometric Results:

Test Condition	Mean Force (N) [Standard Deviation]
Operating Load	
Blocked Force	2.50 [0.12]
0.50 N	2.13 [0.10]
0.75 N	1.97 [0.01]
1.00 N	1.59 [0.11]
1.25 N	1.52 [0.10]
1.50 N	1.36 [0.10]
Precursor Fibre Diameter	
0.21 mm	0.81 [0.04]
0.38 mm	1.78 [0.12]
0.48 mm	2.11 [0.15]
0.71 mm	6.60 [0.38]
Spring Index	
C = 2.17	1.79 [0.04]
C = 2.02	2.29 [0.07]
C = 1.94	2.95 [0.06]
Coil Bias Angle	
21°	2.10 [0.10]
25°	1.81 [0.06]
30°	1.48 [0.05]
Twist Insertion Speed	
60 rpm	1.72 [0.06]
240 rpm	1.77 [0.03]
480 rpm	1.68 [0.05]
720 rpm	1.78 [0.02]
Training Conditions	
0.3 lb (Static)	1.70 [0.04]
0.7 lb (Static)	2.05 [0.02]
1.0 lb (Static)	2.72 [0.02]
k = 0.0319 N/mm (Dynamic)	1.86 [0.00]
k = 0.0929 N/mm (Dynamic)	2.57 [0.03]
Pre-Stretch in Precursor Fibre	
2.5%	1.98 [0.02]
5.0%	1.73 [0.01]
7.5%	1.53 [0.01]
Pre-Stretch in Coiled Sample	
7.5%	1.88 [0.05]
21%	1.68 [0.06]
35%	1.48 [0.01]

Eccentric Results:

Operating Strain Rate:

Test Condition	2 mm/min	5 mm/min	10 mm/min
Temperature	Mean Tensile Modulus (MPa) [Standard Deviation]		
25°C	146.32 [1.34]	146.00 [1.12]	147.04 [1.38]
50°C	235.58 [1.43]	240.20 [2.09]	241.03 [2.14]
80°C	286.77 [3.71]	304.71 [1.86]	330.03 [0.77]
110°C	303.46 [0.99]	321.45 [0.48]	340.24 [0.46]
Range in Stiffness (Max/Min)	2.13	2.20	2.31

Precursor Fibre Diameter:

Test Condition	0.21 mm	0.38 mm	0.48 mm	0.71 mm
Temperature	Mean Average Modulus (MPa) [Standard Deviation]			
25°C	117.85 [0.26]	67.33 [1.19]	56.59 [1.85]	84.55 [1.10]
50°C	88.23 [0.65]	69.41 [1.67]	131.37 [3.43]	124.06 [2.02]
80°C	87.09 [1.45]	188.13 [4.77]	204.09 [6.04]	150.74 [0.80]
110°C	220.67 [2.60]	227.57 [1.24]	276.69 [3.83]	168.75 [4.17]
Range in Stiffness (Max/Min)	2.53	3.38	4.89	2.00

Spring Index:

Test Condition	C = 2.17	C = 2.02	C = 1.94
Temperature	Mean Tensile Modulus (MPa) [Standard Deviation]		
25°C	128.08 [1.62]	207.04 [0.71]	282.12 [3.22]
50°C	162.46 [2.80]	199.74 [1.87]	320.38 [4.08]
80°C	202.30 [1.23]	242.99 [1.45]	384.20 [2.05]
110°C	216.78 [0.89]	330.46 [1.38]	459.84 [2.99]
Range in Stiffness (Max/Min)	1.69	1.65	1.63

Coil Bias Angle:

Test Condition	21°	25°	30°
Temperature	Mean Tensile Modulus (MPa) [Standard Deviation]		
25°C	270.96 [2.05]	236.70 [2.61]	115.77 [3.23]
50°C	269.31 [1.36]	241.52 [1.40]	243.55 [2.60]
80°C	314.92 [2.56]	321.77 [3.40]	319.70 [1.14]
110°C	388.92 [2.91]	361.57 [0.78]	365.32 [1.21]
Range in Stiffness (Max/Min)	1.44	1.53	3.16

Twist Insertion Speed:

Test Condition	60 rpm	240 rpm	480 rpm	720 rpm
Temperature	Mean Average Modulus (MPa) [Standard Deviation]			
25°C	162.46 [4.70]	206.16 [1.64]	136.46 [4.71]	224.74 [3.98]
50°C	314.96 [2.61]	311.61 [4.08]	275.24 [1.29]	245.64 [4.40]
80°C	328.78 [3.32]	332.69 [0.88]	343.97 [2.00]	318.12 [1.97]
110°C	413.72 [2.13]	416.29 [2.97]	362.86 [2.99]	377.15 [2.83]
Range in Stiffness (Max/Min)	2.55	2.02	2.66	1.68

Training Conditions:

Test Condition	0.3 lb	0.7 lb	1.0 lb	k = 0.0319 N/mm	k = 0.0929 N/mm
Temperature	Mean Average Modulus (MPa) [Standard Deviation]				
25°C	115.67 [0.61]	112.91 [0.94]	119.02 [0.61]	123.96 [1.90]	122.41 [2.18]
50°C	263.35 [1.25]	71.72 [2.05]	59.65 [2.87]	145.07 [3.58]	87.87 [1.86]
80°C	380.19 [3.26]	203.92 [1.46]	64.50 [2.53]	301.34 [1.59]	181.78 [1.18]
110°C	386.17 [2.87]	288.79 [3.61]	180.76 [1.33]	398.21 [1.11]	287.09 [0.72]
Range in Stiffness (Max/Min)	3.34	4.03	3.03	3.21	3.27

Pre-Stretch in Precursor Fibre:

Test Condition	2.5%	5%	7.5%
Temperature	Mean Tensile Modulus (MPa) [Standard Deviation]		
25°C	203.05 [2.40]	160.76 [1.32]	140.55 [2.08]
50°C	325.28 [1.78]	271.75 [1.61]	215.62 [1.21]
80°C	346.96 [3.81]	308.13 [2.37]	256.45 [2.96]
110°C	390.69 [1.08]	340.27 [0.88]	298.67 [1.49]
Range in Stiffness (Max/Min)	1.92	2.12	2.13

Pre-Stretch in Coiled Sample:

Test Condition	7.5%	21%	35%
Temperature	Mean Tensile Modulus (MPa) [Standard Deviation]		
25°C	293.44 [2.70]	284.63 [3.51]	281.18 [2.45]
50°C	378.30 [1.46]	327.84 [1.27]	317.37 [1.69]
80°C	396.34 [1.97]	352.21 [1.68]	324.45 [1.14]
110°C	425.95 [1.25]	391.52 [6.72]	374.54 [2.09]
Range in Stiffness (Max/Min)	1.45	1.38	1.33